

ELECTROCATALYTIC UPGRADING OF BIOMASS PYROLYSIS OILS TO CHEMICAL
AND FUEL

By

Chun Ho Lam

A DISSERTATION

Submitted to
Michigan State University
in partial fulfillment of the requirement
for the degree of

Chemistry – Doctor of Philosophy

2014

ABSTRACT

ELECTROCATALYTIC UPGRADING OF BIOMASS PYROLYSIS OILS TO CHEMICAL AND FUEL

By

Chun Ho Lam

The present project's aim is to liquefy biomass through fast pyrolysis and then upgrade the resulting "bio-oil" to renewable fuels and chemicals by intensifying its energy content using electricity. This choice reflects three points: (a) Liquid hydrocarbons are and will long be the most practical fuels and chemical feedstocks because of their energy density (both mass and volume basis), their stability and relative ease of handling, and the well-established infrastructure for their processing, distribution and use; (b) In the U.S., the total carbon content of annually harvestable, non-food biomass is significantly less than that in a year's petroleum usage, so retention of plant-captured carbon is a priority; and (c) Modern technologies for conversion of sunlight into usable energy forms—specifically, electrical power—are already an order of magnitude more efficient than plants are at storing solar energy in chemical form.

Biomass fast pyrolysis (BFP) generates flammable gases, char, and "bio-oil", a viscous, corrosive, and highly oxygenated liquid consisting of large amounts of acetic acid and water together with hundreds of other organic compounds. With essentially the same energy density as biomass and a tendency to polymerize, this material cannot practically be stored or transported long distances. It must be upgraded by dehydration, deoxygenation, and hydrogenation to make it both chemically and energetically compatible with modern vehicles and fuels. Thus, this project seeks to develop low cost, general, scalable, robust electrocatalytic methods for reduction of bio-oil into fuels and chemicals.

ACKNOWLEDGEMENTS

I would like to express my deepest appreciation to my graduate school advisor, Prof. Ned Jackson, who has been a very patient scholar nurturing my academic growth. Ned taught me a lot – from designing experiments for proofing hypothesis to the elegant use of the English language for article composing (he even teaches me Latin and French occasionally). I often admire the fact that Ned can use every word to its full potential to produce a flawless convincing article easily at the tip of his fingers. With an in depth knowledge on almost every subjects, Ned cannot be replaced with a better advisor. Aside from being a great writer, Ned is also an excellent teacher. He would spent enough time for anyone to help them to understand (and think forward!) on chemistry problems. This explains why undergraduate students from his classes always ask for research opportunities in his research group. I am very fortunately that he entrusted me with his carefully selected students, letting them augment my data throughputs and the quality of my research. He taught me the patience required to mentor these students as well as the wisdom needed to guide them forward. I am forever grateful to have him to be my research advisor for the past 5 years – it has been a wonderful experience.

Thanks to Ned, I had the opportunity to work with over 30 undergraduate students over the past five years. Of these many individuals, Miss Kelsey Longe, Miss Michaelyn Lux, Miss Carly Houdek, Miss Christy Lowe, Miss Laura Schultz, Mr. Michael Caldwell, Mr. Jordan Rayburn, Mr. Andrew Henika, Mr. Ryan Barlow and Mr. Jacob Kunan stood out the most. These students took their own time and intellectual power to assist me in my graduate work at MSU. Special mention to Kelsey, who had been working with me for her entire 4 years of college: 2

years as a professorial assistant and 2 years as a volunteer, she continued to work dedicatedly years after years on different projects.

I would also like to thank my co-advisor, Prof. Chris Saffron, and my colleagues in the Jackson group. Dr. Saffron has been a very kind mentor to me in proofreading my work, giving me insightful feedbacks, and introducing me to various connections during academic conferences. His kindness and dedication are the two of his many positive qualities I looked up to. Collaborations with my colleagues have been some valuable experiences to me; learning from other members from different projects often inspires new ideas.

Finally, I would like to thank my family and friends. My parents never had the pleasure to attend college, but they realize the importance of education, and thus providing an enormous amount of support both emotionally and financially for me to complete this PhD degree in Chemistry. I can never reply what they have done for me; it is the best gift I can ever receive from anyone in my life. My friends outside of the program are also very supportive, my graduate life would not be as smooth without them.

There are countless more individuals I would like to mention – perhaps another thesis worth of acknowledgement can be written. I apologize if I missed out anyone on this page but I promise you that your contributions have not been forgotten. So, thank you!

TABLE OF CONTENTS

LIST OF TABLES.....	vii
LIST OF FIGURES.....	x
LIST OF SCHEMES.....	xvi
CHAPTER 1 Literature Review on Common Renewable Mobile Fuel Candidate.....	1
1.1 The Importance of Hydrocarbon.....	1
1.2 Emergence of Hybrid Vehicle	3
1.3 Hydrogen as a Fuel	5
1.4 The Biofuel: E85.....	9
1.5 Biofuel production via Fischer-Tropsch Process	11
1.6 CO ₂ Recycling and Carbon Capture & Storage (CCS).....	13
1.7 Biomass as a Renewable Energy Feedstock	16
1.7.1 The Need of Renewable Energy	16
1.7.2 Common Pathway for Biomass to Biofuels.....	18
1.7.3 Biomass as Feedstock	19
1.7.4 Biomass Fast Pyrolysis (BFP)	20
1.7.5 Nature of Bio-oil	21
1.7.6 Bio-oil Upgrading via ECH	24
1.8 Chapter Summary	26
1.8.1 Summary Table of the Discussed Alternative Fuel Candidates.....	28
1.8.2 Goal of this Research Project.....	31
CHAPTER 2 Literature Review on Electrocatalytic Hydrogenation.....	33
2.1 Introduction.....	33
2.2 Catalytic Hydrogenation for Bio-oil Upgrading and its Concerns	33
2.3 From Catalytic Hydrogenation to Electrocatalytic Hydrogenation	35
2.4 Brief Introduction to Electrocatalysis	36
2.5 Current Efficiency.....	38
2.6 Use of Cationic Surface Active Reagent in ECH	39
2.7 Selection of Electrodes and the volcano plot.....	40
2.8 The use of Raney-Nickel and Other Skeletal Metals.....	43
2.9 Preparation of Raney-Nickel Electrode	44
2.10 Introduction of the Cobalt Phosphate Water Oxidation Catalyst.....	45
2.10.1 Preparation of the Cobalt Phosphate Water Oxidation Catalyst.....	46
2.11 Overview of System Setup.....	47
2.11.1 Constant Voltage vs. Constant Current Electrolysis.....	47
2.11.2 Three Electrode System	50
2.11.3 Two Electrode System	51
2.12 Summary	52

CHAPTER 3	Electrocatalytic Upgrading of Model Lignin Monomers with Earth Abundant Metal	55
3.1	Introduction.....	55
3.2	Electrocatalytic Hydrogenation of Acetophenone in Undivided cell	56
3.2.1	Experimental Procedures	57
3.2.2	Analysis.....	58
3.2.3	Results and Discussion	58
3.3	Reduction of Phenol in Undivided Cell.....	60
3.3.1	Experimental Procedures	60
3.3.2	ECH of Phenol	62
3.3.3	Results and discussion	62
3.4	Reduction of Guaiacol in Divided Cell:.....	63
3.5	Experimental Procedures	64
3.6	Results and discussion	65
3.6.1	Mechanistic Investigation of Guaiacol Demethoxylation.....	68
3.6.2	Material Balance	74
3.6.3	Current Efficiency.....	77
3.6.4	Mechanistic Insight.....	79
3.7	Summary	83
CHAPTER 4	Electrocatalytic Hydrogenation of Aliphatic Model Compounds in a Solid Polymer Electrolyte Electrolyzer (SPEE)	85
4.1	Introduction.....	85
4.2	Preliminary Experiment I – SPEE Designs and Construction	88
4.2.1	Preparation of the Membrane Electrode Assembly (MEA).....	89
4.2.2	Construction of the 1 st Generation SPEE – The Prototype	90
4.2.3	Construction of the 2 nd Generation SPEE.....	92
4.2.4	Construction of the 3 rd Generation SPEE	93
4.3	Preliminary Experiment II – Exploring the 4 th SPEE	95
4.3.1	Construction of the 4 th Generation SPEE – The Current Version	95
4.3.2	Direct Metal deposition on Nafion Membrane	96
4.3.3	MEA Preparation with Different Reductants.....	97
4.3.4	Experimental Procedures	98
4.3.5	Results and Discussion	99
4.3.6	Formation of Ag-Cu Bimetallic Layer Catalyst.....	101
4.4	New Perspective on the SPEE and C.E. % Improvement Effort	105
4.4.1	Experimental Procedures	105
4.4.2	ECH of acetol in the presence of acetic acid	110
4.4.3	Effect of Anolyte on Current Efficiency Improvement	113
4.4.4	Influence of Metal Ion Re-deposition	115
4.4.5	Mesh Size Effect on Current Density	119
4.4.6	The Effect of Current Density on Current Efficiency.....	120
4.4.7	Isopropyl Alcohol Study	122
4.5	Summary	123

4.5.1	Miscellaneous Ideas and Future Directions	126
CHAPTER 5	Pedagogy: Electrocatalytic Hydrogenation of Acetol with US. Coins	128
5.1	Introduction.....	128
5.2	Hazards and Disposals	131
5.3	Experimental Procedures	131
5.3.1	Materials and Preparations.....	131
5.3.2	Experiment.....	132
5.4	Current Efficiency Analysis.....	134
5.5	Results and Discussion	136
5.6	Summary	140
CHAPTER 6	Conclusions	141
6.1	Project I - ECH of Bio-oil Model Compound, Guaiacol to Chemicals and Fuel	141
6.1.1	Improvement I – Electrode Material Synthesis	142
6.1.2	Improvement II – Substrate Scope and Mechanistic Studies.....	144
6.2	Project II – Development of SPEE system for Bio-oil Hydrogenation	144
6.2.1	Improvement I – Deposition of Ruthenium on Stainless Steel Mesh.....	145
6.2.2	ECH of Aqueous Bio-oil using Ru-SPEE.....	147
6.3	New Cell Design – The High Pressure Tube Reactor.....	149
6.4	Overall Progress Summary	153
6.5	Final Remarks – The Carbon Balance	154
REFERENCES	156

LIST OF TABLES

Table 1-1: Composition comparison between bio-oil and crude oil are shown. Note: actual composition of bio-oil varies depending on the biomass feedstock.....	22
Table 1-2: Summary of each discussed alternative energy candidate. 5 major factors: adaption to the current fueling structure, relationship to fossil energy, Cost to consumers, sustainability, and the environmental impacts are explored.....	29
Table 2-1: Terms comparison between chromatography and electronic system.....	48
Table 2-2: An example to illustrate how the absolute potential on individual electrode changes during a constant voltage electrochemical reaction. Note: Ta and Tb describes different stage during the ECH.....	49
Table 3-1: Condition for sacrificial and non-sacrificial of Acetophenone (AP) to 1-phenylethanol (PE) at constant current (50mA)	57
Table 3-2: Deposition rate and deviations on Ni-Al alloy deposition. Mono side physical area (2.5 x 2.5 cm) of the used for the <i>J</i> value calculation	61
Table 3-3: Reduction of 20 mM of Guaiacol in 0.1 M pH 8.2 borate buffer at $82 \pm 2^\circ\text{C}$, and $j= 8 \text{ mA cm}^{-2}$ (current density was calculated by applied current (50 mA) divided by the electrode area that is facing the anode 2.5 x 2.5 cm). G: Guaiacol, P: Phenol, 2M, 2-Methoxycyclohexanol and C: Cyclohexanol	67
Table 3-4: Values are percentages relative to starting material buffer concentration, $12.1 \pm 1.5 \text{ mM}$ as determined by gas chromatography. Reductions employed a Raney-Nickel cathode in 30 ml of 0.1 M pH 8.0 potassium borate buffer, and a stainless steel anode coated with cobalt phosphate catalyst in 30 ml of 0.1 M pH 7 potassium phosphate buffer. Reaction started with 60 minutes of pre-electrolysis and followed immediately by compound addition and then run for 6 hours at 50 mA (8 mA cm^{-2})* at 75°C . Total current passed in this time represents 4.1 x the amount required for substrate reduction to ROH and cyclohexanol. b) Cis and trans product are in equal amounts. c) Only a single peak was observed by GC. *Note: current density is calculated based on the single side electrode facing the membrane and anode compartment.....	70
Table 4-1: 10 ml of 5% acetol (924.5 mM) dissolved in deionized water undergo ECH to propylene glycol after 6 hours at a constant current $98 \pm 2 \text{ mA}$, at room temperature and ambient pressure. All current collectors are mesh 200 in size, and had been cleaned with hexane, acetone and water prior to use. Stainless steel 304 (Mesh 200) was used in a 0.1M pH 7.0 phosphate buffer as an anode for all trials. Material	

balance was calculated by summing acetol and propylene glycol alone. *Initial acetol concentration for the “copper with 5% acetic acid” trial was 716 mM..... 107

Table 4-2: ECH of 10 ml of 5% acetol with 5% (v/v) glacial acetic acid added. Condition: copper mesh with various mesh size at 98 ± 2 mA at 1 atm at room temperature (22 ± 1 °C) for 6 hours. Note: mesh size 2.3×2.3 cm = 5.29 cm²..... 119

Table 4-3: ECH of 10 ml of 5% acetol with 5% (v/v) glacial acetic acid added. Condition: Monel 400 mesh 200 at different current density (mA cm⁻²) 1 atm at room temperature (22 ± 1 °C). Note: charge passed was calculated by the summation of multiplying current level (recorded hourly) with the time interval between sampling time. Note: current density was calculated based on the cut dimension of 2.3×2.3 cm = 5.29 cm²..... 120

Table 4-4: Factors that enhance current efficiency towards organic substrate hydrogenation... 125

Table 5-1: Results of ECH of acetol in various conditions. All trials were run using a penny as the anode at room temperature. Note: results were determined by ¹H-NMR peak integration to verify the formation of propylene glycol (See Figure 5-6). 1) 3 V d.c. power supply; 2) 3 V (two AA cells in series) batteries; 3) 3 V d.c. power supply with bag/coins in an ice bath. 135

Table 6-1: atomic % from EDX analysis on the surface of the electrodes, SS-Ni-Pd and SS-Ni-Pd-Ru, showing palladium and ruthenium were deposited onto the surface. Note: the remaining percentage is made of nickel and chloride. 147

LIST OF FIGURES

Figure 1-1: Comparison of the specific energy (MJ kg ⁻¹) of various common energy carrying chemicals. Hydrogen has a specific energy of 124 MJ kg ⁻¹ and its scale is associated with the secondary axis on the right.	2
Figure 1-2: General operating principle of hydrogen fuel cell	6
Figure 1-3: Comparison of the overall carbon and energy balance in the US transportation sector and harvestable biomass. Red bars compare the weight of the petroleum used, and the weight of the harvestable biomass. Blue bars compare the actual carbon content. Green bars compare the energy spent annual, and the harvestable amount of energy from biomass. Projections are made based on the available biomass by 2030.	17
Figure 1-4: General chemical distribution of organic substrates found in bio-oil. Percentage is given percent of mass.	23
Figure 1-5: Phenol is used as a model compound to illustrate the increases in specific energy (MJ kg ⁻¹) upon hydrogenation and deoxygenation. Note: higher heating values mean the heat of combustion is calculated with the heat of formation of water in liquid state, which is lower in energy compared to gaseous state, and thus gives a greater value of heat of combustion (heating values).	25
Figure 2-1: Cetyltrimethylammonium bromide (CTAB) is used as an example to illustrate the positively charged hydrophilic head and hydrophobic end (the hydrocarbon tail) nature of surfactant	40
Figure 2-2: The volcano plot of the common metals used in electrocatalysis.	42
Figure 2-3: Co-deposition of Ni-Al alloy onto the electrode surface. Condition: Preparation of the Ra-Ni cathode uses the Lessard method of trapping nickel-aluminum alloy particles in an electrodeposited nickel matrix.	45
Figure 2-4: Three electrode system where the reference electrode is referencing the cathode (working), substrate A is oxidized on the anode surface and substrate B is reduced on the cathode surface. The separator, typically a glass frit or Nafion membrane, may or may not be necessary to the system. Note: V = Voltmeter, to measure the voltage between the reference electrode and the working electrode. A = Ammeter, to measure the current at any time during the reaction	50
Figure 2-5: Two electrodes with the cathode (working) and the anode (counter); substrate A is oxidized on the anode surface and substrate B is reduced on the cathode surface. Separator is optional, and is typically a proton exchange membrane or glass frit. Note: V = Voltmeter, to measure the voltage between the reference electrode and the	

working electrode. A = Ammeter, to measure the current at any time during the reaction	51
Figure 3-1: Electrocatalytic Hydrogenation of acetophenone in an undivided cell with different electrodes.....	56
Figure 3-2: Reduction of acetophenone with different electrode at room temperature.....	58
Figure 3-3: Raney Nickel cathode before (left) and after (right) leaching of Al with NaOH at 70 °C for 7 hours.	62
Figure 3-4: Electrocatalytic hydrogenation of Guaiacol and the possible product and their annotations.....	65
Figure 3-5: Electrocatalytic Hydrogenation of Guaiacol in high pressure setting (Left) the physical setup of the overall system (Right) Schematic depiction of the reaction chamber	65
Figure 3-6: Electrocatalytic hydrogenation (ECH) of organic molecule in a divided cell separated by a Nafion 117 proton exchange membrane.....	66
Figure 3-7: Depiction of CTAB at different concentration in solution. Low and optimal will cause CTAB to form on adsorption on surface while medium high to high will encourage formation of micelle and may encourage diffusion of organics through the cationic exchange membrane (Nafion).....	68
Figure 3-8a. (upper) Trial a: 1:1:1 mixture of guaiacol (---), 2-ethoxyphenol (---), and 2-isopropoxyphenol (---) undergoes electrocatalytic hydrogenation (ECH) under the same condition described in table 1. All three reactants form a common intermediate, phenol (---), which is further hydrogenated to cyclohexanol (---). Only traces of the alkoxy cyclohexanol products of direct hydrogenation were detected. Figure 3-8b (lower) Trial b: 1:1:1 mixture of guaiacol (---), 3-methoxyphenol (---), and 4-methoxyphenol (---) undergoing ECH as above. Formation of 3-methoxycyclohexanol (---) and 4-methoxycyclohexanol (---) is observable. Phenol (---) and cyclohexanol (---) were also formed as the major products. Curves are polynomial fits included to guide the eye.	72
Figure 3-9: ECH of Syringol (IUPAC: 2,6-dimethoxyphenol) in 30 ml of 0.1M pH 8.0 Borate Buffer with 0.5mM CTAB at 75 °C. Syringol(---), cyclohexanol(---), guaiacol(---), phenol(---) and current efficiency(---), vertical axis on the right.....	73
Figure 3-10: (a) Reactants, products and C.E. (%) data from ECH at 50 mA (8 mA cm ⁻²)* and 75 °C of 30 ml 18 mM guaiacol in 0.1 M pH 8.0 potassium borate buffer: guaiacol(---), phenol(---), methanol(---), cyclohexanol(---), and material balance (---).	74
Figure 3-11: Adsorption study to investigate the cause of material loss.	76

- Figure 3-12: Diffusion test on guaiacol and phenol under experimental condition. Raney nickel electrode is substituted with a plain nickel bar to prevent the hydrogenation of the substrates. 77
- Figure 3-13: Total charged passed of the reaction vs. amount of charge spent on guaiacol reduction for the reaction shown in Figure 3-10. 78
- Figure 3-14: Proposed mechanism for the alkoxy-demethoxylation. Scheme 1 has been eliminated with ¹H-NMR study. Scheme 2 and 3 are the probable route for the reaction. 79
- Figure 3-15: Competition study of 10 mM guaiacol in the presence of various amount of p-cresol. Upper left (a) guaiacol analysis, upper right (b) phenol analysis, lower left (c) cyclohexanol analysis and lower right (d) p-cresol and 4-methylcyclohexanol analysis: With 20 mM of p-cresol added (----), with 10mM of p-cresol added (----), and no p-cresol added (----). Legends are same across all figures, each figure focuses on the specific compound of interests specified on the vertical axis. 81
- Figure 3-16: Possible mechanism for the de-alkoxylation of 2-alkoxyphenol 83
- Figure 4-1: Schematic diagram to show the (Left) operating principle of a chemical (H₂) fuel cell and (Right) how the SPEE operates. Note: App. is short for electronic applications 86
- Figure 4-2: Solid Polymer Electrolyte Electrolyzer processing unit that connects to the fast pyrolysis unit. Bio-oil can be upgraded immediately upon exit..... 88
- Figure 4-3: Schematic drawings of the 1st SPEE cell made of two identical pieces as shown in the figure on the right, these two halves are held together with a cell metal clip. 90
- Figure 4-4: Schematic drawings of the 2nd SPEE cell which combines conventional dual compartment electrochemical cells with SPEE concepts together..... 92
- Figure 4-5: Schematic drawings of the 3rd SPEE cell – 2 pieces of glass plate that host the MEA supported by a pair of Parafilm gasket and Carpenter clamp..... 94
- Figure 4-6: Production of furfuryl alcohol from furfural ECH in SPEE. (Left) MEA was prepared with sodium borohydride (Right) MEA was prepared with hydrazine. 99
- Figure 4-7: Used Ag-MEA after 3 uses of electrolysis. (Left) a used Ag-MEA prepared with sodium borohydride, and (right) a used Ag-MEA prepared with hydrazine. Conductivity measure was taken using multimeter for both membranes: 100
- Figure 4-8: Visual comparison between (left) before, and (right) after copper plating onto the Ag-MEA 101
- Figure 4-9: (Right) ECH of 10 ml of 10 mM furfural. Condition: Ag is deposited on Nafion using 1% Hydrazine solution. Reactions were run at 98 ± 2 mA at 1 atm at room temperature (22 ± 1 °C) for 6 hours. Note: Cu-Ag is prepared by plating copper onto

the Ag-MEA electrochemically using 50 mM CuSO ₄ at 98 ± 2 mA for 5 minutes. (Left) the voltage log for the reactions displayed on the right	102
Figure 4-10: Reduction of acetol in examining the necessity of the silver foundation and the importance of the current collector.	104
Figure 4-11: Solid Polymer Electrolyte Electrolyzer (SPEE) parts, and the setup.....	106
Figure 4-12: (Left) typical experimental setup of a SPEE. (Right) close-up to a SPEE with alligator clips and silicon tubing connected	106
Figure 4-13: Proposed reaction pathways of acetol. Candidates are proposed based on the observed molecular weight from aqueous phase MS analysis. Percentages of the compounds are given based on the relative intensity of the peak.	109
Figure 4-14: ECH of 10 ml of 5% acetol with <u>5% (v. /v.) glacial acetic acid</u> added. Condition: copper mesh 200 at 98 ± 2 mA at 1 atm at room temperature (22 ± 1 °C) for 6 hours. Copper mesh is being reused multiple times and compared with the Monel 400 mesh 200 Note: reaction is evaluated using the cumulative current efficiency, each point accounts for the product accumulated previously. For equation, see Scheme 2-2..	111
Figure 4-15: SEM examination on copper mesh before (Top, Left) and after (Top, Right) 6 hours of electrolysis. New Stainless Steel (Bottom, Left) and used stainless steel (Bottom, right). Samples were washed with water, acetone and chloroform to remove organic residues. Then they were dried in vacuum desiccator for 2 hours before SEM examination at 12kV and 10 mm working distance under ultrahigh vacuum.....	112
Figure 4-16: ECH of 10 ml of 5% acetol with 5% (v. /v.) glacial acetic acid added. Condition: Monel 400 at 98 ± 2 mA at 1 atm at room temperature (22 ± 1 °C) for 6 hours. The anode compartment conditions are listed in the legend	113
Figure 4-17: ECH of 100 ml of 5% acetol with 5% (v. /v.) glacial acetic acid added. Condition: Monel 400 mesh 200 at 98 ± 2 mA at 1 atm at room temperature (22 ± 1 °C) with a platinum mesh anode in deionized water for 6 – 12 hours. Metal salts were added at the beginning of the experiment.....	116
Figure 4-18: ECH of 100 ml of 5% acetol with 5% (v. /v.) glacial acetic acid added. Condition: Monel 400 mesh 200 at 98 ± 2 mA at 1 atm at room temperature (22 ± 1 °C) with a platinum mesh anode in different analytes for 12 hours.	117
Figure 4-19: ICP-OES analysis of nickel and potassium in the cathode solution for trials described in Figure 4-18. Samples were diluted 125 times with 2% nitric prior analysis (0.2 ml of sample in 25 ml of 2% nitric acid).	118
Figure 4-20: graphical interpretation of A) at low current, hydrogen adsorption is low, resulting in low hydrogenation efficiency. when the applied potential is too low (or too high), energy of the electron and the LUMO is mismatched, causing an inefficient transfer and lower the C.E. B) at moderate level of current, surface is filled with enough	

adsorbed hydrogen and can fit in organics to achieve hydrogenation. C) at high current, surface is saturated with adsorbed hydrogen and disfavors organic adsorption. H₂ formation becomes dominated result. energy of the transfer electron matches the LUMO of the pi bond to give an efficient electron(s) transfer 121

Figure 4-21: ECH of 10 ml of 5% acetol in water or isopropanol, with and without acetic acid. Condition: Monel 400 mesh 200 at 98 ± 2 mA at 1 atm at room temperature (22 ± 1 °C) for 6 hours. 122

Figure 5-1: Schematic diagram of ECH of unsaturated organic molecules (a-d) and hydrogen evolution (e -f)..... 130

Figure 5-2: (left) Experimental setup of ECH of acetol with coins. A copper coin anode is clipped with red wire, and the nickel coin cathode is clipped with the black wire. An extra coin is added on each side to act as a current collector and provide enough pressure for the clamp (right). Setup is in a small sample bag to prevent filter paper drying..... 132

Figure 5-3: Electronic setup of the experiment. Note: Drawing is not to scale..... 133

Figure 5-4: Color changes of Q.B. solution in response to concentration of acetol. From left to right: 100:0, 80:20, 60:40.....0:100 acetol (5% v/v): propylene glycol (5% v/v)... 134

Figure 5-5: Change in absorbance of QB solution in response to % of acetol in standard solution. Note: students can take readings in transmittance and calculate the absorbance using the equation: $A = 2 - \log (\%T)$ 134

Figure 5-6: ¹H -NMR spectrum (Red) propylene glycol standard (Orange) ECH of acetol with penny for 10 minutes; low resolution of the orange spectrum was due to Cu²⁺ ion contamination. (Green) acetol standard (Blue) experiment 10 minutes with no electricity passed 135

Figure 5-7: An example of current-time profile. Total charge passed (C_{total}) can be estimated by calculating area of the curve. Area under the curve can be estimated by simple summing of the trapezoidal areas..... 136

Figure 5-8: (left) SEM spectroscopic analysis of plain penny surface, and (right) the black copper layer after reaction..... 136

Figure 5-9: Change in absorbance of QB solution in response to % of acetol in standard solution. 138

Figure 6-1: ECH of guaiacol using Raney-Nickel cathode. Reaction proceeds with excellent selectivity to form cyclohexanol as the sole product, and does not form the planar 2-methoxycyclohexanol..... 142

Figure 6-2: Multiple layers of metals plated onto stainless steel to support the deposition of ruthenium..... 146

Figure 6-3: GC-MS results on the aqueous fraction of bio-oil before hydrogenation in SPEE cell. Temperature program: 50 °C hold for 3 minutes, then 15 °C/minute until 270 °C and hold for 5 minutes.....	148
Figure 6-4: GC-MS results on the aqueous fraction of bio-oil after hydrogenation in SPEE cell. Temperature program: 50 °C holds for 3 minutes, then 15 °C/minutes until 270 °C and hold for 5 minutes	148
Figure 6-5: HPLC-Flow style cell anatomy.....	150
Figure 6-6: the general overall setup of the Flow cell reactor	150
Figure 6-7: Prototype testing of the flow cell reactor. Reaction condition: 5% of acetol dissolved in 0.25 M of ammonium acetate, 50 mA (117.9 mA cm ⁻²), room temperature, 1 ml min ⁻¹ . Anolyte was the platinum wire inside of 0.1 M H ₂ SO ₄ solution. 0.01 ml of sample was taken hourly and was mixed with 0.75 ml of D ₂ O for H-NMR analysis. The absolute concentration of product was calculated by the internal concentration reference, 1,4-dioxane, that was pre-dissolved in the D ₂ O solvent. Note: the current efficiency is calculated based on the charge passed and product formed hourly, NOT accumulatively.....	152
Figure 6-8: Overall time summary of the progress of this research project.	153

LIST OF SCHEMES

Scheme 1-1: General descriptive chemical equation describes common biomass to biofuel processing pathways. Fermentation and Gasification both disposes 33% of the carbon content as CO ₂ while fast-pyrolysis retains most carbon in the form of bio-oil: 70% bio-oil, 15% bio-char, and 15% gas.	18
Scheme 1-2: Overall scheme of the research project: a maximum carbon retention strategy to produce renewable carbon fuel through biomass pyrolysis, followed by electrocatalytic upgrading that is powered by renewable electricity.	24
Scheme 2-1: general chemical equations for electrocatalytic hydrogenation of organic substrate	37
Scheme 2-2: chemical equations illustration on how H ₂ can be generated on the electrode surface with two different mechanisms	38
Scheme 4-1: Possible cathodic reactions: a) Hydrogen evolution b) acetol undergoes ECH to propylene glycol using electrons and protons c) acetol undergoes ECH to propylene glycol using water and electron as a reductant. d) cathodic water reduction forming hydroxide anion.	109
Scheme 4-2: Revised mechanism for the SPEE cell that accounts for all observed reactions. Reaction mechanism is proposed based on the conditions described in the diagram.	124
Scheme 5-1: Acetol hydrogenation to propylene glycol electrocatalytically. and hydrogenation evolution	134

Chapter 1 Literature Review on Common Renewable Mobile Fuel Candidate

1.1 The Importance of Hydrocarbon

There is no replacement for hydrocarbon's low toxicity, well-developed and ease of handling as storable stable liquid. These excellent qualities make liquid hydrocarbon fuels irreplaceable by any other energy carriers. It is the ideal source of energy for transportation purposes owing to its high energy: mass ratio, formally known as specific energy (MJ kg^{-1}). Today, hydrocarbon fuels are still playing a key role in the transportation sector. In 2011, over 250 million cars were thought to be on the roads in the US.¹, but only 1.19 million of these were powered by non-traditional sources such as batteries, hydrogen, propane, or ethanol². Although the trend towards alternative fuel vehicle usage is rising, traditional fuels will still play a key role far in the foreseeable future. At a glance, gasoline carries approximately 25 times more energy per kilogram (45 vs. 1.8 MJ kg^{-1}) than the most advanced commercially available lithium battery, as shown in Figure 1-1.³ The difference in energy immediately explains why gasoline is still the predominant choice of energy carrier for transportation; it has a high energy to mass ratio compared to other carriers available. Specific energy is a particularly important factor in transportation fuel consideration because spending energy on moving the fuel itself is an energy wasting process. Even if energy supply were easily available and come in unlimited quantity, the mass of the energy carrier would still matter. Vehicle that is powered by low specific fuel would suffer from frequent fuelling stops and low transportation capacity as the majority of the vehicle space would be occupied by the energy carrier.

Therefore, this is why crude oil is being refined to hydrocarbon fuel to power internal combustion engine (ICE) rather than being used to generate electricity in a power plant to power electric motors. This is because hydrocarbon stores a lot more energy than battery per given weight, so hydrocarbon can cover a lot more mileage compared to battery. It is worth noting,

however, using a hydrocarbon fuel cell to generate electricity in a hydrocarbon fuel cell would be a different story because it would still be best to have an efficient way of converting hydrocarbon energy to electricity without the ICE. The vast value difference in specific energy between hydrocarbons and batteries makes the ICE still the preferred converter of chemical to mechanical energy, even though it has a lower energy efficiency than the electric motor. For the foreseeable future, hydrocarbons will continue to be to the predominant form of energy carriers over any other sources.

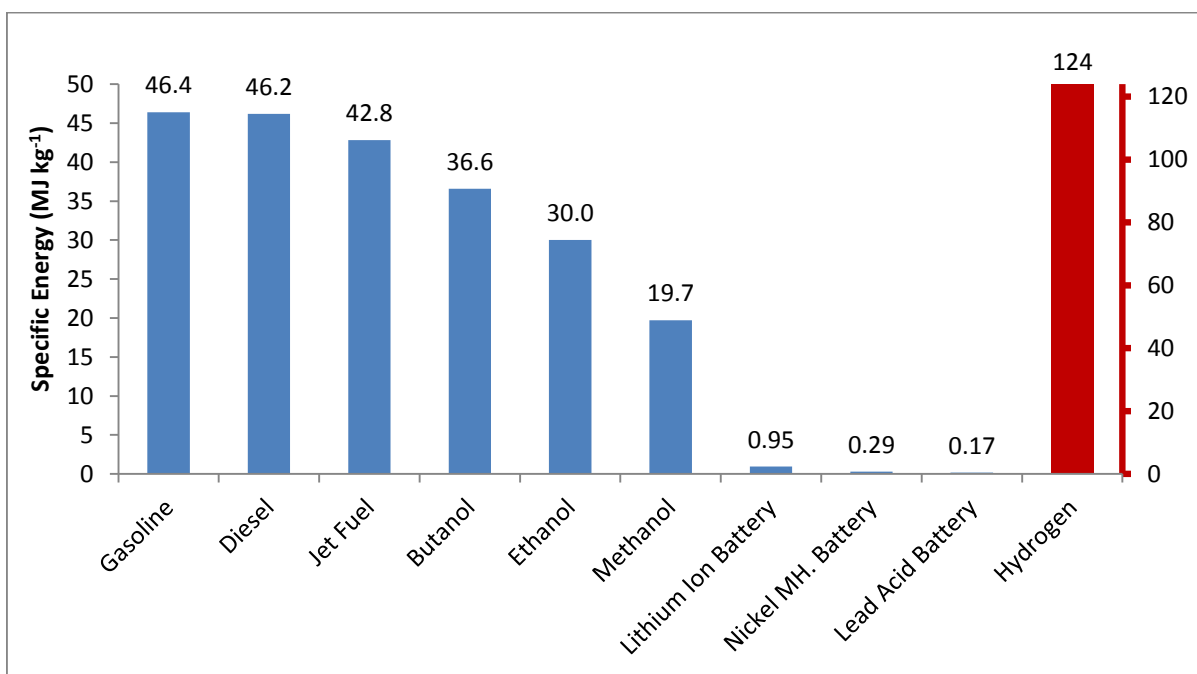


Figure 1-1: Comparison of the specific energy (MJ kg⁻¹) of various common energy carrying chemicals. Hydrogen has a specific energy of 124 MJ kg⁻¹ and its scale is associated with the secondary axis on the right.

Nature has affirmed this assessment: hydrocarbon-like fats and oils have been powerfully selected by evolution as the ideal lightweight energy carriers for essentially all mobile organisms. The use of hydrocarbons in engines is thus not a coincidence, but a logical practice that mimics nature's highly optimized energy transport materials. However, this practice and the combustion

of the fuel, does not only depletes the earth's finite reserves of fossil resources, but also increases the CO₂ concentration in the atmosphere causing global warming and various unpredictable climate changes.

The world is making great efforts to develop CO₂ emission free technology while accommodating the energy needs of the ever growing population. However, as of today, *NO* technology is entirely free from CO₂ emission because these technologies, e.g. hydrogen fuel, E85, Fischer-Tropsch diesel synthesis and electric vehicles all depend on the current energy framework. As long as fossil fuel continues to serve as the fundamental energy source, these “renewable fuel” options can only be considered mitigation plans that minimize localized CO₂ emission.

In this chapter, these renewable fuel options will be explored, their pros and cons will be evaluated from various viewpoints such as cost, safety and ease of implementation within the current fueling infrastructure, and in some cases the overall environmental impact. Bio-oil will be presented as the renewable fuel candidate with the most immediate promise to potentially displace the current fossil fuel demand in the transportation sector.

1.2 Emergence of Hybrid Vehicle

Hybrid vehicles powered by gasoline and batteries together have begun to emerge as the world is slowly moving towards low carbon-emission technologies. Such hybrid vehicles operate by converting the spare mechanical energy produced from internal combustion in the engines, or by braking, into the form of electrical energy, which is then reversibly stored in the rechargeable batteries installed in the vehicle. The stored energy is delivered when driving conditions call for acceleration or other heavy duty work that would otherwise require high gasoline input. This electrical energy compensation mechanism reduces gasoline consumption and thereby improves

the vehicle's gas mileage. Today, some of the hybrid models even come in "plug-in" versions with zero vehicle emission modes in which the vehicle can be recharged from the electrical grid and be driven modest distances without combusting gasoline. Although the zero emission mode typically only lasts several tens of miles, it is certainly a great step in the right direction towards reducing greenhouse gas emission. However, as mentioned before, since the majority of electrical power on the grid still comes from combustion of fossil fuels, mainly coal and natural gas, this mode of powering transport is not actually "emission free" when the source is considered.

Along the same line, some companies, such Nissan, Honda, and Tesla have begun to market total zero emission vehicles – cars that run completely on electricity, and release zero carbon dioxide. This seems excellent at a first glance, but it does come with drawbacks when viewed in the bigger picture. First, electricity from the grid is still generated from coal or natural gas burning, so zero emission vehicles are not entirely emission free. But localized, fixed source CO₂ emission could potentially enable effective CO₂ recapturing, a process that will be discussed later. Second, even if these vehicles are powered by renewable electricity, their manufacture requires intensive energy inputs from the grid which as noted comes mainly from fossil sources. Lastly, these vehicles typically suffer from high production costs and frequent fueling stops because the energy storage module is manufactured with costly advanced materials and limited by weight in the vehicle. Tesla Motors, a leading company in production of electric cars, has been marketing its latest model, capable of travelling more than 300 miles (driving at 40 mi/hr)⁴, a typical driving distance of a passenger car with a 14 gallon gasoline tank. Unfortunately, such performance does not come without cost. A car from Tesla costs anywhere between \$58,570 -

\$106,570 depending on the model and accessories purchased, while most cars today on the market cost between \$25,000 – \$45,000.

Although the US government has introduced various tax subsidies to promote the growth of the alternative fuel vehicle business, the current cost is simply beyond what an average American household can afford. These overwhelming prices are mainly due to the advanced patented battery technology, and high unit production costs due to low present demand. After all, battery charging stations are not yet widely established in the country compared to gasoline stations. As of March 2014, only 7700 fueling sites in the US come with charging option.⁵ Recharging the battery to cover 300 miles in the Tesla takes approximately 53 hours on a 120 volt outlet⁶ whereas filling a 14 gallon gasoline tank takes less than 5 minutes. So even though the fueling option of electric car seems more convenient – plug the vehicle at home vs. driving to gas station, the long refueling time without high cost equipment is a major setback to its sales. Though a world operating with 100% zero emission vehicles would be wonderful, the high production and long refueling time will continue to let conventional gasoline cars dominate the transportation system for years to come.

1.3 Hydrogen as a Fuel

One highly touted carbon free transportation energy carrier has also been the focus of great effort – Hydrogen. In 1970, John Bockris coined the term “hydrogen economy” in which hydrogen would serve as the fundamental energy source to power various applications run in a society.^{7, 8} In his theory, hydrogen could be generated from hydrocarbon steam reforming ($\text{CH}_4 + \text{H}_2\text{O} \leftrightarrow \text{CO} + 3 \text{H}_2$) or water electrolysis ($2\text{H}_2\text{O} \rightarrow \text{O}_2 + 2\text{H}_2$). However, steam reforming makes use of methane which is a fossil fuel, and electrolysis requires electricity that usually comes from burning coal or natural gas. In other words, the hydrogen economy can merely serve

as a strategy to alleviate the global dependence on fossil fuel but it not a long term solution unless there is affordable means to practice water electrolysis through renewable electricity.

Unlike hydrocarbons, which generate carbon dioxide and water upon combustion, hydrogen only generates water in the form of steam, which is bio-friendly and hazard free. To maximize the energy extraction from hydrogen, the hydrogen fuel cell (HFC) is currently one of the most studied topics of research. In an HFC, electrical energy is directly generated through oxidation of hydrogen and reduction of oxygen. Electrons are driven in the circuit by the formation of water, which is a more thermodynamically stable product. This direct conversion of chemical to electrical energy is substantially more efficient than the conventional internal combustion engine. (ICE). The ideal efficiency of a hydrogen fuel cell can be as high as 83% under standard testing conditions (1 atm and 25 °C) while an ICE only gets up to 34%.⁹ The general fuel cell operation principle is depicted in Figure 1-2.

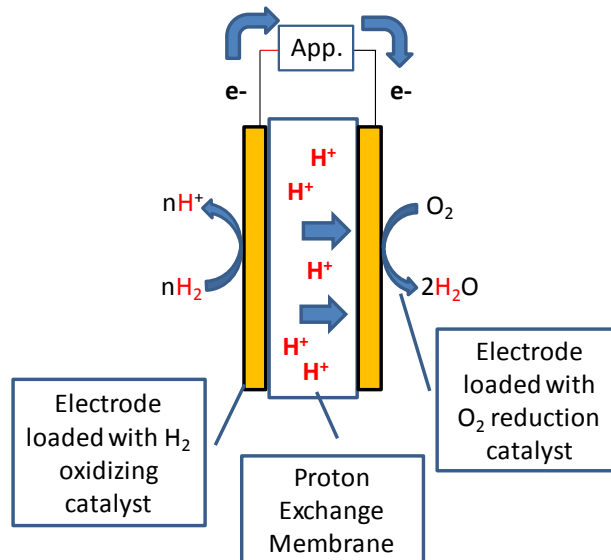


Figure 1-2: General operating principle of hydrogen fuel cell

H₂ fuel cell powered mass transport vehicles (buses) have been produced by various manufacturers such as Toyota and Mercedes-Benz since early 2000 and are becoming

increasingly popular in several European countries.^{10, 11} The H₂ tank and the fuel cell system are typically located on the roof of the bus. Electricity generated is stored or dissipated through a super capacitor or battery to fuel the motion of the vehicle. H₂ refilling typically takes place at a central H₂ storage and fueling station. Prototype of passenger fuel cell vehicles have also begun to emerge from many different vendors such as Audi, BMW, Nissan, Toyota, and Volkswagen. They are often showcased in automobile expositions. However, H₂ powered small cars have generated less interest than gasoline powered cars for several reasons: H₂ is a highly flammable and, when in a mixture with air, explosive gas upon ignition. The 1937 Hindenburg disaster in which a German passenger airship with a flawless safety record caught fire and burned in seconds, resulted in the death of 35 of the 97 on board. While risk assessment reports indicate H₂ can be handled safely with proper public education on its properties, the general public would still fear driving with such a highly explosive gas that reminds them of the airship tragedy.^{12, 13} Furthermore, the H₂ economy has failed to take off because of the need for a completely new infrastructure of H₂ filling stations, a distribution system, and low cost H₂ storage methods and equipment.^{14, 15}

While large vehicles have room for large H₂ tanks sufficient to cover moderate distances, H₂ tanks for passenger cars significantly increase the engineering challenge, weight, and production cost for high pressure vessels or cryogenic systems. Moreover, fuel cell systems lack durability compared to internal combustion engines; they are sensitive to real world fluctuations in environmental variables such as humidity and temperatures. Although service life improvements from 29,000 to 75,000 miles have been made in the last few years, consumers are still better off with the internal combustion engines which typically last more than 150,000 miles.¹⁶ The cost per unit power of the H₂ fuel cell technology has improved greatly over past

decade. The delivery and dispensed price of hydrogen has lowered to \$4.10/gge (gallon of gasoline equivalent) in 2012, but there remains a substantial gap to the ultimate target of \$1-2/gge,¹⁷ a value that would give H₂ fueled vehicles an economical advantage over gasoline fueled vehicle.

The needed infrastructure of H₂ fueling/delivering systems is still unavailable for commercial use. H₂ fuel cell powered public transportation has the advantage of centralized, company-built H₂ refilling facilities, standard fleets of vehicles, and regular travel patterns, but there are only a handful of H₂ refilling station in the US for H₂ fuel cell car owners. This lack is mainly due to the extreme capital investments required, ranging from \$500,000 to \$5,000,000 per station.¹⁸ Even if H₂ refilling stations were subsidized by the government (i.e. taxpayers), and were built across the nation, the current high cost of H₂ (\$4.10/gge) would still put H₂ powered vehicles at an economic disadvantage compared to gasoline (~\$3/gal) for the general public due to lower durability, higher vehicle costs, and safety concerns.

Although production of H₂ through biomass gasification has been shown to cost as little as \$2.00/gge,¹⁷ the gasification process requires both intensive energy input and heavy capital. As a path to valuable chemical product, gasification would be a reasonable strategy because its large energy demand does not contradict with the goal. However, production of fuel in an energy intensive environment would be counterintuitive (with the exception of making rocket fuel or military jet fuel). Therefore, even if the government would subsidize construction of H₂ fueling stations and advanced H₂ storing and fuel cell technology, the H₂ fuelling option cannot be considered as carbon free technology, unless H₂ comes from water electrolysis and every stage of the process, from production to distribution, is powered by renewable electricity.

Hydrogen has the highest specific energy of any chemical energy storage medium,¹⁹ though that is still several orders of magnitude lower than uranium-235 nuclear fission reaction, which has a specific energy of $6.73 \times 10^7 \text{ MJ kg}^{-1}$.²⁰ It must be noted, however, that the number does not include the weight of the nuclear plant, and various safety structures associated with it. While nuclear power plant construction is becoming more of a common practice, nuclear power as a transportation fuel is impossible because of the mass of the energy extraction system (with the exception of large scale military vessels). Along the same time, hydrogen fuel also requires heavy gas tanks, compression pumps, cryogenic system for storage. When these weights were included in the specific energy calculation, the effective specific energy value is lower. Hydrocarbon fuel (gasoline), on the other hand, bypasses the necessity of heavy tanks, because it exists naturally in liquid form under ambient conditions; gasoline storage requires much less attention than that of hydrogen. Their safety, established practice, chemical stability and high specific energy make hydrocarbons still the ideal choice of energy carrier in today's and tomorrow's markets.

1.4 The Biofuel: E85

The most popular and developed alternative fuel today is 85% ethanol (E85), which is a blend of 85% denatured ethanol and 15% gasoline by volume. To date, E85 is viewed as a promising renewable energy candidate. Like gasoline, E85 is a stable liquid and as such requires no major modification to the current fueling infrastructure. It is a blend of gasoline with ethanol produced from corn starch. In other words, this strategy opens a route to turn CO₂ and sunlight into mobile carbon fuel. Production of ethanol starts with mixing ground corn kernel or other starch rich component with water and enzymes. The starch is converted enzymatically into glucose for fermentation, and the fermenting processing typically takes 40 – 50 hours. The

resulting ethanol is dehydrated, by distillation (an energy intensive process in its own right) denatured, and then blended with gasoline.²¹

E85 was proposed as a means to alleviate the US dependence on foreign crude oil imports and to reduce greenhouse gas emissions. E85 compatible vehicles, aka flexible fuel vehicles (FFV), require only little modifications to their engine and fuel systems, and hence do not pose significant production costs to consumers.

In sum, E85 establishes a connection between biomass and carbon fuel, avoids the safety concerns posed by H₂ fuel, and most importantly requires only modest effort to implement within the current transportation infrastructure. All these positive qualities explain why E85 quickly became the first national renewable fuel option, making its appearance in many local gasoline stations. Of the 121,446 gas stations in the nation, 2400 of them offer E85 refueling.⁵ Although that is merely a 2% coverage, it is nonetheless a good start toward widely available renewable carbon-based biofuel.

As wonderful as the E85 scheme sounds, there are several problems associated with the E85 productions. First of all, Atmospheric simulation studies have shown that use of E85 actually makes no improvement to emissions of CO₂ or to tropospheric formation of NO_x and ozone. In fact, NO_x increased in the Midwest and Southeastern region as a result of rising biogenic emissions from increased corn acreage.²² Moreover, detailed environmental studies reveal that increasing production of E85 may cause increases in CO₂ emission over conventional gasoline when other factors were considered. Second, production of fertilizer and pesticides, and fueling of tractors actually boosted the energy consumption in the big picture. Furthermore, boosting corn farming to match fuel demand has led to undesired environmental effects. Increased water usage, smog formation and land use are all negative impacts due to expanded

corn cultivation, and hence disfavor corn ethanol production.²³ Third, nitrogen rich fertilizers, and pesticides themselves, require energy to synthesize and are potential pollutants to the ecosystem upon disposal.^{24, 25} Fourth, Although the US currently has no shortage in food supply, increased use of food materials for fuel production may eventually lead to an increase in food prices due to land displacement.^{26, 27} Most importantly, E85 only slightly reduces the usage of fossil petroleum and is not a permanent solution to the energy problem. Efforts today should be devoted to seeking long term solutions that are environmentally friendly, sustainable, and can address the scale of the US's liquid fuel economies.

1.5 Biofuel production via Fischer-Tropsch Process

Aside from glucose fermentation, a long studied catalytic process known as the Fischer-Tropsch process (FT) is another approach to fuel production. It was invented by Franz Fischer and Hans Tropsch in Germany 1925 as a strategy to convert other forms of carbon resources such as natural gas, coal, or biomass into liquid hydrocarbons for production of long chain oil lubricants and synthetic fuels. Depending on the target products, FT processes and conditions can vary vastly, but the overall process can be broken down into three stages: synthesis gas (syngas) generation, FT synthesis of hydrocarbons from syngas, and FT product refining. Biomass gasification via FT process has been considered as one of the most attractive routes towards fuels and chemicals production.

Syngas is essentially a 1:2 mixture of carbon monoxide and hydrogen, which are chemicals of high reducing power. The production of syngas starts with gasification of biomass or other carbon feedstock in the temperature range of 900 – 1600 °C. Gasified carbon feedstocks become syngas, which occasionally includes some fully oxidized species such as carbon dioxide (CO₂) and water (H₂O). This mixture can be refined downstream via the water gas shift

equilibrium ($\text{CO} + \text{H}_2\text{O} \leftrightarrow \text{CO}_2 + \text{H}_2$). The resulting mixture of gases is then purified of contaminants such as H_2S and NH_3 which may be present if the feedstock contained nitrogen or sulfur.

The purified syngas can then be converted to a variety of hydrocarbon products: $n\text{CO} + (2n+1)\text{H}_2 \rightarrow \text{C}_n\text{H}_{2n+2} + n\text{H}_2\text{O}$, where $\text{C}_n\text{H}_{2n+2}$ represents any hydrocarbon product desired. Among many conditions criteria, temperature plays the most important role in dictating the growth of the hydrocarbon product. The high temperature Fischer-Tropsch (HTFT) reaction, typically operating at 340°C , tends to favor production of relatively short chain hydrocarbons $\text{C}_1\text{-C}_{30}$ that consist mostly of alkenes along with some alkanes and aromatics²⁸. On the other hand, the low temperature Fischer-Tropsch (LTFT) reaction, typically around $220 - 240^\circ\text{C}$, favors long chain hydrocarbon formation, $\text{C}_1\text{-C}_{120}$, producing waxes and saturated alkanes along with some alkenes.^{29, 30} The flexibility of FT synthesis enables production of various organic chemicals from virtually any common carbon feedstock. In the context of renewable fuels as the target, ideally non-food-grade biomass would serve as feed.

Hydrocarbon synthesis, particularly diesel fuel production, using biomass gasification has been an attractive strategy in the recent years. The sulfur free and low nitrogen nature of biomass makes it a better candidate than coal in the gasification process. Syngas ($\text{CO}:\text{H}_2$ in ratio of 1:2) conversion yields $\text{CO} + 2\text{H}_2 \rightleftharpoons (-\text{CH}_2-) + \text{H}_2\text{O}$. Production of $(-\text{CH}_2-)$ creates building block for hydrocarbon production.^{31, 32} However, gasification of biomass, which has a general formula of “ $-\text{CH}_2\text{O}-$ ”, yields a syngas ratio of $\text{CO}:\text{H}_2$ of 1:1. As a result, CO_2 will be generated as a result of hydrogen production. via the water gas shift $6\text{CO} + 6\text{H}_2 + 2\text{H}_2\text{O} \leftrightarrow 4\text{CO} + 8\text{H}_2 + 2\text{CO}_2 \leftrightarrow 4\text{H}_2\text{O} + 2\text{CO}_2 + 4(-\text{CH}_2-)$ To avoid wasting carbon as CO_2 in the product, addition of H_2 is required. As discussed before, today’s H_2 supply principally comes from reforming methane in

steam, or high cost water electrolysis. The addition of H₂ towards fuel production limits the sustainability of FT synthesis using biomass.

Moreover, FT plants come with high capital and operating energy costs. This is because the actual chemical process is rather complex and energy demanding. These difficulties and costs explain why common commodities today are still produced from refining petroleum. Nonetheless, there are circumstances when a FT plant is favored over a petroleum refinery. For example, when crude oil supplies are distant or unstable, or transportation of petroleum feedstocks is economically impractical, the FT process can be useful in the sense that it can condense low energy density feedstocks into higher energy value products, which lowers the cost for the chemical transportation. Of the several stages of the mentioned FT process, the gasification utility poses the most significant cost and has the greatest energy demand. While FT could serve as a flexible hydrocarbon production platform, the energy input and inefficient carbon utilization (water gas shift equilibrium produces CO₂ when the syngas ratio is CO: H₂ 1:1) may exceed the value of products formed, and hence it is less attractive as a strategy for the renewable fuel chemist. Nonetheless, addition of H₂ from water splitting could represent a strategy to maximize carbon utilization and raise its energy content. However, that would be a different subject matter.

1.6 CO₂ Recycling and Carbon Capture & Storage (CCS)

Replacing fossil fuel with bio-fuel can reduce the atmospheric CO₂ because biomass is considered as a carbon neutral fuel, a source that does not put fossil carbon into the current atmosphere. In principle, the emitted CO₂ from coal plant can be collected and stored in pressurized vessels underground. The stored CO₂ could potentially be recycled to chemicals or fuels using electrochemistry.

Electrocatalytic hydrogenation of carbon dioxide (CO₂) to chemicals and fuels is one of the current biggest areas of research. It aims to fix CO₂ in the form of methanol or related mono carbon substrates. Electricity captured from renewable sources such as solar, wind, hydroelectric and geothermal could be used for the formation of carbon hydrogen bonds. In other words, CO₂, a greenhouse gas, could be recycled into an energy rich chemically valuable resource through storing captured renewable energy. These efforts could be fruitful in reducing global warming if CO₂ could be captured and effectively recycled.

Electrocatalytic Hydrogenation of CO₂ was first reported in the beginning of the 19th century, when a zinc cathode was used to reduce (hydrogenate) CO₂ to formate (HCOO⁻) in an aqueous environment. Today, hydrogenation of CO₂ has been explored to a great extent both homogeneously and heterogeneously.³³ In general, the reaction is done in a neutral to basic environment in which CO₂ is solubilized as carbonate (CO₃²⁻).³⁴ Mechanistic insights into CO₂ reduction have been reported in many review articles or book chapters.³⁵ Product selectivity seems to be dependent on choice of electrolyte and electrode. In general, inorganic electrolytes seem to afford formate (HCO₂⁻) as the sole product while organic electrolytes, e.g. tetraalkylammonium salts, favor formation of a series of organic products, such as formate (HCO₂⁻), glycolate (HOCH₂COO⁻), malate (C(O)CH₂CHOHC(O)O)²⁻, oxalic ((OC(O)C(O)O)²⁻), and other carboxylic acids.³⁶⁻³⁸ Other reviews noted that the coinage metals, gold, silver, and zinc yield mostly CO as the major product while indium, lead, tin and cadmium yield mostly formate as the major products with the condition unspecified. Recently, interest has begun to shift towards the use of copper, an abundant and environmentally friendly metal, showing formation of a variety of hydrocarbon products depending on applied potential.³⁹⁻⁴¹ Although research on

CO₂ hydrogenation has taken off and began to demonstrate promising results (CO is a valuable chemical), there are yet any effective scheme in recapturing atmospheric CO₂.

Some newly built coal plants are designed with carbon capture and storage (CCS) features. CCS concentrates the CO₂ released from fuel combustion, and stores it deep underground.⁴² A CCS power plant is estimated to release 88% less CO₂ into the atmosphere.⁴³ However, CCS is not a sustainable option to address the energy problem. First of all, CCS power plants are still burning fossil coal to generate electricity; CO₂ recapture may be carbon neutral in terms of the atmosphere, but it is no solution to the greenhouse effect. Moreover, gas collection and compression takes 10 – 40% extra energy from the power plants.⁴⁴ Manufacture of CO₂ capturing chemicals such amine, ammonia, or amino salt for CO₂ recapture is also an energy investment.⁴⁵

In a CCS scheme, CO₂ generated from fossil fuel combustion is pumped and sealed deep underground permanently. Even if, hypothetically, the stored CO₂ can be retrieved and recycled to CO electrocatalytically, hydrogen is still required to mix with CO for fuel production. In summary, CO₂ hydrogenation is a promising technology that is crucial for greenhouse gas reduction in the future. However, it is not a practical solution for fuel production today because a) mono-carbon species carry too little energy as fuel, and b) fuel production using CO generated from biomass gasification requires addition of H₂ to become effective synthesis gas. In theory, CO₂ could be reduced to methanol (CH₃OH) to power methanol fuel cell device. However, the specific energy of methanol is much smaller than that of hydrogen or hydrocarbons. Methanol is also much more chemically aggressive towards polymer based container and is lesser likely fit the current transportation infrastructure.

In summary, CO₂ recycling to fuel and chemicals is a potentially wonderful technology. But CCS is flawed; even if the underground CO₂ can be retrieved and reduced to CO, it will require addition of H₂ for hydrocarbon production. Most important, CCS is not a sustainable option, it merely reduces the net CO₂ output to the atmosphere while consuming an ever depleting fossil. A low cost renewable carbon based strategy that can be implemented easily within the current infrastructure. If the cost is too high, it will lack the economic driving force to displace fossil fuel. This fuel must be carbon based so that it can be implanted to the current system without major modification, similar to E85. The fuel must be free from using any fossil related products for its processing. For this, the project seeks biomass to be the optimized candidate towards renewable fuel production.

1.7 Biomass as a Renewable Energy Feedstock

1.7.1 The Need of Renewable Energy

As of 2012, the US continue to be the world greatest oil consumer, consuming 18.49 million barrels of oils daily.⁴⁶ Although the consumption has declined slightly from 19.18 million barrel/day since 2010 owing partly to improved gas mileage in modern engine design⁴⁷ and partly to less use of liquid fuels in fixed settings (natural gas boom), the US is still leading by far compared to the 2nd runner, China, where 10.3 million barrels of oil are consumed daily. Moreover, over half of the oil supply is dependent on foreign regions; as such the US should find a renewable domestic source of fuels to secure its energy supply and independence.⁴⁸ Even more important, ongoing combustion of fossil carbon-based fuels continues to raise atmospheric CO₂ concentrations, causing ever-increasing greenhouse warming and ocean acidification with the attendant drastic shifts in the earth's global climate, sea levels, and biosphere.⁴⁹ In January 2014, the atmospheric CO₂ concentration, corrected for seasonal fluctuation, at Mauna Loa was 397.80

ppm.⁵⁰ a 24.4% increase compared to 50 years ago (Jan. 1964. 319.67ppm); transportation fuels contribute roughly 1/3 of this excess CO₂ load.⁵¹ Meanwhile, individual vehicle use is ever growing in the United States.⁵² Ultimately, if humans are to continue enjoying the quality of life we have built on a hydrocarbon foundation, future supplies of these critical substances must come from renewable, carbon-neutral (or preferably carbon-negative) sources.

As of 2011, US petroleum use is roughly a 9.6×10^{11} kg of petroleum per year, almost all for fuels. Estimates for annual potential production by 2030 of non-food biomass are very optimistically 1.4×10^{12} kg.⁵³ But the carbon and energy contents of these starting materials are vastly different, as shown in data from the US Energy Information Agency (EIA) and the US Department of Energy’s (DOE) office of Energy Efficiency and Renewable Energy, presented in Figure 1-3 below:

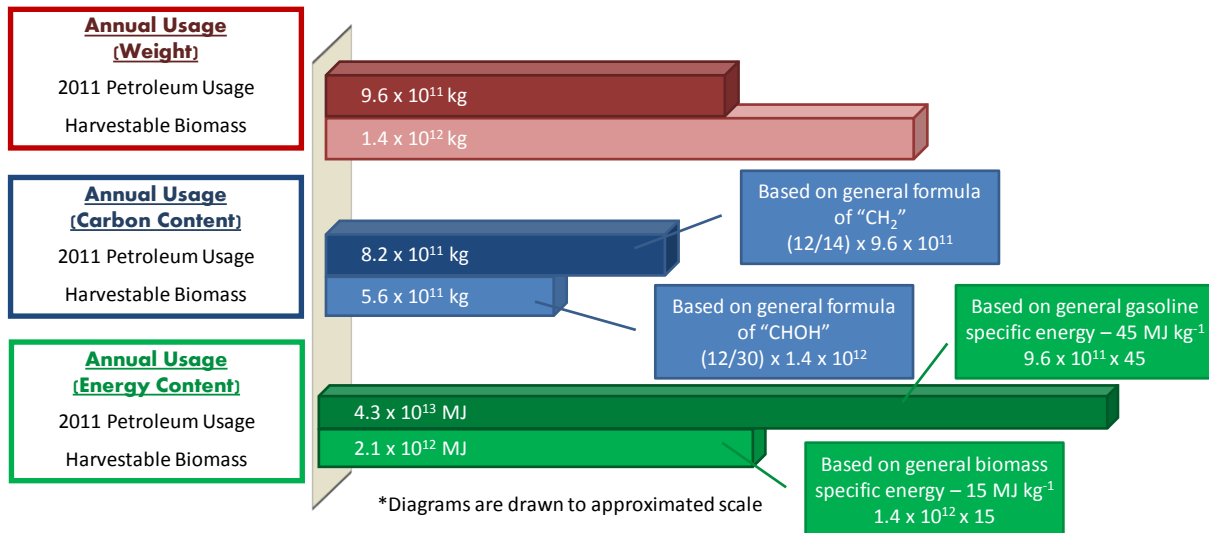


Figure 1-3: Comparison of the overall carbon and energy balance in the US transportation sector and harvestable biomass. Red bars compare the weight of the petroleum used, and the weight of the harvestable biomass. Blue bars compare the actual carbon content. Green bars compare the energy spent annual, and the harvestable amount of energy from biomass. Projections are made based on the available biomass by 2030.

In the US, there is neither enough carbon nor enough energy in the most optimistically projected biomass supply to match the amounts in the petroleum used. The scenario is even less optimistic when coal and natural gas are considered. Both biological and thermochemical processes to convert biomass to desirable fuels have seen impressive advances in recent years, yet most of these biofuel strategies simply extract the small energy content of biomass as fuel, and discard the remaining carbon, usually as CO₂.

1.7.2 Common Pathway for Biomass to Biofuels

Method	General Descriptive Chemical Equations	Carbon Loss
Fermentation	$\text{C}_6\text{H}_{12}\text{O}_6 \xrightarrow{\text{Ferment}} 2 \text{CH}_3\text{CH}_2\text{OH} + 2 \text{CO}_2$	33%
Gasification (F-T Process)	$\text{C}_6\text{H}_{12}\text{O}_6 \xrightarrow{900 - 1600 \text{ }^\circ\text{C}} 6 \text{CO} + 6 \text{H}_2 \xrightarrow[\text{Water Gas Shift Equilibrium}]{+ 2\text{H}_2\text{O}} 4 \text{CO} + 8 \text{H}_2 + 2 \text{CO}_2$ $4 \text{H}_2\text{O} + 2 \text{CO}_2 + 4 \text{ "CH}_2\text{ " } \xleftarrow{\text{F-T Process}}$	33%
Fast-Pyrolysis	$\text{C}_6\text{H}_{12}\text{O}_6 \xrightarrow{\text{Fast Pyrolysis}} \text{C}_6\text{H}_{10}\text{O}_5 + \text{H}_2\text{O} \xrightarrow{6 \text{ H}_2} \text{C}_6\text{H}_{12} + 5 \text{H}_2\text{O}$ <p style="text-align: center; margin-left: 100px;">"Bio-oil"</p>	0%

Scheme 1-1: General descriptive chemical equation describes common biomass to biofuel processing pathways. Fermentation and Gasification both disposes 33% of the carbon content as CO₂ while fast-pyrolysis retains most carbon in the form of bio-oil: 70% bio-oil, 15% bio-char, and 15% gas.

Both gasification and pyrolysis could in principle capture all the input carbon as fuel, if H₂ were freely available. But current production of H₂ comes from reforming natural gas (methane) with CO₂ as a byproduct. So despite its lack of carbon, H₂ is a fossil fuel product in today's market; its use as primary reductant in the field would bring extra costs in complexity, energy, and fossil carbon. Of course, hydrogen can be produced by electrolysis of water, and a large amount of effort has been put into development of water splitting catalysts. An optimistic estimation, based on today's electricity cost from burning cheap coal, of H₂ production will be still at the high end of the overall candidates (\$6.75/kg) – 4.5 times more expensive than methane

reforming (\$1.47/kg).⁵⁴ The associated high cost of H₂ production from water electrolysis would substantially increase the cost of fuel production. If these productions were carried out with renewable electricity, the fuel prices will increase dramatically.

In summary, any renewable fuel scheme that uses gaseous hydrogen as a reductant or that releases CO₂ during its process is flawed as a long term solution towards creating a sustainable carbon fuel cycle. A new approach is necessary to address all the mentioned challenges. This renewable fuel must be able to fit into the current fueling structure, have must a high specific energy, and must be independent from fossil carbon. Hence, this project seeks an innovative strategy to produce a carbon-based fuel using the renewable carbon from biomass, via the unprecedented combination of fast-pyrolysis and electrocatalytic upgrading.

1.7.3 Biomass as Feedstock

Any strategy for direct biomass-to-fuels conversion is fundamentally a solar energy capture scheme. Plants, natural CO₂ collectors designed by evolution, are the cheapest carbon collectors available. However, while excellent at fixing carbon, plants are inefficient at capturing the sun's energy and storing it in chemical form. With the sun rising every day, they have no evolutionary driving force to store more energy than they need for growth. Most plants in nature has a photosynthetic efficiency ranged 1 – 2%; the other 98% energy is lost to optimal wavelength mismatch, respiration, reflection and transmission.^{55, 56} Furthermore, biomass has only about one third of the specific energy of gasoline as mentioned above; therefore, unmodified plant matter is energetically unsuitable as transportation fuel.

Human technologies can capture solar energy much more efficiently than plants, but they do so in the form of electricity. Commercially available lower-end solar voltaic cells, mostly made of single crystalline silicon, have an energy efficiency of 12 – 15%.⁵⁷ In other words, even

the oldest form of photovoltaic device on the market still captures solar energy at least ten times more efficiently than plants. It is a national goal to replace as much fossil (petroleum oil) with biological carbon in liquid fuels as possible. If solar electricity could be used to raise the energy content of biomass, the limiting quantity would become the content of carbon rather than energy, enabling higher yields of biomass-derived fuels. Furthermore, due to a mismatch between the times of human power demand and the cycles of light and wind availability, electric power generating capacity may go unused at some times, so an alternative, time-insensitive method of using and storing alternative energy is sorely needed.

1.7.4 Biomass Fast Pyrolysis (BFP)

Biomass Fast Pyrolysis is one of the most popular strategies in biomass liquefaction. It heats up biomass rapidly to 400 – 600 °C for a few seconds in the absence of oxygen and causes it to “melt”.⁵⁸ The resulting products can be categorized based on their physical states: gas, which can be used as a fuel for the pyrolyzer; liquid, also known as “bio-oil” that consists of hundreds of different small organic compounds to be discussed in detail in the next section; and solid “bio-char” which is used primarily as a soil amendment for plant cultivation.

BFP may seem simple – it is not. It is a complex physical and chemical process that transforms solid matter under rapidly changing temperature. Various factors such as feedstock powder size, feed rate, temperature program and heat transfer mechanisms, vessel pressure, and residence time can control the quality and quantity of bio-oil⁵⁸⁻⁶⁶ which is the key ingredient in biofuel production. This research focuses on upgrading of bio-oil to bio-fuel and hence BFP will only be discussed at an introductory level in this chapter.

Biomass must first be dried and ground prior to feeding to the pyrolyzer. Drying minimizes water input to the system, which reduces the amount of water in the product bio-oil.

Small particle size of the ground biomass ensures the uniformity of heat transfer to maximize bio-oil production. In general, the particle size can range from less than 1 – 6 mm.⁶¹ The optimal biomass particle size depends on the type of reactor, feedstock, and feed rate. Different feedstocks require different temperature programs to decompose properly. For instances, hemicellulose and cellulose decompose in a fairly narrow temperature range compared to lignin, which degrades slowly over a wider temperature range. The ratio of cellulose to lignin varies among plants, and hence there is no one single best universal setting for bio-oil production. In general, maximum bio-oil product yield is obtained in the range 500 – 520 °C with less than a 2 second residence times.^{58, 66} Prolonged residence times trigger secondary reactions, in which dehydration of oxygenated organics occurs and leads to char formation, thus decreasing the bio-oil yield.

1.7.5 Nature of Bio-oil

Compared to crude oil, bio-oil is a dark syrupy emulsion comprising many low carbon number organics and water. It cannot be used directly as transportation fuel without pre-treatment for several reasons, most important of which is its low energy density. Like biomass, bio-oil has ca. 1/3 the energy content of hydrocarbons (ca. 15 vs. ca. 45 MJ/kg). In addition, bio-oil is highly acidic and contains many oxygenated organics. In fact, almost 20% of bio-oil is comprised of compounds like acetic acid, hydroxyacetaldehyde, hydroxyacetone, furfurals, levoglucosan (derived from sugars), and a variety of lignin-derived aromatics.⁶⁶ A general chemical distribution of bio-oil⁶⁷⁻⁷⁰ is depicted in Figure 1-4. This mixture corrodes steel storage and pipes aggressively, especially at elevated temperature.⁷¹ Furthermore, the reactivity and viscosity of bio-oil are both high; bio-oil tends to polymerize via acid-catalyzed condensation of its high content of reactive oxygenates such as aldehydes and ketones and phenols. Lastly, bio-

oil has a high water contents. Bio-oil is an emulsion, consisting of liquid phase organic compounds and water. All of the above properties make it incompatible with storage and transport over extended periods. Table 1-1 shows a composition comparison between bio-oil and crude oil.⁶³

Table 1-1: Composition comparison between bio-oil and crude oil are shown. Note: actual composition of bio-oil varies depending on the biomass feedstock.

Characteristics?	Bio-oil	Crude Oil
Moisture wt%	15-30	0.1
pH	2.5	-
Specific gravity	1.2	0.82 – 0.875
Element composition wt%		
Carbon	39.5-55.8	85.2
Hydrogen	6.1-7.5	11
Oxygen	37.9-52.6	1.0
Nitrogen	<1	0.3
Specific Energy MJ/Kg	18 - 22	43 – 46

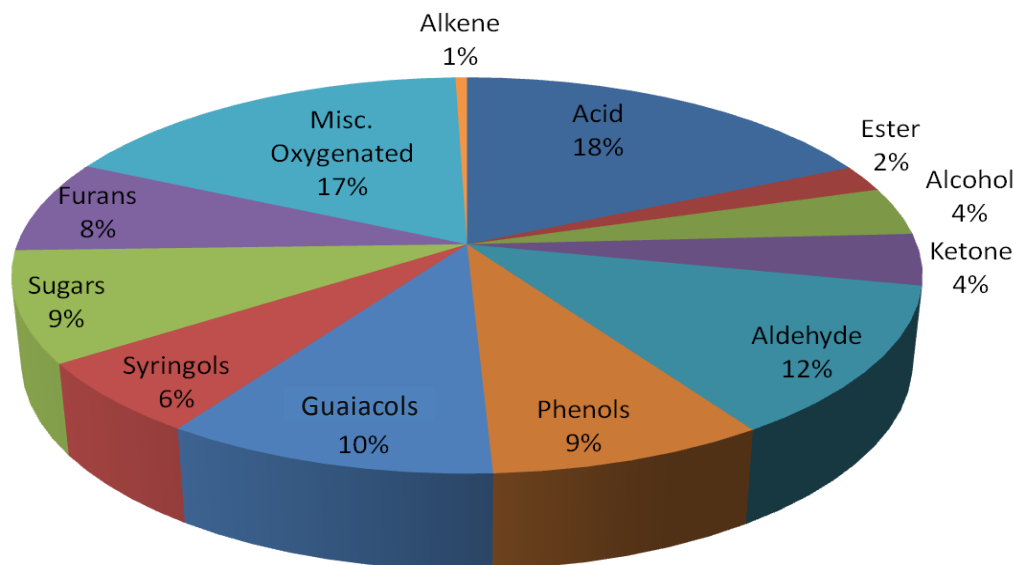
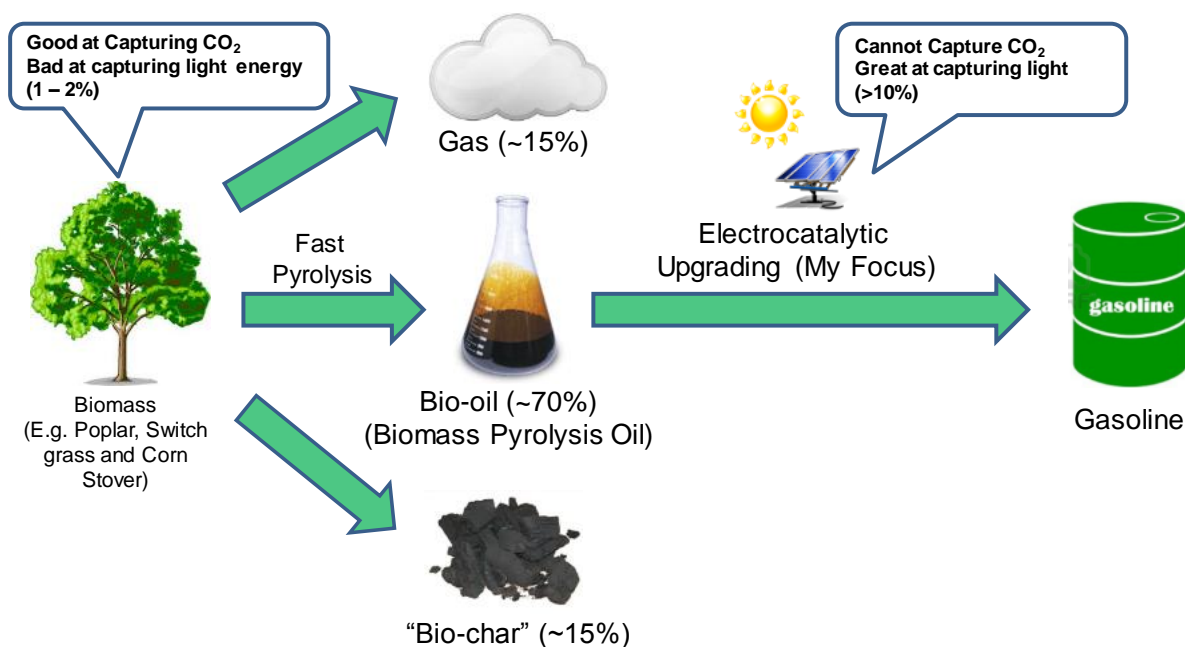


Figure 1-4: General chemical distribution of organic substrates found in bio-oil. Percentage is given percent of mass.

Bio-oil must be pretreated for stabilization before it can even be considered as a crude fuel because of its reactivity and aggressive character. The primary key to effective stabilization is the reduction of the carbonyl moieties of the ketone and aldehyde functional groups, and acid neutralization. Ideally, such reductions would occur immediately downstream of the pyrolysis process. The stabilized material could then be further upgraded and refined, or transported to a central facility such as a petroleum refinery for classical upgrading by hydrotreating, a process that upgrades the energy value and stability of bio-oil using hydrogen. However, as noted earlier, the current supply of hydrogen comes from steam reforming of methane, and thus it is a non-renewable fossil-based product. Moreover, even if water electrolysis becomes cost feasible for H₂ production, the need for a storage system for H₂ would pose an economic barrier towards bio-oil upgrading. However, it is worth noting that substantial work has gone into direct petroleum style upgrading of bio-oil with H₂, and more detail will be discussed in detail in Chapter 2.

Fortunately, electrocatalytic hydrogenation (ECH) upgrading bypasses both issues. It achieves hydro-upgrading of organic compound without an explicit H₂ gas supply. H₂ (or more precisely a supply of H-atom) is generated on the surface a catalytic electrode that can be used to hydrogenate organic substrates adsorbed from solution. The details of ECH will be discussed in the next chapter. In short, ECH can serve as a relatively energy feasible alternative to chemical H₂ hydrogenation. With this in mind, the overall scheme of this research project, biomass to biofuel production through BFP and ECH, is depicted in Scheme 1-2.



Scheme 1-2: Overall scheme of the research project: a maximum carbon retention strategy to produce renewable carbon fuel through biomass pyrolysis, followed by electrocatalytic upgrading that is powered by renewable electricity.

1.7.6 Bio-oil Upgrading via ECH

For fuel upgrading purposes, ECH could be the ideal route because it operates at mild conditions below the electrolyte's boiling temperature (typically water), while at the same time it avoids the storage and use of H₂ gas. By reducing the carbon-oxygen and carbon-carbon double bonds of the organic compounds in bio-oil, it is possible to eliminate carbonyl condensation

processes that lead to a polymerization to form tars. Also, hydrogenation incorporates the additional heat of combustion of H₂ into the reduced species as shown in Figure 1-5.

Bio-oil also contains many oxygenated aromatic compounds. Hydrogenation of such electron-rich aromatic compounds in general is difficult due to their aromatic stability. However, under favorable pH and surfactant conditions, efficient ECH results can be achieved.⁷² The design and investigation of an efficient ECH system is one of the major goals of this research project.

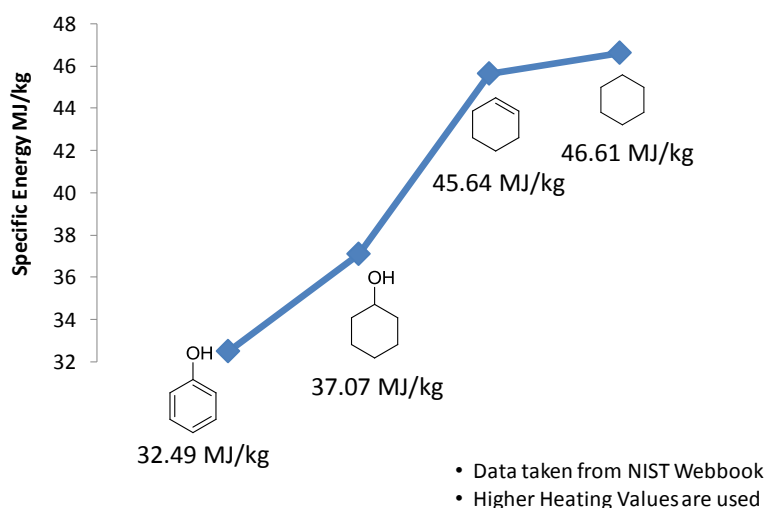


Figure 1-5: Phenol is used as a model compound to illustrate the increases in specific energy (MJ kg⁻¹) upon hydrogenation and deoxygenation. Note: higher heating values mean the heat of combustion is calculated with the heat of formation of water in liquid state, which is lower in energy compared to gaseous state, and thus gives a greater value of heat of combustion (heating values).

It is noticeable in Figure 1-5 that the specific energy increases substantially between cyclohexanol (37.07 MJ/kg) and cyclohexane (46.61 MJ/kg) by replacing an –OH with –H. This is because the weight of oxygen (15.999 g/mol) is 16 times heavier than hydrogen (1.008 g/mol), and the presence of oxygen decreases the value of the heat of combustion, and thus decreases the energy per unit weight. In terms of fuel mass, oxygen is considered as a free supply from the air

in the heat of combustion equation, so its mass is not counted in the specific energy calculation. This explains the importance of bio-oil hydrogenation and hydrogenolysis; not only does it incorporate the heating value of H₂ into the liquid, but it can also potentially achieve deoxygenation to increase the specific energy of the compound.

Conventional hydrogen upgrading is done in an industrial style where a reactant is subjected to high pressure and high heat environment. These conditions require heavy energy input, counter to the purposes of renewable fuel production. ECH avoids the use of H₂ gas, operates at relatively mild conditions, and most important of all, it incorporates the renewable energy captured from solar, wind, and geothermal electricity, into the bio-oil to raise its energy content. In other words, bio-oil is acting like a “battery” to store energy captured from renewable sources.

1.8 Chapter Summary

Several alternative energy schemes such as electric/hybrid vehicles, hydrogen fuel, E85 fuel, FT biomass gasification, CO₂ capture and storage, and bio-oil have been surveyed in this chapter. Their pros and cons have been evaluated from the stand point of sustainability, cost, environmental impact, and infrastructure compatibility.

Hybrid vehicles are becoming more popular for their high gas mileage and successful integration into the current fuelling system, but they suffer from high production costs and they still use petroleum fuel as their major fuel source. Electric cars and hydrogen fueled vehicles, on the other hand, have the potential to run on fossil free energy, but they suffer from both high production costs and a lack of fueling stops. Also, current electricity supplies come from coal or natural gas combustion, and hydrogen is generated from methane steam reforming. So even though these vehicles provide a means to alleviate local gasoline consumption and CO₂ emission,

they remain dependent on burning fossil carbon and so are not the ultimate solution to the fuel problem. Also, H₂ gas raises significant safety concerns for drivers.

Current strategies for biomass-derived fuel also have limitations; although E85 is making its way to be the first available renewable fuel nation-wide, in-depth analyses have revealed that an increase in ethanol production from corn starch poses a greater environmental burden to local farming than petroleum refining. The FT process enables production of a great variety of hydrocarbon products from virtually any carbon feedstock including biomass. However, FT plants are both energy demanding capital cost intensive. Also, like E85, FT throws away about 33% of the carbon as CO₂ during the water gas shift equilibrium stage because of the wrong CO:H₂ ratio. Although CO₂ recycling has been explored as an option towards renewable fuel production, it is still far from practical to be able to create a sustainable fuel cycle to support the U.S. transportation sector.

Continued use of fossil coal via CCS is by no means a renewable energy strategy; it merely puts the released CO₂ back underground at the expense of greater energy consumption. In a way, CCS may speed up fossil reserve depletion while causing just as much negative impact on the environment because of chemical production for CO₂ recapture. Land drilling and sites construction requires careful selection around the shore area and close enough to the CO₂ emission locations to minimize transportation costs. Ultimately, the multiple factors adds up making it a challenge option to execute.

Hydrogen fueled vehicle is relatively more promising in creating a sustainable cycle compared to other mentioned candidate. However, the high cost associated with water splitting and gas storage makes it less favorable to the transportation system. Steam methane reforming for hydrogen production is not a sustainable strategy. In terms of safety, hydrogen is a highly

explosive gas combining with oxygen. This put a greater safety and psychological burden to the drivers . Hydrogen fuel cell has a shorter life time compared to gasoline engine, and the operating efficiency fluctuates with the real world environment – carbon fuel is still a better option even with its low specific energy that is only 1/3 of hydrogen.

Making hydrocarbon from FT synthesis using biomass as a feedstock seemed like an attractive option, but the energy investment and the capital cost of a FT plant is too high to be economically feasible for fuel production (chemicals would be fine). Gasification of biomass requires high energy input, and worse, the produced bio-syngas ratio will require addition of H₂ to prevent CO₂ formation during the water-gas shift equilibrium. Although the CO₂ release from bio-syngas WGSE does not consider as carbon positive to the atmosphere, throwing away value biomass carbon that was insufficient in the first place is problematic in the bigger picture.

BFP can produce liquid fuel through liquefaction of biomass. Biomass is heated rapidly in an oxygen-free environment to produce an emulsive liquid called bio-oil. The highly oxygenated bio-oil can be upgraded to gasoline through catalytic hydrogenation and hydrogenolysis (discussed in Chapter 2) and be directly substituted into the current fueling infrastructure. Although only 70% of the carbon of biomass will end up in bio-oil, the other 30% (15% gas + 15% bio-char) can be used for process heat to the reactor or for soil amendment, which will be recycled into biomass carbon again. This is the only option that can effectively produce a carbon fuel without heavy involvement of fossil energy.

1.8.1 Summary Table of the Discussed Alternative Fuel Candidates

The overall argument of how biomass can be favored over other alternative energy is summarized in Table 1-2 below:

Table 1-2: Summary of each discussed alternative energy candidate. 5 major factors: adaption to the current fueling structure, relationship to fossil energy, Cost to consumers, sustainability, and the environmental impacts are explored.

Hybrid Vehicle

Adaptation to the current fueling structure	Highly adaptable to the current fueling system as they are run on gasoline. (121,446 gasoline stations in the US as of March 2014)
Relationship to fossil energy	Gasoline production comes from refining petroleum, a form of fossil fuel
Cost to consumer	Hybrid vehicles are more expensive than non-hybrid vehicles, although tax credits are given towards hybrid vehicle purchase, they are still cost typically \$10K - 20K more.
Sustainability	Although hybrid vehicles have better gas mileage, it is not a sustainable option because fossil fuel is a finite resource.
Environmental Impact	Gasoline from fossil sources will continue to release fossil carbon into the atmosphere, though the rate of CO ₂ will reduced as a result of the hybrid technologies

E85 Fuel

Adaptation to the current fueling structure	Around 2400 gasoline stations offer E85 fueling option ⁵ , a 2% coverage of the current gasoline stations
Relationship to fossil energy	Only 85% of the fuel is ethanol from corn starch fermentation. The other 15% is gasoline from fossil fuel
Cost to consumer	E85 in general costs \$0.6 – 0.7 less per gallon of gasoline. E85 fuel only requires minor engine modification (flex fuel engine) and so poses no significant financial burden to consumers. However, FFVs are 30% less efficient on ethanol and hence, lower fuel price still does not compensated for that.
Sustainability	Not a sustainable option because 15% of which is still gasoline that comes from petroleum refinery
Environmental Impact	Combustion of E85 release lesser greenhouse gas to the atmosphere. However, increases in agriculture land mining, production and use of fertilizer, fermentation processing have negative impact towards the environment in a overall picture

Electric Vehicle

Adaptation to the current fueling structure	Around 7700 charging stations available nationwide ⁵ - 6% of the current gasoline stations, however, home charging is also available for most models in the market.
Relationship to fossil energy	Current electricity comes from burning natural gas and coal, with minor supply from nuclear reactors and tiny fraction from renewable sources like solar and wind
Cost to consumer	Vehicles powered by electric motors in general are only slightly more expensive than those of gasoline engines. However, high end electric vehicles can cost more than 100k.
Sustainability	Potentially sustainable is in a distant future when electricity is generated from completely renewable sources.
Environmental Impact	Electric Vehicles themselves are emission free but the increase of electricity consumption will lead to greater coal or natural gas consumption meaning more CO ₂ release to the atmosphere. Greater demands on battery (E.g. lithium ions or Lead acid) and power plants have impacts on the environment

Table 1-2: (cont'd)

CO₂ Capture and Storage

Adaptation to the current fueling structure	Not applicable - CCS does not alter the current fueling infrastructure
Relationship to fossil energy	CCS requires more 10 - 40% more energy to transport and store the CO ₂ generated. ⁷³ Thus increases the consumption of coal. ⁴⁴
Cost to consumer	Although no literature found on how CCS plant would change the electricity price, it is reasonable to assume electricity price would go up as a result of the CCS recapture system construction.
Sustainability	CCS is not a sustainable option; it only reduces fossil carbon release into the atmosphere and makes fossil fuel more “environmentally friendly”.
Environmental Impact	CCS should have positive impact on the environment, but increase in chemical production for CO ₂ capturing, extra land use for CO ₂ storage site construction with deep drilling would all have a great negative impact on the environment.

Hydrogen Fuel Cell

Adaptation to the current fueling structure	Only 10 H ₂ fueling stations are available nationally ⁵ , 9 of them are in California, a 2% coverage of the current gasoline stations in that state.
Relationship to fossil energy	Current H ₂ supply comes from methane reforming, making H ₂ a non-renewable energy source.
Cost to consumer	\$3 - 4 /gge but projected to drop in the course of next decade. Hydrogen vehicle, however, in general costs around \$50K and the fuel cell unit has a lower lifetime (most recent reported ca. 75,000 miles) compared to internal combustion engine (typically around 150,000 miles)
Sustainability	Although current hydrogen supply comes from methane reformation, hydrogen in the future may come from water electrolysis powered by renewable electricity.
Environmental Impact	Hydrogen fuel probably has the least environmental impact in the pool of candidates – it releases water upon combustion. However, manufacture of fuel cell requires precious metals that would have negative environmental impact to the land mining.

Bio-Fuel via FT Process

Adaptation to the current fueling structure	FT produces conventional hydrocarbon fuel through biomass, and so it can benefit from the current fueling infrastructure
Relationship to fossil energy	This uses biomass as feedstock; however, the bio-syngas formed has a 1:1 ratio of CO: H ₂ which leads to formation of hydrocarbon and CO ₂ . Addition of another equivalent of H ₂ , produced from methane reforming or water electrolysis, is required to avoid CO ₂ formation
Cost to consumer	F-T produces hydrocarbon fuel that requires no modification on the vehicle. However, FT plants comes with a high capital cost, and hence may boost the fuel prices due to increase in cost production
Sustainability	As mentioned above, H ₂ is required to set the CO: H ₂ ratio right. Even if H ₂ can be made from water electrolysis via renewable electricity, the energy demand of gasification will most likely supplied by coal or natural gas burning
Environmental Impact	The increase in H ₂ demand will increase steam reforming thereby putting more CO ₂ into the atmosphere. Higher energy demand from the power plant may increase coal and natural gas consumption. Biomass are selected to no interfere with the current food supply.

Table 1-2: (cont'd)

Biomass Fast Pyrolysis (BFP)

Adaptation to the current fueling structure	BFP produces bio-oil that can be upgraded to bio-oil fuel for gasoline engine use, and so it benefits from the current fueling infrastructure.
Relationship to fossil energy	BFP liquefies biomass to bio-oil. However, energy for the fast pyrolysis is likely to come from power plants fueled by non-renewable sources. Depending on the upgrading scheme, the H ₂ needed for upgrading can either come from methane for catalytic hydrogenation or <i>in-situ</i> formation for electrocatalytic hydrogenation.
Cost to consumer	Product of upgraded bio-oil should function identically to gasoline fuel, and so does not require more financial investment.
Sustainability	Almost - projection of harvestable non-food grade biomass by 2030 cannot cover the fuel usage in the transportation sector for today.
Environmental Impact	Unlike E85, where corn is the sole crop plant for fuel production, BFP includes different biomass feedstocks. The multi-crop cultivation may cause lesser impact on the environment due to mono cultivation. Moreover, BFP doesn't throw away 33% of its carbon unlike ethanol production. 15% of the biomass will become bio-gases, and can be fed back to the pyrolyzer for further heating.

1.8.2 Goal of this Research Project

Of the options explored, bio-oil is the renewable fuel candidate that can maximize carbon utilization and potentially fit into the current fueling infrastructure after it is upgraded. Without needing to change the fueling infrastructure, bio-oil could be marketed nationally similar to the case of E85. The hydrocarbon nature of bio-oil allows consumers to continue to drive with a peace of mind just like driving with gasoline. Utilization of non-food grade biomass does not compete with the land for edible agriculture production, thus making bio-oil an economically favorable route on a grand scale.

However, as discussed before bio-oil only carries 1/3 of the energy content compared to gasoline. Bio-oil contains large amounts of water and polymerizable oxygenated organic compounds, making bio-oil incompatible with modern vehicle engines. Hence, bio-oil must be upgraded with a maximum carbon retention strategy to an energetically compatible and chemically stable fuel. Such upgrading ideally does not require energy intensive processes such as high heat or pressure or the use of H₂. Hence, this project seeks to develop an electrochemical hydrogenation method that would be an effective bio-oil upgrading strategy for renewable

carbon fuel production. The goal is a chemically and economically scalable electrocatalytic reactor system in which bio-oil can be hydrogenated in a continuous process with good current and energy efficiency. In the past, Lercher reported the use of Raney nickel catalyst to achieve Hydrodeoxygenation on common bio-oil aromatic compounds such as eugenol, guaiacol, syringol in a high H₂ pressure and high heat setting.^{74, 75} The ideal short term goal would be translate Lercher's chemistry from catalytic to electrocatalytic cost efficiently. Traditional ECH makes use of expensive catalysts such as platinum and ruthenium, which are fine for small scale chemical productions, but they are insufficient to address the scale of transportation fuel production. Hence, investigation on low cost catalytically active metals is the first stage of the project, and will be discussed in chapter 2 in detail. An ultimate ideal scenario would be for a farmer to make a bucket of bio-oil through the fast pyrolysis reactor, use the electrodes or reactor developed from this project to upgrade it to a fuel, an organic mixture that has the comparable specific heat to fossil transportation fuel, and finally, use it for her tractor using the electrodes or reactor developed from this project.

Hydrocarbon fuel is deeply rooted in today's society but it comes from a finite resource – fossil carbon compounds. An innovative strategy that does not disturb the current fueling infrastructure will be needed to replace fossil fuel with biomass for a sustainable future. Liquefaction of biomass to bio-oil has been shown to be a promising way to replace fossil hydrocarbon fuel. Unfortunately, bio-oil itself comes with low specific energy, and is not a good fuel. Moreover, bio-oil contains a large amount of acetic acid and oxygenated compounds which makes it highly unstable to store, and energetically incompatible as fuel. Hence, this project seeks an energetically feasible strategy that can utilize renewable electricity to stabilize and

upgrade bio-oil to usable fuel. The details of the upgrading strategy will be discussed in Chapter 2.

Chapter 2 Literature Review on Electrocatalytic Hydrogenation

2.1 Introduction

Due to Bio-oil's low stability, low energy content and highly oxygenated nature, it must be upgraded before it can be used as a transportation fuel. These negative properties can be circumvented by hydrodeoxygenation (HDO), in which bio-oil undergoes catalytic hydrogenation at high temperature (150 – 400 °C) and high pressure (~150 – 200 psi H₂). HDO can achieve deoxygenation by hydrogenating all possible carbonyl, alkene, and aromatic sites. The resulting increase in the hydrogen to carbon ratio effectively raises the specific energy of bio-oil (See Figure 1-5). The current HDO strategy is performed in the current petroleum refinery setting, so it does not require major infrastructure modifications and is thus economically appealing. Many bio-oil upgrading studies have shown promising results toward fuel production using petroleum upgrading catalysts such as cobalt or nickel molybdenum sulfur.

2.2 Catalytic Hydrogenation for Bio-oil Upgrading and its Concerns

In the petroleum refinery industry, many upgrading catalysts are designed to remove sulfur, a process known as hydrodesulfurization (HDS). Without HDS, fuel combustion emits sulfur dioxide (SO₂) leading unpleasant smell and to acid rain in the environment. Also, sulfur poisons noble metal catalysts such as platinum, and therefore reduces the life time of the catalytic convertors at the exhaust. The most commonly used catalysts for HDS are a cobalt molybdenum (Co-Mo) and a nickel molybdenum (Ni-Mo) alloy, both of which are available on different supporting materials such as aluminum oxide (Al₂O₃) and silicon dioxide (SiO₂).

Lifetimes of these catalysts and their catalytic functions have been studied extensively and reported in these selected reviews.⁷⁶⁻⁷⁹

Today, HDS is a well-established technology in every petroleum refinery site. Knowing oxygen and sulfur are both group VI elements and the promising future that bio-oil can offer in renewable fuel production, one might expect that petroleum HDS chemistry would be applicable for hydrodeoxygenation (HDO) of bio-oil. Hence, HDO on reactive bio-oil aromatic model compounds such as phenol, anisole, or guaiacol, using petroleum refinery catalysts has become a popular research area in recent years.^{74, 75, 80-88} The results of these studies support the possible transition from crude oil to bio-oil inside the current refinery infrastructure.

As discussed in the section on the hydrogen economy in chapter 1, the use of hydrogen in renewable fuel production is questionable because H₂ comes from methane, a fossil resource. Moreover, the intensive energy requirement for HDO would most likely be supplied from burning coal, which is the cheapest form of energy currently in the US. In other words, upgrading bio-oil by HDO in a petroleum refinery would still be a fossil fuel dependent process; it could partially mitigate US dependence on crude oil but it is not a completely sustainable solution.

Ideally, bio-oil upgrading would be done without using fossil energy. While all commercial forms of energy today are built on a fossil foundation, renewable sources (e.g. solar electricity) are being rapidly implemented. This project seeks to develop a new chemical tool--Electrocatalytic Hydrogenation (ECH)—as an alternative HDO method for the fuel production cycle based on these alternative energy inputs.

2.3 From Catalytic Hydrogenation to Electrocatalytic Hydrogenation

Compared to catalytic hydrogenation, ECH achieves hydrogenation using electrical energy at atmospheric pressure and below the boiling temperature of its electrolyte, typically water. ECH allows renewable electricity, captured from solar, wind, geothermal and other alternative schemes, to be incorporated into bio-oil, raising its chemical energy content. Although CH and ECH are run under vastly different conditions, both methods achieve effective hydrogenations, suggesting that the harsh requirements of CH can be improved by using electricity in ECH. In the following discussion, some reactions from the literature have been selected to illustrate the similarities between CH and ECH. Benzene can be hydrogenated with a Raney-Nickel catalyst at 300 °C and 20 atm pressure, but a reasonable conversion can also be achieved at 45 °C with ECH.⁸⁹ In the past, the Jackson group uncovered a similar reaction improvement. Lactic acid had been chemically hydrogenated to propylene glycol in H₂O with H₂ over 5% Ru/C at 150 °C and 14.5 MPa H₂.⁹⁰ Using the same Ru/C catalyst as had been used for chemical hydrogenation, lactic acid was hydrogenated electrocatalytically at 70 °C with traces of perchloric acid as the electrolyte.⁹¹

For fuel upgrading purposes, ECH could be an ideal route because a) it operates at mild conditions; b) it avoids the storage and use of H₂ gas; c) the chemisorbed hydrogen density and reactivity on the cathode surface can be controlled by current density. Protons can be generated in-situ by anodic water oxidation and then recombine with electrons at the catalytic cathode to reduce the organic components in bio-oil. By reducing C=O and C=C double bonds, it is possible to eliminate carbonyl condensation processes which polymerize bio-oil, while increasing the energy density of the bio-oil.

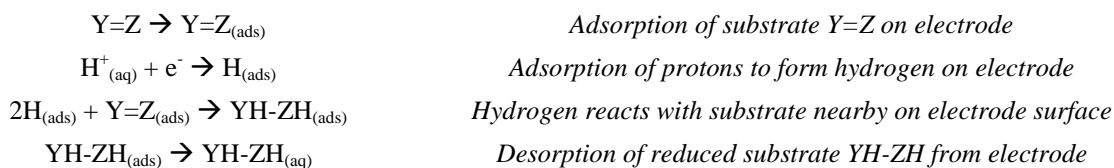
Bio-oil also contains many oxygenated aromatic compounds. Hydrogenation of such electron-rich aromatic compounds is generally difficult due to aromatic stability. Under favorable pH and surfactant conditions, useful ECH results can be achieved.^{92, 93} Because it avoids use of H₂ gas, operates at relatively mild conditions, and allows the potential incorporation of renewable energy into the bio-oil to raise substrate energy content, ECH will be the focus of this research project.

2.4 Brief Introduction to Electrocatalysis

Electrocatalysis is a familiar reaction in the field of organic electrochemistry, which itself has been known since the late 18th century when Faraday first electrolyzed an acetate solution and obtained a gaseous product, ethane.⁹⁴ In that experiment, potassium acetate was electrolyzed with platinum at high anodic potential to generate CO₂, CH₄, C₂H₆. This oxidative electrochemical reaction is known today as the Kolbe oxidation (oxidation of fatty acids to hydrocarbons with the loss of CO₂). Another famous oxidative process is the Simons electrochemical fluorination (replacement of all hydrogens and double bonds with fluorine using a nickel anode). These reactions play vital roles in many industrial processes and natural product syntheses. Fewer electrochemical organic reductions are familiar; perhaps the best known is the reduction and dimerization of acrylonitrile to form adiponitrile.⁹⁵

In general, reduction rates and selectivities depend on applied conditions such as catalytic electrode material, supporting electrolyte and solvent, applied voltage, current density, temperature, and pressure. Of the mentioned conditions, the supporting electrolyte and cathode materials have the greatest influence on ECH.⁹⁶ These two factors dictate how well the reactants interact (adsorb) on the surface, which in turns affects the rate of hydrogenation reaction. When the compound and hydrogen are adsorbed on the metal surface in close proximity, hydrogen can

bond with the substrate, reducing it. This set of cathode processes can be described in the form of chemical equations:



Scheme 2-1: general chemical equations for electrocatalytic hydrogenation of organic substrate

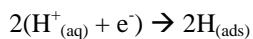
Although no one single material is universally better, in general, the platinum group tends to have a better catalytic effect. The reason was summarized by Navarro in his recent publication.^{97, 98}

“In the Co family ([Ar] 3d⁷ 4s²), the differences in energy between s and d orbitals hinder the re-hybridization of s valence electrons. These orbitals cause Pauli repulsion....Metals such as Ni, Pt, and Pd have closer d and s orbitals, thereby allowing the re-hybridization of s electrons and leading to chemisorptions of both hydrogen and unsaturated organic compounds”
-Navarro, M.

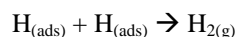
The cost of platinum is undesirably high so this metal is best avoided if other options are available. Thus, the primary focus of this research project is to find a low cost, robust, and simple catalyst that can achieve ECH of bio-oil at ambient conditions.

As mentioned above, substrate reduction takes place when there is enough adsorbed hydrogen in close proximity with the substrate. However, this situation also would place two adsorbed hydrogens close to each other, favoring formation of hydrogen gas, a process known as the Tafel reaction. The closely related Heyrovsky reaction involves a proton from the electrolyte solution reacting with a surface hydrogen and an additional electron from the cathode (effectively, solution proton reacting with surface metal hydride). In either case, H₂ is formed and current is wasted by being diverted from substrate reduction. Both mechanisms are illustrated in Scheme 2-2.

The Tafel mechanism

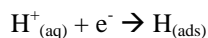


2 protons are adsorbed on the electrode surface

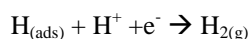


Both adsorbed protons combine to form H₂

The Heyrovsky mechanism



1 proton is adsorbed on the electrode surface.



The adsorbed proton combines with a proton and electrons to form H₂

Scheme 2-2: chemical equations illustration on how H₂ can be generated on the electrode surface with two different mechanisms

If there is too much adsorbed hydrogen on the cathode, the reaction will favor hydrogen evolution. In order to quantitatively evaluate the fraction of electrons spent on substrate hydrogenation verses those spent on H₂ formation, the Columbic efficiency for the desired reaction is calculated. If the efficiency drops during the reaction, either the electrode surface is being deactivated for catalytic hydrogenation or the surface concentration of the reactant is declining which diverts the reaction to form H₂ instead.

2.5 Current Efficiency

Current efficiency is the percentage of total charge passed that effects the desired reaction. An example of a Columbic efficiency calculation is as follows. In the case of acetophenone hydrogenation to 1-phenylethanol, a 2e⁻ transfer reaction, if 6 moles of electrons were passed to form 1 mole of 1-phenylethanol, the Columbic efficiency would be 2/6 = 33.3%. That means 33.3% of the electrons were used to perform the hydrogenation and the other 66.6% were used for side reactions such as hydrogen evolution. The Columbic efficiency by the end of the reaction can be calculated by:

$$\text{Coulombic Efficiency (\%)} = \left(\frac{\text{Mole} \times F \times n}{C_{\text{total}}} \right) \times 100\%$$

where Mole = moles of product formed. F = faraday's constant, 96485 C mol⁻¹, n = number of electrons per reaction, and C_{total} = the accumulative charge passed

For bio-oil hydro-upgrading, it is preferred to have an electrode that has a high Coulombic efficiency; an electrode that prefers hydrogenating the organic substrate rather than forming H₂. In general, Coulombic efficiency of ECH in aqueous phase, which sometimes contains small portion of organic co-solvent (e.g. methanol) to improve organic substrate solubility, has Coulombic efficiency ranges vastly. ECH of small aliphatic molecules (6 carbon atoms or fewer) typically has a greater Coulombic efficiency (~50 – 60%) than the larger ones (10 – 30 %); most likely owe to how the organic molecules adsorb on the electrode surface. Given the majority portion of bio-oil consists mostly small organic molecules, such as acetols, butandiones, and furfurals, ECH is a promising strategy for bio-oil upgrading. However, bio-oil is a complex mixture that also contains a large quantity of larger size aromatic substrates, like phenol, guaiacol, and eugenol, which are harder to hydrogenate due to their aromaticity. ECH of these molecules will require more catalytically active electrodes to break these stable π bonds. The selection of electrode will be discussed later in the chapter. Aside from electrode surface, there are chemical means to improve Coulombic efficiency to favor hydrogenation of organic substrate over side reactions such as hydrogen evolution.

2.6 Use of Cationic Surface Active Reagent in ECH

Surfactants are typically long molecules that have two ends with very different chemical character – specifically one has hygroscopic, polar character and other is nonpolar and hydrophobic.

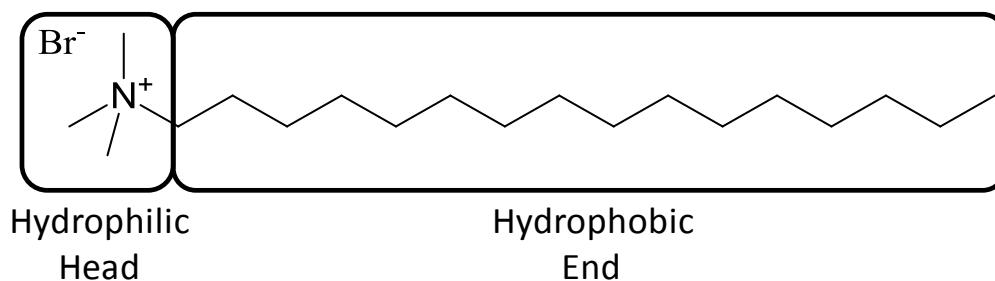


Figure 2-1: Cetyltrimethylammonium bromide (CTAB) is used as an example to illustrate the positively charged hydrophilic head and hydrophobic end (the hydrocarbon tail) nature of surfactant

As a surface active reagent, the hydrophilic end of the reagent adheres on the charged surface of the electrode while the hydrocarbon end makes increases the hydrophobicity of the surface. At an optimal concentration, the surface becomes more hydrophobic to favor organic adsorption. As emulsifying reagents, surfactants can increase the solubility of the organic solute. This in turn speeds up the exchange rate of organic between the surface and the bulk solution.

With these attractive properties, cationic surfactants have been employed in many ECH reactions to increase CE.⁹⁹⁻¹⁰⁴ A common example would be cetyltrimethylammonium bromide $C_{19}H_{42}NBr$ (CTAB). However, if the concentration exceeds a limit, known as the Critical Micelle Concentration (CMC), CTAB (or almost any surfactant) will form micelles and no longer behave as a surfactant. For CTAB, the concentration necessary for the CMC varies a lot depending on experimental conditions. In neutral water systems, it typically ranges from 0.9 – 0.98 mM at room temperature.¹⁰⁵ For high Columbic efficiency, it is important to adjust the amount of CTAB such that it is just below the CMC.

2.7 Selection of Electrodes and the volcano plot

The choice of electrode is critical to product selectivity and Columbic efficiency in ECH. For instance, ECH of acetophenone on different surfaces changes the selectivity from simple hydrogenation (forming 1-phenylethanol) to dimerization (forming pinacol).¹⁰⁶ Other factors

such as current density, cathodic potential, temperature, and electrolyte can also change the product outcome,⁹⁸ but these factors typically have lesser influence on product selectivity compared to cathode properties. In ECH, electrode metals can be categorized based on their H₂ evolution overpotential. To understand this subject further, it is necessary to introduce the use of the volcano plot.

The volcano plot shows the relationship between the metal-substrate binding energy versus activity (typically measured in current density). The concept of a volcano plot is derived from the Sabatier principle, which states that high activity happens only when the substrate and metal binding energy is just right.¹⁰⁷ If the metal-substrate binding energy is too low, the substrate will not bind with the surface in the first place or binds too loosely to carry out the reaction. On the other hand, if the metal-substrate binding energy is too high, the substrate will be held tightly on the metal surface, and it will not be released for the reaction. The metals with too low and too high binding energies are shown in the bottom left and bottom right corner, respectively, of the volcano plot in Figure 2-2.^{108, 109} During the H₂ evolution reaction, these metals generate low current density, a measure of hydrogen evolution activity due to the formation and release of every H₂ which consumes 2 electrons, because hydrogen either adsorbs too weakly or too strongly on their surfaces. Metals on the apex are the ones with the optimal binding energy, which thus give the highest current density. However, these metals are typically the precious metals that should be avoided if possible. Hence, the 2nd highest activity group, which consists of copper, nickel, cobalt and iron, are of great interest to the ECH project.

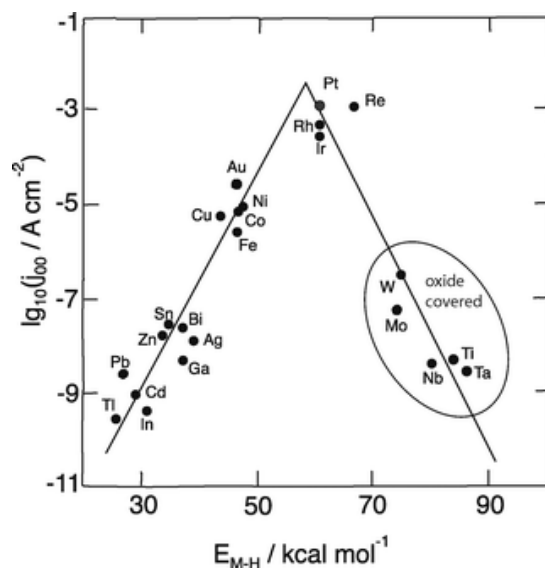


Figure 2-2: The volcano plot of the common metals used in electrocatalysis.

In the past, the ECH literature has surveyed electrodes made of the metals in the volcano plot. In general, high H_2 activity metals tend to hydrogenate organic substrates giving the expected hydrogenation product, whereas the low H_2 activity metals tend to favor a radical transfer mechanism, in which the surface prefers to transfer an electron to the substrate and causes organic dimerization. In the case of acetophenone, 1-phenylethanol is the major product when high H_2 activity metals (Ni, Cu, Fe, Pt) are used,¹¹⁰⁻¹¹³ but the product selectivity shifts to acetophenone pinacol when the reaction is done with low H_2 activities metals (Hg, Sn, Pb, Cd).^{106, 114-116} The difference in product distribution is owed to the nature of hydrogen adsorption on the electrode surface. Lead lies in the region of the “mismatched area” for hydrogen evolution compared to nickel. In this case, under the same voltage, the hydrogen coverage on lead’s surface is less than that of nickel due to the low M-H energy. The adsorbed organic species on the lead electrode is therefore less likely to encounter an adsorbed hydrogen atom. Therefore, hydrogenation of organics is less preferred on a lead surface. By comparison, dimerization is more favorable compared to hydrogenation. In the case of nickel, the surface is

more frequently covered with adsorbed hydrogen compared to that of lead. So when an organic species is adsorbed on the nickel surface, it will likely to meet an adsorbed hydrogen leading to hydrogenation.^{94, 117}

It is important to remember the mechanism of organic ECH consists of adsorption of both hydrogen and the organic substrate shown in Scheme 2-1. Therefore, the hydrogen volcano plot only covers half of the scenario.¹¹⁸ Unfortunately, the complexity of bio-oil would require the survey or generation of many more volcano plots which is both time consuming and cost ineffective (calculating organic adsorption energy costs computer time, especially with complicated organic substrate). Hence, only the hydrogen volcano plot will serve as a model for the electrode selection.

2.8 The use of Raney-Nickel and Other Skeletal Metals

Within the 2nd highest group in the volcano plot shown in Figure 2-2, nickel shows up as the highest activity metal after gold, which is an expensive choice. This suggests the hydrogen will be adsorbed on the nickel surface with the optimal amount of energy. For this reason, nickel has been a popular catalyst for many organic ECH reactions.^{98, 119, 120} Various organic substrates have been hydrogenated electrocatalytically under ambient conditions using a nickel cathode. These ECH reactions occur at moderate voltages with reasonable efficiency in an aqueous environment. However, plain nickel cannot hydrogenate aromatic rings. Fortunately, a special nickel catalyst was discovered in the early 1900s that can address this problem – Raney Nickel.

Raney-Nickel, more formally known as skeletal nickel, was developed by the American engineer, Murray Raney in 1924.¹²¹ In his original invention, a mixture of fine silicon powder and nickel were mixed together in a 1:1 ratio before melting them together in coal fire temperature. The resulting alloy was then treated in a basic solution (sodium hydroxide) to

dissolve (leach) out the silicon, leaving behind a porous, reduced nickel surface, which was found to be surprisingly active in cottonseed oil hydrogenation. Two years after his discovery, he modified the design by substituting silicon with aluminum forming the nickel-aluminum alloy, which improved catalytic activity dramatically.¹²² Because of the porous surface, Raney-nickel is also known as skeletal nickel for its non-uniform, high surface area, reticulated framework. Since Murray's discovery, other types of skeletal metals have been investigated with the same methodology: melting aluminum powder with the metal of interest followed by leaching the aluminum. Non-electrocatalytic hydrogenation using skeletal cobalt, copper, iron, platinum, ruthenium have been examined and documented in great detail.^{123, 124}

Today, Raney-Nickel is one of the most widely used catalysts in many areas. Although it is made of low cost abundant metals, its catalytic effect is comparable to precious metal catalysis in terms of aromatic hydrogenation.^{125, 126} It has been studied extensively in terms of leaching rate, dopants,^{127, 128} temperature treatment,¹²⁹ chemical adsorption,¹³⁰⁻¹³⁹ organic hydrogenation,^{126, 140-145} catalysis surface,¹⁴⁶ kinetics¹⁴⁷, hydrogen evolution^{148, 149} and more.

2.9 Preparation of Raney-Nickel Electrode

With its attractive properties, Raney nickel has been explored as an electrode in many ECH reactions for organic substrates.^{103, 104, 129, 150-154} In these studies, preparation of Raney-Nickel is either done by the hard pressing method¹⁵¹ or an electro-codeposition method¹⁵⁵. In the hard pressing method, the Ni-Al alloy is mixed with small portion of binding reagent and is hard pressed into a cylinder shape before it is treated with in a hot base bath to leach out the aluminum. The electro-codeposition works by trapping the Ni-Al alloy powder into the forming nickel matrix during the nickel plating process. The trapped Ni-Al alloy powder is thus in good

electrical contact with the electrode and functions well electrochemically. A schematic depiction is given in Figure 2-3 to illustrate to the plating process.

The deposition began with a 2.5 x 2.5 cm stainless steel 314 mesh 60 screen submerged in 50 ml nickel-ammonia plating solution¹²⁹ with 1.5 g of nickel-aluminum powder stirred in suspension. A nickel plate facing parallel to the mesh screen serves as a sacrificial anode. Plating current density, calculated in terms of the mesh side facing the anode, is maintained at 60 mA cm⁻² for 2 hours. The electrode is turned 180° every 30 minutes to ensure even deposition on both sides.

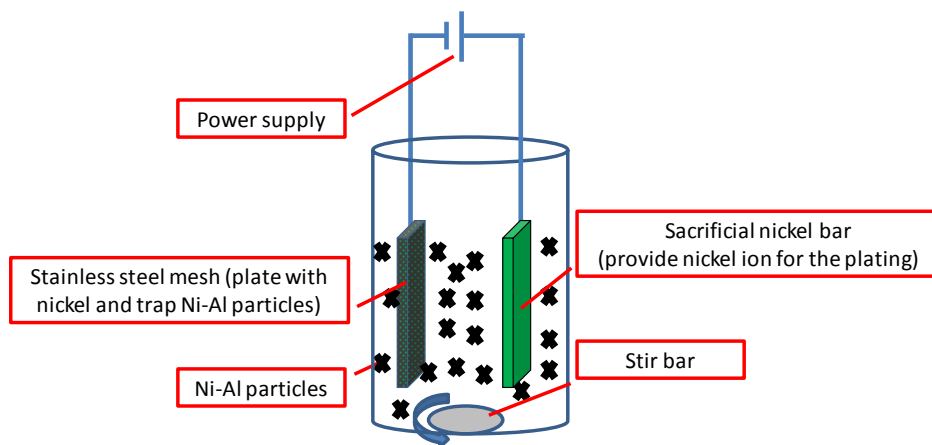


Figure 2-3: Co-deposition of Ni-Al alloy onto the electrode surface. Condition: Preparation of the Ra-Ni cathode uses the Lessard method of trapping nickel-aluminum alloy particles in an electrodeposited nickel matrix.

The resulting Ni-Al deposited electrode is treated with 30% NaOH (6M) at 75 °C for 6 hours, and the electrode is stored in 4% NaOH solution until use.

2.10 Introduction of the Cobalt Phosphate Water Oxidation Catalyst

Platinum has always been a popular choice for the anode because of its high oxidative potential and good catalytic activity compared to many other metals. When it is used in an aqueous environment, it oxidizes water on its surface instead of being oxidized itself like other

more abundant metals such as nickel, copper, iron oxidize. However, platinum is not suitable for large scale synthesis because of its preciousness and scarcity. For this reason, the use of a low cost earth abundant metal water oxidation catalyst was proposed to satisfy the need of platinum.

Water oxidation catalyst development has been highly active for the last two decades for renewable energy production purposes. In general, these studies explore and mimic photosynthesis oxidation systems using different transition metals such as ruthenium, platinum, cobalt, manganese, in combination with different ligand. These catalysts are designed to split water to produce hydrogen and oxygen: $2\text{H}_2\text{O} \rightarrow \text{O}_2 + \text{H}_2$, effectively using electricity presumably generated from renewable sources. When the O_2 and H_2 combine in a fuel cell to form H_2O , the reaction is exothermic releasing the stored energy to generate electricity.

In recent literature, the cobalt phosphate (Co-P) water splitting catalyst from 2008 has received the most attention in the community for several of its outstanding merits.¹⁵⁶ First of all, compared to platinum, Co-P has a lower water oxidation overpotential, which means less energy is required to split water. Second, the simplicity and low cost of the catalyst makes it easily scalable so that it has great potential to address the global energy demand.¹⁵⁷⁻¹⁶⁰ Most reported water splitting catalysts before 2008 either make use of precious metal or sophisticated ligands to tune the catalyst reactivity.^{161, 162} Also, these catalysts typically operate in high pH environments whereas Co-P can function in the neutral pH range (pH 6 – 8).

2.10.1 Preparation of the Cobalt Phosphate Water Oxidation Catalyst

Preparation of Co-P is very simple: dissolve 0.5 mM Co^{2+} in 0.1 M pH 7 phosphate buffer followed a constant potential electrolysis reference to anode at (+1.3 vs. Ag/AgCl) for a few hours. The formation of a black film with gas (oxygen) evolved marks the successful deposition of the Co-P. The formed catalyst can be removed from its preparative solution and be

used in a new aqueous environment. Professor Daniel Nocera, whose group developed the catalyst, demonstrated that the catalyst can operate in the water collected from the famously polluted Charles River. Because of its inexpensive nature and ease of preparation, cobalt phosphate will be explored as a low cost alternative to replace the use of platinum. The results may dramatically increase the chances of applying ECH in large scale Bio-oil production.

2.11 Overview of System Setup

2.11.1 Constant Voltage vs. Constant Current Electrolysis

Before the discussion on cell setup, it is important to identify the difference between constant current and constant voltage electrolysis because the reaction cell setup or apparatus requirements can differ depending on setting. This concept requires an entry level background on electricity that is usually taught in an introductory college level physics class. In here, the level of knowledge will be covered just enough for the reader to understand how an electrochemical system functions – however readers are still encouraged to learn how the basics of electronics though.

In any electrical circuit, assuming the electrical resistance is constant, higher voltage will result in higher current. This is because voltage is the driving force that pushes the electrons through the circuit, and the current is the speed of the electrons travel. To make this more understandable for organic chemists, imagine running a chromatography column; the mobile phase travels slower if the gel is packed too tight. For the solvent to elute at a higher speed in the same gel, pressure is needed to “push” the solvent harder in addition to the gravitational force. In terms of electricity, the “push” from the chromatography example represents the voltage; the speed of the mobile phase travel represents the current; and the tightness of the gel packing

represents the resistance of the electrical load. The overall analogical terms are summarized in Table 2-1.

Table 2-1: Terms comparison between chromatography and electronic system

Chromatography	Electronics terms
Gel packing	Resistance
Flow of solvent	Current
Solvent driving force (gravity)	Voltage

If the gel gets tighter during the chromatography process, then a higher driving force is need to push the solvent to maintain the same flow rate. The idea is the same for constant current electrolysis: if the flow of electrons is required to continue at a fixed rate, the voltage needs to be adjusted to compensate for resistance changes. On the other hand, for constant voltage electrolysis, a change in the resistance will result in a change in current. This is because when the driving force is fixed, changing the resistance will result in a change in the electron flow rate (current). The relationship between resistance, voltage and current is summarized with $V/R = I$, where V means voltage, R means resistance, and I means current.

For constant voltage setting, the subject can get more complicated when “absolute potential” is required for some experiments. Although this project does not use constant voltage (with or without absolute potential applied), knowing the topic will be beneficial for future development.

A conventional direct current (DC) power supply can only regulate the voltage difference between the cathode and anode in a constant voltage setting. However, the actual potential for the individual electrode can fluctuate. In other words, the voltage potential on the cathode may become increasingly negative while the anode shift more and more positive to compensate for the change in cathode. The problem is depicted in Table 2-2.

Table 2-2: An example to illustrate how the absolute potential on individual electrode changes during a constant voltage electrochemical reaction. Note: T_a and T_b describes different stage during the ECH

	Cathode Potential	Anode Potential	Potential Difference
Initial	-2	+3	-5
T _a	-3	+2	-5
T _b	-1	+4	-5

In all 3 stages of the electrolysis, initial, T_a and T_b, the potential difference are all +1 while the absolute potentials of both electrodes are shifting. Such effect can dramatically affect the results because the voltage dictates the energy level of the passing electrons (this subject will be discussed in Chapter 5 with experimental data). To accurately maintain the absolute potential on the electrode of interest, which is often referred as the working electrode, a reference electrode is needed.

Reference electrode is an electrode that is electrochemically stable over a range of potentials. The universal standard reference electrode is the Standard Hydrogen Electrode (SHE), which generates H₂ electrochemically and has a 0 v potential by definition. However, the construction and maintenance of a SHE is rather inconvenient and time consuming. So, silver chloride on silver wire electrode (Ag/AgCl) is the preferred choice for small scale short duration reactions, such as cyclic voltammetry. (For preparation of a Ag/AgCl reference electrode, please refer to the cited book chapter¹⁶³). By controlling and monitoring the potential between the reference electrode and the working electrode, an absolute potential electrolysis can be achieved. Note that absolute potential electrolysis requires a sophisticated digital potentiostat that supports three electrode inputs (working, counter, and reference electrodes) to operate.

2.11.2 Three Electrode System

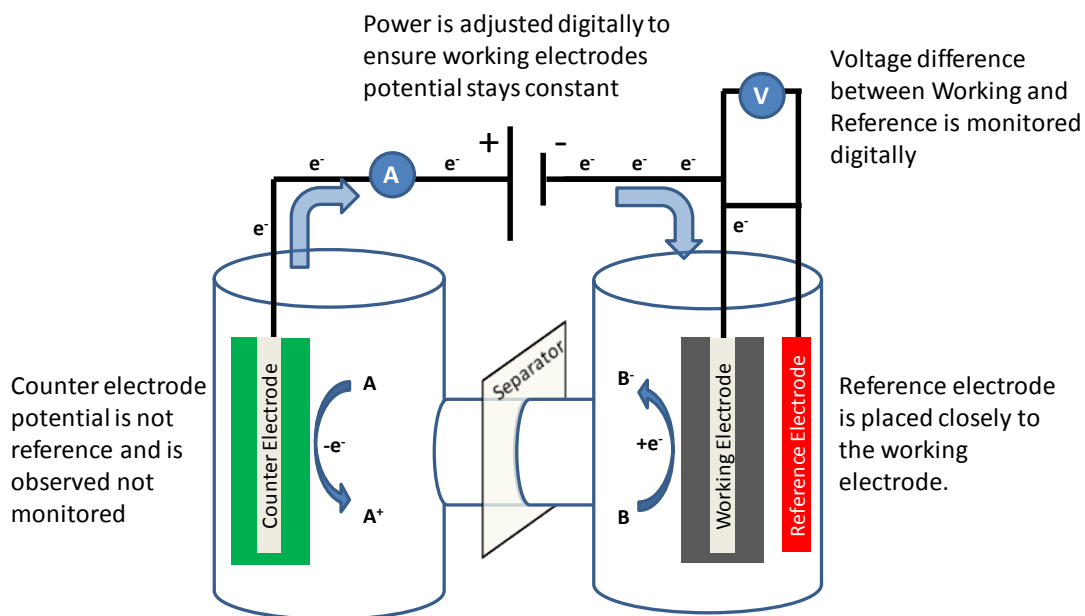


Figure 2-4: Three electrode system where the reference electrode is referencing the cathode (working), substrate A is oxidized on the anode surface and substrate B is reduced on the cathode surface. The separator, typically a glass frit or Nafion membrane, may or may not be necessary to the system. Note: V = Voltmeter, to measure the voltage between the reference electrode and the working electrode. A = Ammeter, to measure the current at any time during the reaction

The three-electrode system shown in Figure 2-4 is a typical electrochemical setup employed in various electrochemical techniques. Among them, cyclic voltammetry is the most frequently used technique to study redox mechanisms, substrate diffusion, and various electrochemical aspects on the working electrode surface. (Note: working electrodes can be either cathode or anode, depending on the reaction of interest) The potential of the counter electrode in this case is not regulated, and is considered as a part to complete the circuit. The separator, typically a glass frit or proton exchange membrane, is optional and is used to separate the two compartments in order to isolate the reaction product.

2.11.3 Two Electrode System

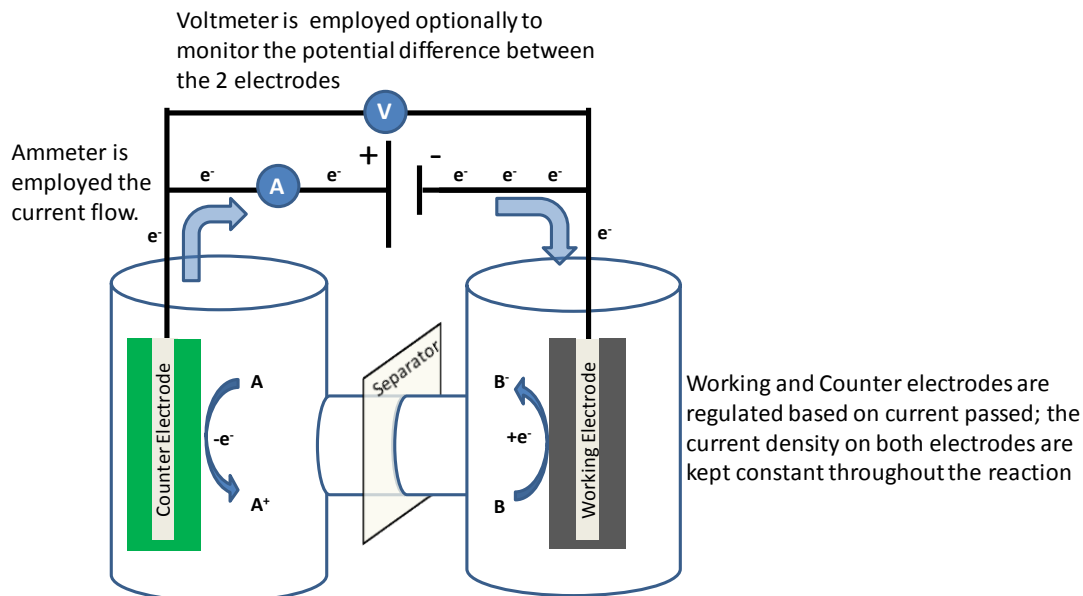


Figure 2-5: Two electrodes with the cathode (working) and the anode (counter); substrate A is oxidized on the anode surface and substrate B is reduced on the cathode surface. Separator is optional, and is typically a proton exchange membrane or glass frit. Note: V = Voltmeter, to measure the voltage between the reference electrode and the working electrode. A = Ammeter. to measure the current at any time during the reaction

Without the reference electrode, the electrolysis is simplified to two electrodes with a power source shown in Figure 2-5. Since there will be no electrode potential regulation, the only sensible setting would be a constant current electrolysis, in which the flow of electrons is maintained at a fixed setting by an automated control potential. For electrocatalytic hydrogenation, constant current is preferred because the surface hydrogen adsorption can be controlled via applied current regulation. Also, in this research project, the use of Co-P catalyst requires either a constant anodic potential or a fixed current density (current per given area) to maintain the catalyst functionality. If a reference electrode (3 electrode system) is employed to regulate the anode potential, the cathode current density will fluctuate making the hydrogenation process difficult to monitor. However, if the cathode potential is regulated, then the anode potential will fluctuate and disfavor the Co-P catalyst formation. Therefore, this project has

chosen the constant current electrolysis setting – fixing the current density to keep the flow of electrons on both electrodes regulated. Also, Columbic efficiency calculations are simplest with constant current electrolysis as opposed to constant potential electrolysis. This is because the electrons are passed at a fixed rate and so the amount of charge is constant over every hourly sampling block. Thus, no additional equipment, such as a coulometer, is needed to measure the charge passed.

The undivided cell is essentially the two compartment cell without the separator. Undivided cells can minimize voltage consumption because the contact between the two electrodes is not “obstructed”. Moreover, the cost of large scale electrolysis can be reduced because proton exchange membranes or glass frits are costly items and require regular replacement. However, the lack of separator can result in undesired reactions. For example, the reduced product released from the cathode can get oxidized when it contacts the anode or vice versa. For bio-oil upgrading, a divided cell is preferable due to reactivity reasons. The large amounts of oxidizable organics in bio-oil can undergo oxidation on the anode surface and then potentially undergo polymerization. However, the lower voltage demand aspect of an undivided cell is very attractive for large scale processing especially in the context of energy upgrading, so it is worth trying to develop a system, or an anode that does not oxidize the organic substrate during the bio-oil upgrading process. For this reason, this research project began by mimicking Navarro’s work in organic hydrogenation in an undivided cell.^{97, 119}

2.12 Summary

With low energy content, high acidity, and polymerizable nature, bio-oil has to be upgraded via hydrogenation to increase its energy content and stability before it can be used as fuel. Although the petroleum hydrodesulfurization catalysts studied are extensive and well

implemented in the current industrial upgrading infrastructure, the energy intensive environment will decrease the sustainability of bio-oil as a fuel. Therefore, an alternative hydrogenation scheme is needed – electrocatalytic hydrogenation (ECH).

ECH can serve as an alternative low cost strategy compared to catalytic hydrogenation. It achieves hydrogenation using electrical energy at ambient conditions below the electrolyte boiling temperature at atmospheric pressure. The electrical input of ECH allows incorporation of renewable electricity capture from solar, wind, geothermal and various schemes and stores it as chemical energy in the bio-oil during the upgrading process. In other words, ECH can be viewed as an energy-upgrading bridge between biomass and fuel – allowing a vehicle to be powered using renewable energy.

Two electrodes, skeletal nickel cathode, and cobalt phosphate coated anode, are proposed as the key electrodes towards bio-oil hydrogenation. Skeletal nickel is effective in aliphatic and aromatic hydrogenation, while the cobalt phosphate catalyst serves as a low cost alternative to platinum to provide H^+ (for hydrogenation) via water oxidation. The process would ideally use electricity generated from renewable sources, and store the energy as chemical energy during the upgrading process.

The goal of this project is to develop a scalable and low cost electrocatalytic system in which bio-oil can be hydrogenated to fuel, thereby addressing the national demand for renewable fuel. With this in mind, the first part of the project is to investigate the viability of using the cobalt phosphate catalyst to bypass the use of platinum. Since the use of cobalt phosphate coated anode in conjunction to cathodic organic hydrogenation is unprecedented, the first part of the project will be devoted to understand the function of cobalt phosphates catalyst and its limits. In

addition to the cobalt phosphate study, other factors such as surfactants and current density will be explored to build a solid foundation for the actual bio-oil hydrogenation.

Chapter 3 Electrocatalytic Upgrading of Model Lignin Monomers with Earth Abundant Metal

3.1 Introduction

Electrocatalytic Hydrogenation (ECH) has been shown as the most promising upgrading strategy in bio-oil. Compared to catalytic hydrogenation (CH), which operates at 150 – 200 psi H₂ and 150 – 400 °C, ECH can achieve hydrogenate pi bonds at atmospheric pressure and relatively low temperature, typically below water boiling temperature. For fuel production purposes, it will be the more preferred strategy because the upgrading stage will be consuming much less energy. The energy required for the upgrading process will presumably come from renewable sources generators.

This research project collaborates with Bio-system Engineering, where biomass will be liquefied into bio-oil via fast pyrolysis (see Chapter 1 for details). The project aims to achieve bio-oil upgrading electrocatalytically and investigation of the optimal conditions in which maximum Columbic efficiency can be obtained. Several goals were set out during the project initiation stage.

Achieve ECH of organic substrate in an undivided cell: traditional ECH experiments are conducted in a divided cell where cathode and anode compartments are separated by an ion exchange membrane, e.g. Nafion®. However, the membrane itself imposed a significant amount of electrical resistance thereby increases the potential difference and thus the energy cost for same amount of current delivered. To minimized resistance (or lower potential difference) it is preferable to conduct ECH in an undivided cell.

Design of long life, low cost reaction system: for long duration system, the anode material must have a high overpotential to prevent self-oxidation. This is why platinum is usually

employed for research purposes. However, the cost and rare nature of platinum would decrease the cost effectiveness of the project. As mentioned above the Co-P Nocera catalyst has a great current density (for oxygen evolution) compared to platinum. Hence, it is a goal to incorporate the Nocera catalyst in the undivided cell.

Optimization of condition for multi substrate hydrogenation at minimal applied voltage: Bio-oil consists of various different organic components. It is necessary to characterize the selectivity and reduction order when different functional groups are present in the same reaction, and to optimize potential to achieve efficient reduction of the multi-component system.

3.2 Electrocatalytic Hydrogenation of Acetophenone in Undivided cell

Navarro reported a sacrificial nickel anode system where simple non-aromatic olefins can be reduced with high efficiency.^{96, 164, 165} Being able to reproduce literature results will be a key step to design a non-sacrificial system, and gaining understanding of the reduction is crucial to the project. Setup of the reaction is rather straight forward; it consists of two electrodes connected to a power supply shown in Figure 3-1.

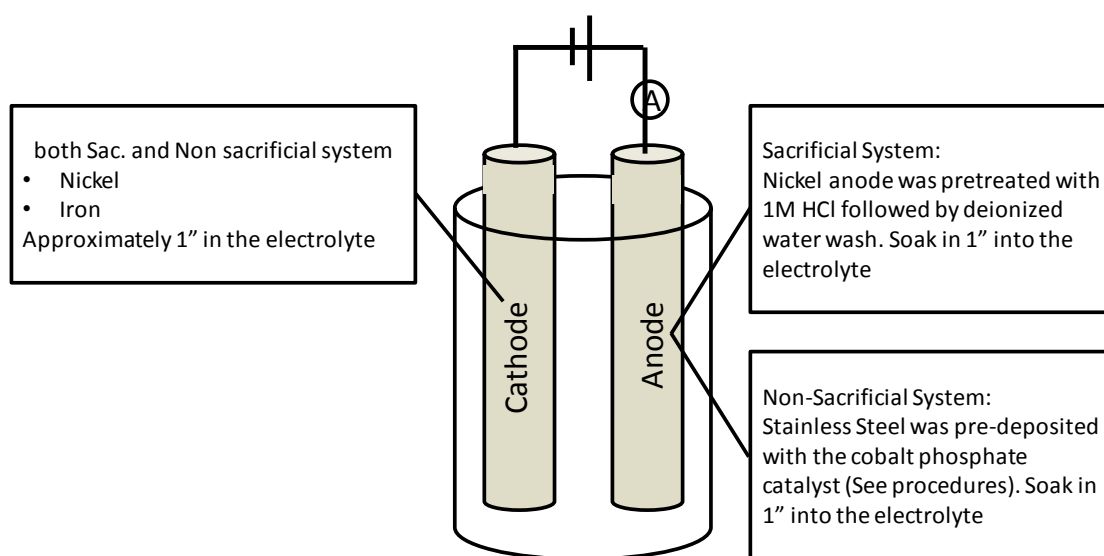


Figure 3-1: Electrocatalytic Hydrogenation of acetophenone in an undivided cell with different

3.2.1 Experimental Procedures

Sacrificial anode system, both electrodes were brushed with sandpaper. Then iron cathode was pretreated with 1M CH₃COOH and the nickel anode was pretreated with 1 M HCl for 1 hour followed by a de-ionized water wash. Both electrodes were then immersed into 75 ml of electrolyte (see Table 1) containing the organic substrate. Samples (0.5 ml) were taken initially and at 30 minute intervals over the 150 minute reaction time.

Non-sacrificial system, the water oxidation catalyst was prepared separately in 0.1 M pH 7 potassium phosphate buffer with 0.5mM CoCl₂•6H₂O dissolved. Traces of white precipitate were observed upon mixing of this solution due to the insolubility of Co₃(PO₄)₂. Two pieces of 2.5 x 3 cm 304 stainless steel (60 mesh) screens were immersed as cathode and anode. Constant voltage (Anode +1.30 vs. Ag/AgCl) was applied for 1 hour and the anode screen turned black indicating the formation of the Co-P film. Analysis of the Co-P catalyst with cyclic voltammetry and SEM imaging with EDS analysis both showed that the described procedure yields results in agreement with the literature. Applications of such prepared anodes were explored with various cathode materials. Results are summarized in Figure 3-2.

	Sacrificial Anode	Non-Sacrificial System
Supporting Electrolyte	4:1 (Water:MeOH), 0.25M NH ₄ Cl	4:1 (KPi : MeOH)
Cathodic Reaction	$AP + 2H^+ + 2e^- \rightarrow PE$ $2H^+ + 2e^- \rightarrow H_{2(g)}$ $2Ni^{2+}_{(aq)} + 2e^- \rightarrow Ni_{(s)}$	$AP + 2H^+ + 2e^- \rightarrow PE$ $2H^+ + 2e^- \rightarrow H_{2(g)}$
Anodic Reaction	$Ni_{(s)} \rightarrow Ni^{2+}_{(aq)} + 2e^-$	$2H_2O \rightarrow O_{2(g)} + 4H^+ + 4e^-$

Table 3-1: Condition for sacrificial and non-sacrificial of Acetophenone (AP) to 1-phenylethanol (PE) at constant current (50mA)

3.2.2 Analysis

Samples were extracted with 1 ml CDCl_3 and filtered with dry MgSO_4 in disposable glass pipette to filter out paramagnetic nickel ions (as their insoluble sulfate salts). Control experiments show that extraction efficiency is 99.2% and extraction selectivity of both reactant and product is in a good 50:50 ratio. Reaction conversions were then determined by NMR based on the aromatic proton integration. For calculations for precautions of using H-NMR quantitatively, please refer to Chapter 2.

3.2.3 Results and Discussion

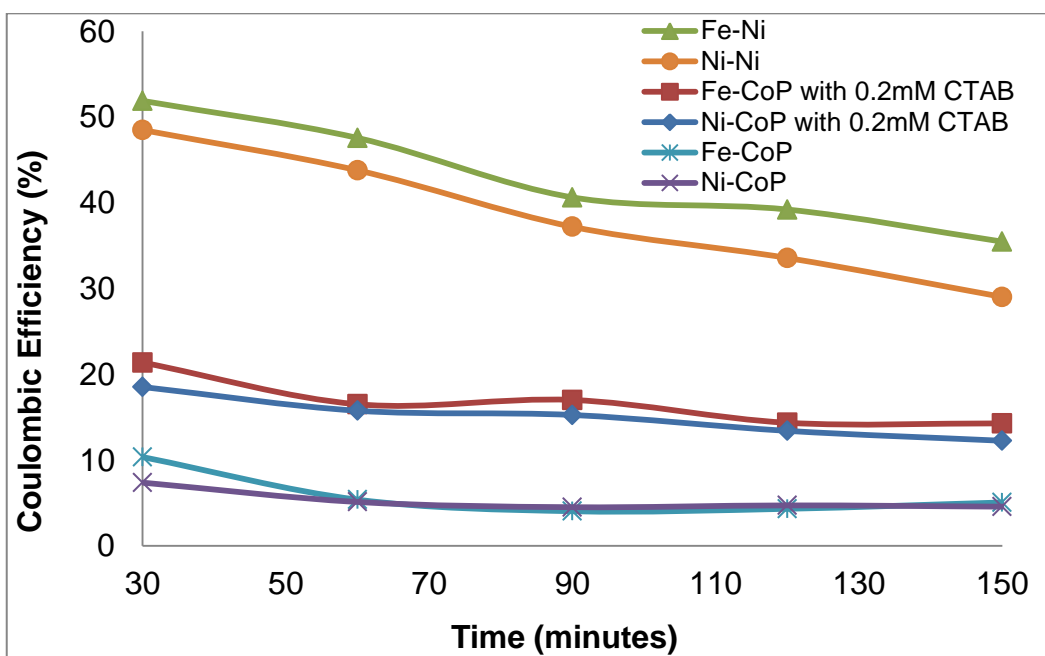


Figure 3-2: Reduction of acetophenone with different electrode at room temperature

The reduction of non-aromatic double bonds occurring at room temperature and high electronic efficiency marks the beauty of the sacrificial anode system. However, the drawback is that the metallic nickel of the anode must lose electrons, undergoing oxidation in order to send electrons as current to the cathode. Thus the mass of the nickel anode limits the lifespan of the system. Though not all were tried, experiments from the Navarro paper were easily and reliably

reproduced. For instance, results with an iron and nickel cathode were in good agreement with the paper. The re-deposition (plating) of nickel onto the cathode constantly renews the surface with Ni, which allows reduction to take place. Interestingly, the efficiency is slightly diminished when the iron cathode is replaced with nickel or, even worse, with a Raney-Nickel cathode. This was suggested by Navarro that the Fe-Ni combination may give special catalytic effect. As for Raney-nickel, the high surface area and morphology was known to favor hydrogen evolution, which decreases the coulombic efficiency. As for the coulombic efficiency, both Iron and Nickel sacrificial system has agreeable and good C.E. However, even of the high surface area, Raney-Nickel has a rather low C.E. which suggests it favors hydrogen evolution by far.

By replacing the sacrificial nickel with a stainless steel anode coated with the Co-P catalyst, the duration of the system's effective run-time increases significantly. No sign of anode oxidation was observed even after 48 hours. However, the tradeoff of the long duration is a low reduction rate. For the same amount of time, the overall C.E. dropped dramatically when switching from sacrificial anode to non-sacrificial anode. To address this problem, cationic surfactant was added in attempt to improve the C.E. With 0.2 mM of CTAB, the overall C.E. of Fe-CoP increased from 7% to 15%.

The optimal concentration of CTAB was not investigated further because this preliminary experimental was designed to test out the compatibility of the Co-P catalyst in conjugation with organic hydrogenation. The effect of CTAB concentration verses efficiency will be shown later in the chapter.

In summary, an electrochemically inactive surface can be modified with traces of surfactant. More importantly, undivided cell with abundant material is demonstrated despite the

low C.E. This finding sets the path for ECH of other molecules that would be difficult to reduce otherwise.

3.3 Reduction of Phenol in Undivided Cell

Seeing this promising system with the Co-P catalyst, reduction of phenol was investigated with Raney-Nickel Cathode. Acidic, easily oxidized and polymerized phenolic compounds are the main lignin-derived components in bio-oil, so successful reduction and deoxygenation of these aromatics to simpler cycloalkanes represents an important mode of upgrading and stabilization. In powder form, the high surface area Raney-Nickel catalysts are effective in reduction of aromatic systems via classical hydrogenation and electrocatalytic hydrogenation.¹⁶⁶⁻¹⁶⁸ Raney-Nickel particles can be electrochemically deposited in the matrix of Nickel metal¹⁶⁹ and the procedure is described below. Previously, Menard have shown that reduction of phenol to cyclohexanol is possible with Raney-Nickel cathode in a divided cell compartment even at 35 °C. With traces of cationic surfactant, CTAB, the Columbic efficiency further improved. These experiments were repeated and the results are agreeable. Hence, the second phase of the project was devoted to the development of an undivided cell for aromatic reduction using Raney-Nickel as a cathode.

3.3.1 Experimental Procedures

The Raney-Nickel electrode was prepared by co-depositing Ni-Al alloy powder onto stainless steel screen along with the electroplated nickel. The nickel plating bath consists of (213g/L NiCl₂•6H₂O, 30g/L NH₄Cl, ~200ml/L NH₄OH) and pH is maintained at 9-10 with NH₄OH. 3g of Ni-Al powder is added to an 80ml plating bath. Nickel rod is used as an anode and a 2.5 x 3.0 cm stainless steel plate is used base support for the Raney-nickel cathode. The aluminum is then leached out by 30% NaOH at 70 °C for 7 hours. The leached cathodes were

stored in 4% NaOH. The storage period was good for at least 3 months. The leaching condition was studied carefully by Lessard based on the efficiency of ECH of phenanthrene.¹⁷⁰ On average, 10 mg of Ni-Al alloy were deposited and deposition is every uniform with the constant current density, 60mA cm⁻². The deposition rate deviates on average 10 – 15 from average implying the position and geometry of the plating plate may have influence to the results. The results are summarized in Table 3-2 below. Dried samples of the cathode before and after leaching were examined by SEM and EDX analysis to check the presence of nickel, aluminum and changes on surface morphology.

Table 3-2: Deposition rate and deviations on Ni-Al alloy deposition. Mono side physical area (2.5 x 2.5 cm) of the used for the *J* value calculation

Current (A)	<i>J</i> (mA cm ⁻²)	Rxn Time (s)	Before (g)	After (g)	Dif. (g)	Ni-Al (g)	Deposit Rate (µg s ⁻¹)	% Deviation
0.45	60.0	7680	0.8911	1.9978	1.107	0.107	13.99	12.4
0.45	60.0	7200	0.8569	1.8772	1.020	0.084	11.60	15.9
0.45	60.0	7260	0.8739	1.8951	1.021	0.077	10.55	17.4
0.45	60.0	7380	0.8970	1.9348	1.038	0.078	10.52	17.1
0.45	60.0	7260	0.8970	1.9366	1.040	0.095	13.09	14.0
0.45	60.0	7260	0.8720	1.9192	1.047	0.103	14.13	13.0
0.45	60.0	7380	0.8975	1.9330	1.036	0.075	10.20	17.7
0.45	60.0	9000	0.9033	2.1714	1.268	0.097	10.79	13.7

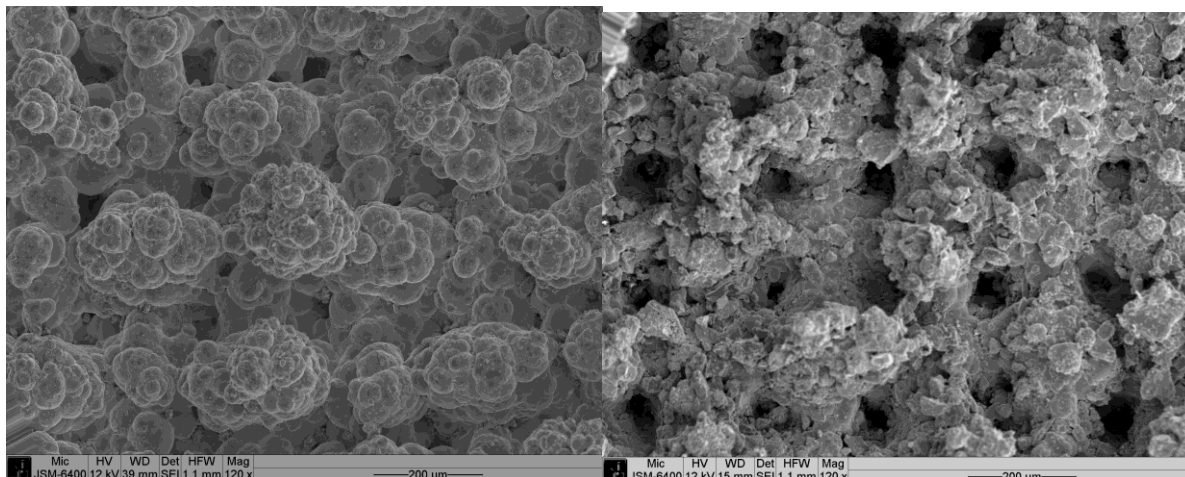


Figure 3-3: Raney Nickel cathode before (left) and after (right) leaching of Al with NaOH at 70 °C for 7 hours.

3.3.2 ECH of Phenol

A solution of 0.022g of phenol (without drying) was dissolved in 20ml of 0.1M KPi buffer. Using Raney-Nickel cathode and the Co-P catalyst on stainless steel as anode, constant current electrolysis was applied until the number of coulomb passed reaches 100% of theoretical (assuming perfect Columbic efficiency). A 0.5 ml sample was taken, saturated with NaCl, and extracted with CDCl_3 . NMR was used to determine the relative ratio of Phenol and cyclohexanol.

3.3.3 Results and discussion

Unfortunately, having tried almost all combination with pH 3, 5, 7, 0.25 mM, 0.5 mM CTAB, 25, and 74 °C, none of these combinations showed reasonable amount of cyclohexanol. At pH 7 and pH 9, with 0.25 mM, traces of cyclohexanol can be observed with NMR in the baseline noise level. During the reaction, electrolyte turned to a brown color and the anode surface turned brown. The color cannot be removed even with concentrated THF, HCl or HNO_3 , which implies they were not attributed by the water oxidation catalyst. Literature revealed that phenolic compounds can be polymerized even at low oxidation potential (+1.44 vs. Ag/AgCl) in both acidic and basic environment on 304 stainless steel surface.¹⁷¹ The phenolic film adheres

strongly on the anode surface, blocking Co-P catalyst formation and water oxidation reaction and the resistance of the system. Hence, reduction of phenol in undivided cell with the Nocera anode was an unexpected challenge. Other phenolic derivatives, Guaiacol (2-methoxyphenol) and Syringol (2,6-dimethoxyphenol) showed similar behavior. Hence, reduction of phenolic compounds at this stage can only be done with a sacrificial nickel or in a divided cell where cathodic material is separated from the anode compartment to prevent polymerization.

3.4 Reduction of Guaiacol in Divided Cell:

Having seen phenolic derivatives oxidized and polymerized, a divided cell is necessary to achieve ECH of bio-oil. Further investigation on phenol reduction in divided cell will not be conducted because a) it has been investigated in the past with platinum group metal and Raney-nickel cathode.^{166, 167} b) the presence of phenolic derivatives is relatively less than Guaiacol derivatives in bio-oil. Guaiacol derivatives are not costly, and they are good models compounds for preliminary data purposes. To the best of our knowledge, ECH of guaiacol has never been reported. Although Lessard has reported lignin treatment with Raney-nickel catalyst,¹⁷² in which guaiacol was formed and maybe hydrogenated but the ECH of guaiacol was not studied executively. Furthermore, Thomalla has reported ECH of phenol with traces of cationic surfactant at different temperature and obtained reasonable yield.⁹² Hence, it is highly possible that guaiacol can be hydrogenated into 2-methoxycyclohexanol electrochemically with the help of cationic surfactant. However, the electron donating methoxy group may decrease the reduction rate because it can stabilize the aromatic system through resonance with the oxygen lone pair.

3.5 Experimental Procedures

Nafion 117 was boiled in 5mM H₂SO₄ for 1 hour, and boiled in 1% H₂O₂ solution for 1 hour. Cleaned Nafion membranes were stored in 1 mM H₂SO₄ solutions. All solutions were prepared with HPLC grade water. Raney-nickel cathode preparation was described in part II and a Co-P on stainless steel mesh was used as anode. 30mL of electrolyte was heated to the desired temperature in water bath. Electrodes were connected through a rubber stopper by stainless steel wire to slow down evaporation of electrolyte. Both cathodes and anode were placed closely to the membrane to minimize internal resistance. After 20 minutes of pre-electrolysis, 20 mM of guaiacol was added. Reaction time was based on charge passed for 100% theoretical yield assuming perfect Coulombic efficiency. 1 ml of sample will be taken at the end of the reaction from cathode and anode compartment, saturated with NaCl, and extracted with CDCl₃ for NMR analysis. Another 1 ml from both compartments will be analyzed by HPLC using mixed mode C18 cation column using 13% acetonitrile in water as mobile phase and 0.8 ml min⁻¹ flow rate. Phenol and guaiacol are analyzed by the UV detector while 2-methoxycyclohexanol and cyclohexanol are analyzed by water reflective index detector. Response curve of both detectors and retention times were determined by standards injection. Note: Phenol was dried by sublimation and checked with NMR for standard preparation. GC-MS also was employed to analyze some of the samples due to unexpected technical difficulties with the HPLC system. Standards with known concentrations were prepared in dichloromethane for standard curves. 0.1 ml of samples from experiment were taken from experiment and extracted with 1.0 ml of dichloromethane and products were identified based on retention time and M.S.

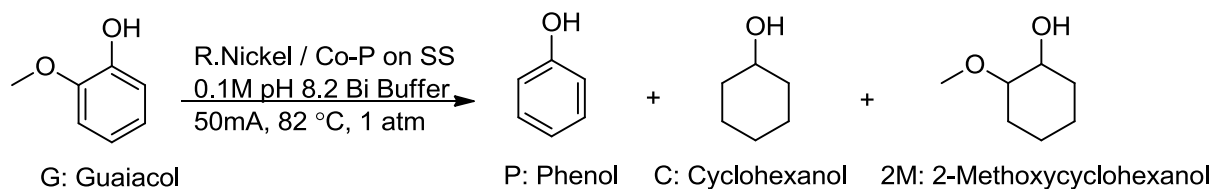


Figure 3-4: Electrocatalytic hydrogenation of Guaiacol and the possible product and their annotations.

3.6 Results and discussion

As expected, reduction of guaiacol is more challenging than phenol. In absence of CTAB, guaiacol does not get reduced at 80 °C at 3 different pH buffer solutions: Ammonium Acetate, Phosphate and Borate Buffer. Strong acid, such as HI, HCl, even SAC-13 (Nafion-H solid superacid), have no effect on reduction of guaiacol. To achieve reduction without CTAB, a pyro-reactor was modified with two stainless steel wire as electrical couple to achieve temperature above boiling point.

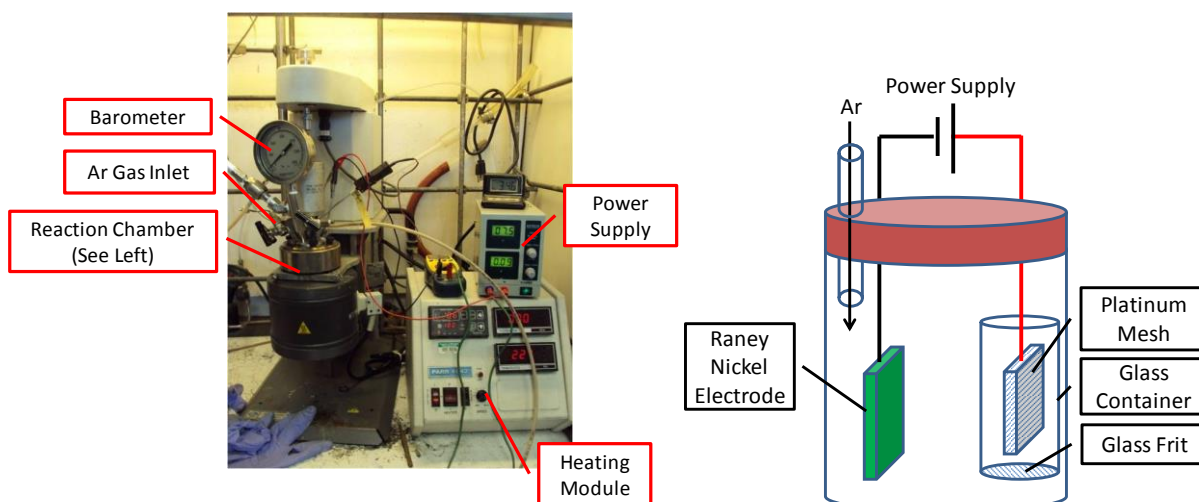


Figure 3-5: Electrocatalytic Hydrogenation of Guaiacol in high pressure setting (Left) the physical setup of the overall system (Right) Schematic depiction of the reaction chamber

Trace of transformation (<4%) was observed at 120 °C at 100 psi of argon gas at both pH 7 and 8.2, but not with pH 3 ammonium acetate. However, with 0.50 mM of CTAB, guaiacol began to undergo reduction at 80 °C in the normal atmosphere as shown in Table 3-3. Reaction

was carried out in a dual compartment cell without an elaborated pressurized setup shown in Figure 3-6.

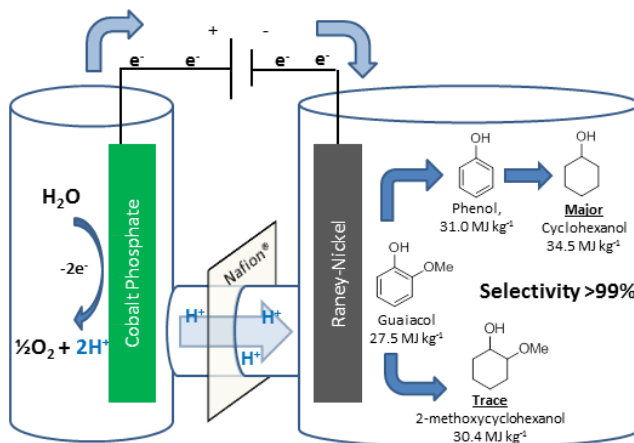


Figure 3-6: Electrocatalytic hydrogenation (ECH) of organic molecule in a divided cell separated by a Nafion 117 proton exchange membrane.

At pH 8.2, reduction of guaiacol becomes more preferable as the relative ratio of guaiacol to hydrogen on cathode surfaces decreases as the electrolyte becomes more basic. In the presence of CTAB, the Coulombic efficiency reaches as high as 35.9% at 0.50 mM, showing hydrogen evolution is still the dominant reaction. At higher concentration of CTAB, the current efficient drops again due to the formation of micelle and CTAB no long functions as a surface modifying reagent.

Table 3-3: Reduction of 20 mM of Guaiacol in 0.1 M pH 8.2 borate buffer at $82 \pm 2^{\circ}\text{C}$, and $j=8 \text{ mA cm}^{-2}$ (current density was calculated by applied current (50 mA) divided by the electrode area that is facing the anode $2.5 \times 2.5 \text{ cm}$). G: Guaiacol, P: Phenol, 2M, 2-Methoxycyclohexanol and C: Cyclohexanol

Use	CTAB mM	G	P	2M	C	Coulomb (C)	C.E. (%)	M. Bal (%)
1	0.25	12.36	0.63	0.39	3.21	363.80	23.31	82.97
1	0.50	10.63	0.66	0.52	5.25	374.59	35.89	85.29
1	0.75	15.06	0.59	0.37	3.58	376.50	24.65	98.02
1	1.50	14.16	0.05	0.19	0.66	364.54	5.22	75.36
2	0.50	14.84	0.28	0.39	2.11	380.97	15.04	88.09
2	0.75	16.68	0.38	0.19	1.51	382.38	10.60	93.83
2	1.50	14.21	0.00	0.23	0.11	390.52	1.67	72.73

The influence of CTAB in mass balance was also examined. Interestingly, the mass balance increased from 0.25 mM reaches highest at 0.75 mM CTAB and dropped after. This may due to the positively charged micelle assisting the guaiacol diffuse across the membrane as below in figure 8. A similar phenomenon is also observed in fuel cell application such as the PEM-fuel cell and Methanol-fuel cell and is known as electro-osmosis (EOS).¹⁷³ Despite the membrane separation, neutral substrates are assisted by charged species to diffuse from one compartment to another. In this case, it is possible that the micelle which has a positively charged surface binds with guaiacol and the complex diffuses across the membrane. Interestingly, EOS also occurs in the absences of CTAB as NMR shown traces of guaiacol was present in the sample from the anode compartment. In this case, it may be the formation of water-guaiacol complex to facilitate the diffusion across the membrane as shown in Figure 3-7.

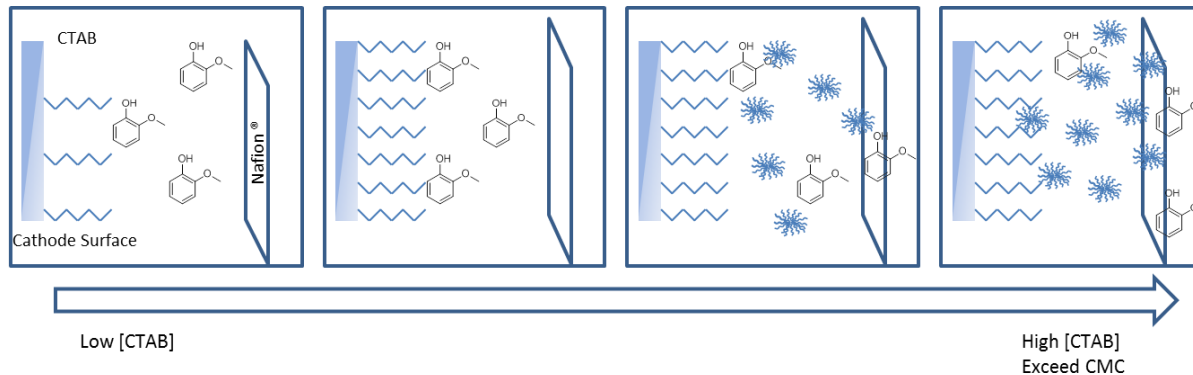


Figure 3-7: Depiction of CTAB at different concentration in solution. Low and optimal will cause CTAB to form on adsorption on surface while medium high to high will encourage formation of michelle and may encourage diffusion of organics through the cationic exchange membrane (Nafion)

After the 1st trial of experiment, the Raney-Nickel electrodes were washed with distilled water, rinsed with acetone, and stored back in the 4% NaOH for 24 hours before the 2nd use. It was expected that Raney-nickel electrode prepared by the described method would have a good life time and the C.E. would only decrease by a small amount.¹¹⁷ Surprisingly, in a second identical application condition the Columbic efficiency dropped almost 50%. This unexpected result may due to the diffusion of Co^{2+} ions, which was part of the oxidation catalyst, migrates from anode to cathode compartment and be reduced on the Raney-Nickel electrode surface. Further investigation with be done with ICP-MS to determine the concentration of Co^{2+} in the cathode compartment. The result will be compared with control experiment where Pt wire substitute as anode. If such hypothesis is valid, it is important to minimize the Co^{2+} deposition by either employing ion participation method or consider other catalysts to prolong the life time of Raney-Nickel electrode.

3.6.1 Mechanistic Investigation of Guaiacol Demethoxylation

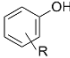
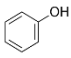
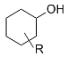
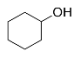
Production of guaiacol to cyclohexanol was serendipity. The elimination of an oxygen atom from guaiacol to phenol effective increased the energy content from 27.5 MJ kg^{-1} to 31.0

MJ kg⁻¹ an increase of 12.7%. When phenol is hydrogenated to cyclohexanol, the specific energy increased to 34.5 MJ kg⁻¹, an additional boost of 11.3% of the energy.

The alkoxydemethoxylation occurred at an ambient condition was highly encouraging. In the past, similar alkoxy cleavage was achieved by a purpose-built homogeneous nickel catalysts with various reductants have also been reported.¹⁷⁴⁻¹⁷⁶ However, the conventional reductant, molecular H₂, is derived from natural gas or petroleum refining in today's markets, so despite its lack of carbon, it must be viewed as a fossil resource. An interesting transition metal-free alkoxy cleavage system makes use of organosilane but requires stoichiometric amounts of reagent and strong base which limits its potential for scale-up.¹⁷⁷ The formation of phenol from guaiacol under an ambient condition, atmospheric pressure, and in the absence of external H₂ supply is remarkable. Furthermore, the heterogeneous electrocatalytic nature of the reaction makes it more favorable to industrialization compared to homogenous reaction.

Driven by the serendipities, a series of mechanistic investigation experiments were conducted to see how the demethoxylation occurred, and see if the same transformation could be performed other compounds with similar structure.

Table 3-4: Values are percentages relative to starting material buffer concentration, 12.1 ± 1.5 mM as determined by gas chromatography. Reductions employed a Raney-Nickel cathode in 30 ml of 0.1 M pH 8.0 potassium borate buffer, and a stainless steel anode coated with cobalt phosphate catalyst in 30 ml of 0.1 M pH 7 potassium phosphate buffer. Reaction started with 60 minutes of pre-electrolysis and followed immediately by compound addition and then run for 6 hours at 50 mA (8 mA cm^{-2})* at 75°C . Total current passed in this time represents $4.1 \times$ the amount required for substrate reduction to ROH and cyclohexanol. b) Cis and trans product are in equal amounts. c) Only a single peak was observed by GC. *Note: current density is calculated based on the single side electrode facing the membrane and anode compartment.

R Group					Material Balance
2-MeO	1.1	-	Traces ^b	78.9	80.0
2-EtO	1.8	-	-	90.7	92.5
2- <i>i</i> PrO	4.6	1.3	-	82.8	88.7
3-MeO	9.9	0.6	32.7 ^c	41.1	84.3
4-MeO	Traces	Traces	48.1 ^b	44.6	92.7

As shown in Table 3-4, when guaiacol is subjected to exhaustive galvanostatic ECH, cyclohexanol is the main product observed; only traces of 2-methoxycyclohexanols, direct aromatic ring hydrogenation products, are seen. Thus, ECH effects both methoxy ether cleavage and phenol hydrogenation. Importantly, under these same conditions, phenol itself readily and rapidly undergoes hydrogenation to cyclohexanol. This excellent selectivity for deoxygenation and hydrogenation appears promising for bio-oil energy upgrading. Though this aryl ether cleavage had been seen in earlier work by Lessard et al., it was not particularly noted as unusual.¹⁵¹

One possible model for interaction between the catalyst and phenolic substrates involves the aryl ring lying flat on the catalyst surface.^{178, 179} Inhibition of such binding might be expected as side chain bulk increases from methyl to isopropyl. However, with guaiacol analogues 2-ethoxy- and 2-isopropoxy phenol, the results are essentially similar to those from guaiacol. As shown in the time sequence in Figure 3-8a, the ether alkyl group size seems to have little effect, at best slightly increasing reaction rate.

The guaiacol isomers 3- and 4-methoxyphenol were also subjected to the above reduction conditions and produced cyclohexanol as major products, Figure 2b. Observable quantities of 3- and 4-methoxycyclohexanol, the direct aromatic hydrogenation products, were also observed. Individual trial results, shown in table 1, found that alkoxy group cleavage appears to be favored by closer proximity to the phenolic hydroxyl group.

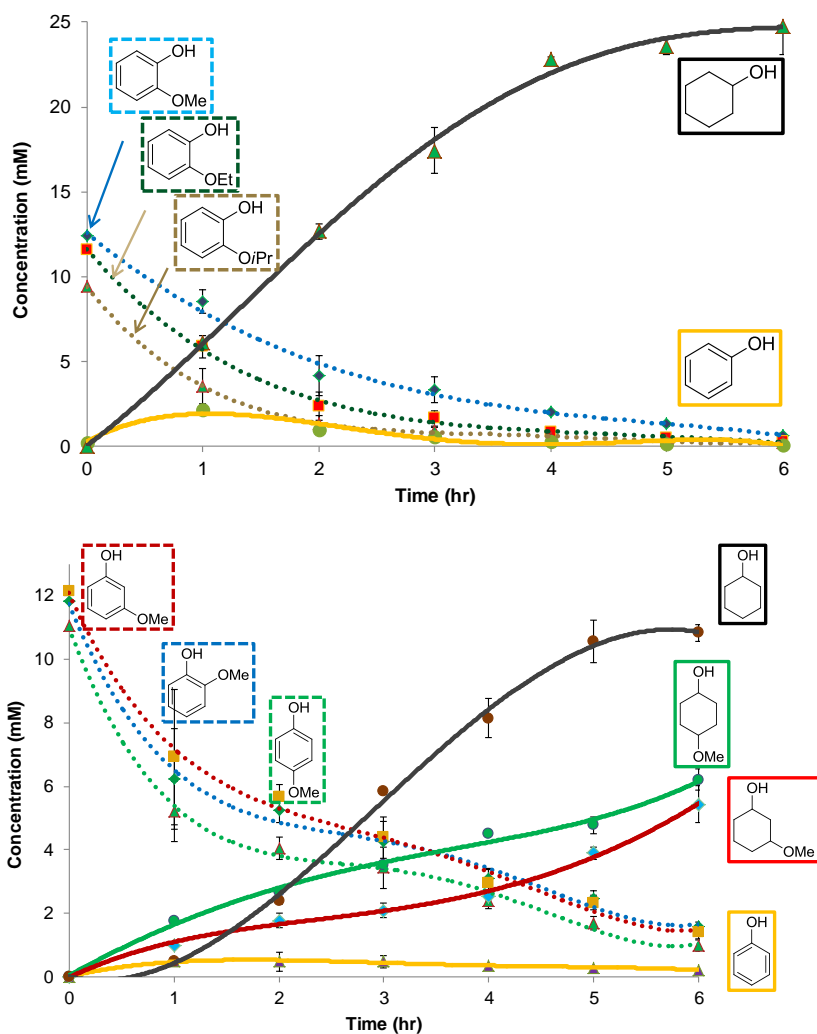


Figure 3-8a. (upper) Trial a: 1:1:1 mixture of guaiacol (---), 2-ethoxyphenol (---), and 2-isopropoxyphenol (---) undergoes electrocatalytic hydrogenation (ECH) under the same condition described in table 1. All three reactants form a common intermediate, phenol (---), which is further hydrogenated to cyclohexanol (---). Only traces of the alkoxy cyclohexanol products of direct hydrogenation were detected. Figure 3-8b (lower) Trial b: 1:1:1 mixture of guaiacol (---), 3-methoxyphenol (---), and 4-methoxyphenol (---) undergoing ECH as above. Formation of 3-methoxycyclohexanol (---) and 4-methoxycyclohexanol (---) is observable. Phenol (---) and cyclohexanol (---) were also formed as the major products. Curves are polynomial fits included to guide the eye.

In further exploratory studies, Raney Cobalt (Raney Co) and Devarda copper, skeletal metals other than Raney nickel, were examined as cathodic catalysts. Cobalt-aluminum and Devarda copper¹⁵⁰ (copper zinc aluminum) electrodes were prepared using the same method as

for the Raney nickel. Only Raney Co formed observable traces of phenol and cyclohexanol after prolonged reaction time, as expected based on Raney Co's previously noted lower reactivity relative to Raney nickel.^{124, 180} Importantly, control experiments showed that a plain nickel bar electrode completely failed to reduce guaiacol or phenol. Together, these results indicate that both demethoxylation and hydrogenations require a highly active skeletal nickel surface.

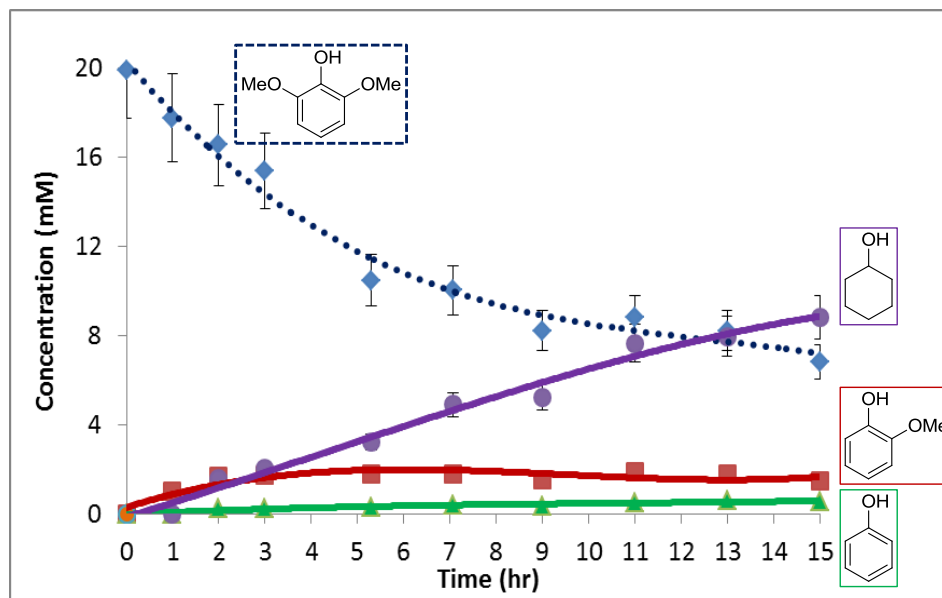


Figure 3-9: ECH of Syringol (IUPAC: 2,6-dimethoxyphenol) in 30 ml of 0.1M pH 8.0 Borate Buffer with 0.5mM CTAB at 75 °C. Syringol(---), cyclohexanol(---), guaiacol(---), phenol(---) and current efficiency(---), vertical axis on the right

Syringol (2,6-dimethoxyphenol) was also studied under the same condition, but the efficiency of the process is a lot lower compare to the 20 mM trials (Figure 3-9) . The di-methoxy character of syringol further increases the electron density of the ring and decreases of the rate of demethoxylation. This supports demethoxylation is indeed the rds. Throughout the reaction, concentration of guaiacol and phenol stayed at low level while cyclohexanol continue to build up. To our delight, we observe no formation of the 2,6-dimethoxycyclohexanol, implying the system is exclusively de-alkylation process occurs regardless the nature of the

aromatic ring. Such results show this strategy is ideal for bio-mass pyrolysis liquid processing and energy upgrading.

3.6.2 Material Balance

To probe the sequence of events in the dealkoxylation and phenol hydrogenation processes, Columbic efficiency (C.E.), the percentage of current spent on the de-alkoxylation and reduction to form cyclohexanol, was studied as a function of reaction time.

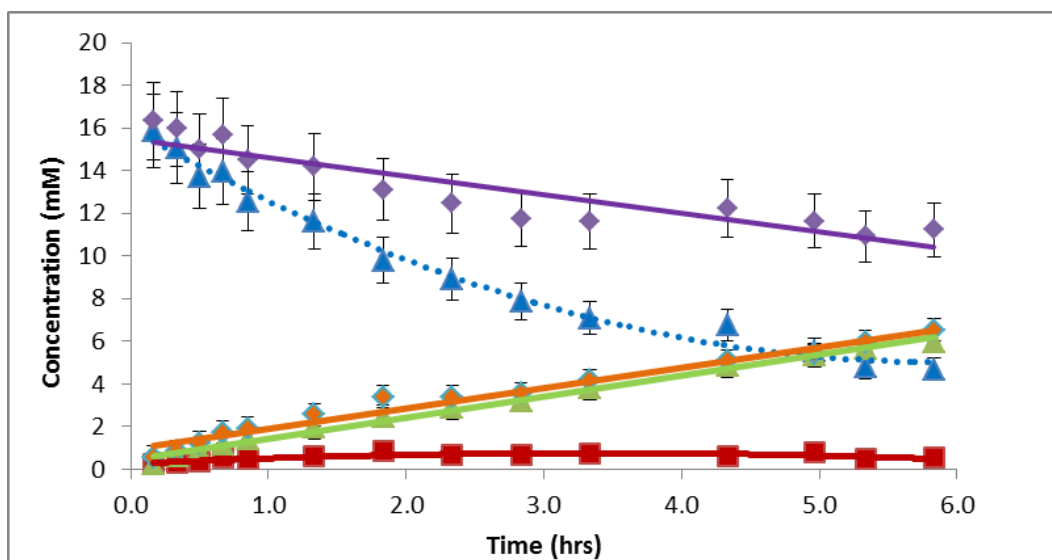


Figure 3-10: (a) Reactants, products and C.E. (%) data from ECH at 50 mA (8 mA cm^{-2})* and 75°C of 30 ml 18 mM guaiacol in 0.1 M pH 8.0 potassium borate buffer: guaiacol(---), phenol(---), methanol(---), cyclohexanol(---), and material balance (---).

As seen in Figure 3-10, cyclohexanol is produced at the expense of guaiacol. Once reaction began, phenol was observable in small amounts throughout, suggesting that it is formed and liberated but undergoes hydrogenation much faster than guaiacol conversion to phenol. In other words, the demethoxylation of guaiacol appears to be the rate limiting step.

The material balance of the reaction is calculated by the sum of substrate, and is dropping slowly during the course of reaction. A small amount of cyclohexanol was detected in the anodic chamber and suggests that diffusion of organics across the membrane may account for the

observed material losses. Compare to cyclohexanol, the alkoxyphenols might be more vulnerable to membrane crossing diffusion. The deprotonated hydroxyl group might be attracted to the positively charged anode and encouraged the diffusion process as a result. Although guaiacol and phenol were not detected in the anodic chamber, it is possible that these aromatic molecules might have been oxidized and polymerized on the anode surface.¹⁸¹

At the present stage, adsorption study on highly porous surface remains challenge to present spectroscopic techniques, we deduce the possible mechanism through various literature results with our experimentation data. Hence, we took the data Ni (111) surface adsorption as the ground of our analysis. Studies suggested that phenol and aniline both adsorbed through the pi-ring interaction on metallic nickel surface^{178, 179} This suggests hydrogenation of the pi-bond between the hydroxy group and methoxy group shown in scheme 3 is unfavorable as both oxygenated group will disfavor the adsorption for such reaction to occur.

This could be due to the retention of the adsorption of the aromatic substrate, which eventually got hydrogenated and desorbed from the electrode surface. A simple adsorption experiment was conducted to investigate the amount of adsorption of phenol, the intermediate substrate, on the electrode surface and the method is illustrated in Figure 3-11. A new Raney nickel electrode was submerged into 30 ml of electrolyte solution containing 295.5 μmol (9.85 mM) of phenol without current passing for 5 minutes, and then washed with the borate buffer electrolyte for 5 minutes. The electrode was then subjected to a new electrolyte bath for 30 minutes of electrolysis. After the initial adsorption step, only 228 μmol (7.6 mM) remained in the original phenol electrolyte solution. The electrode was the washed with clean electrolyte, in which 1.1 mM of phenol was washed away before subjecting to ECH. This purpose of this is to allow the adsorbed phenol would undergo ECH to become cyclohexanol and desorbed from the

surface. During the electrolysis, cyclohexanol was detected from the solution, indicated the amount of adsorbed phenol must have been hydrogenated on the electrode surface.

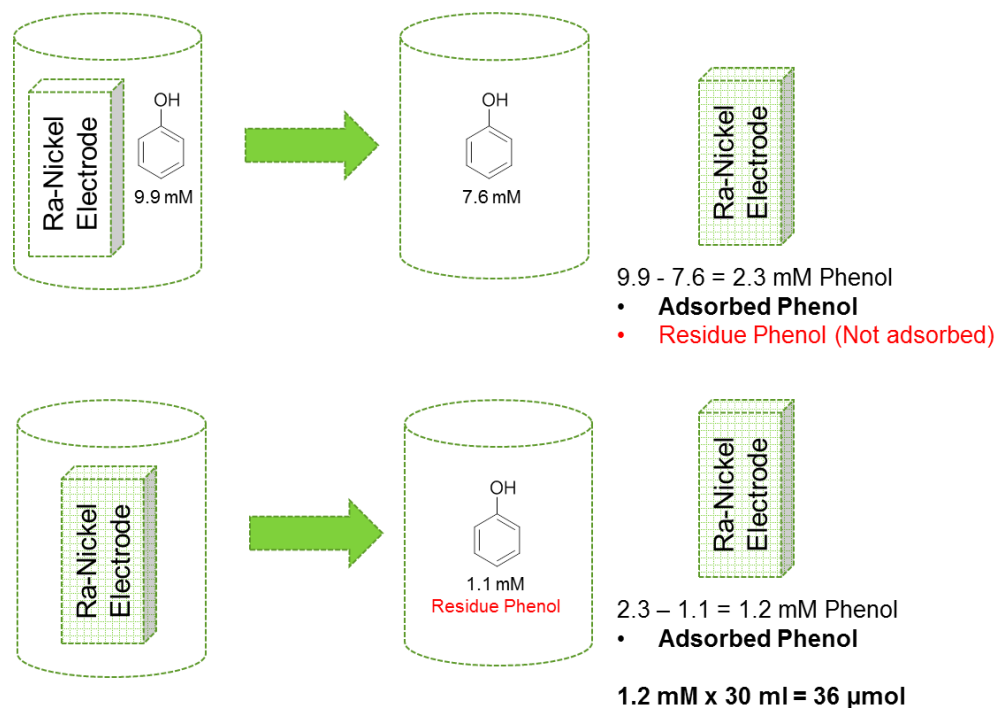


Figure 3-11: Adsorption study to investigate the cause of material loss.

The adsorption of aromatics is fall from accounting all the materials loss during the 6 hours guaiacol electrolysis shown in Figure 3-10b. Hence, a simple diffusion study of organic molecule was studied. In this control experiment, a plain nickel with use to mimic the reactions but to prevent aromatic hydrogenation. The results reviewed guaiacol and phenol were vulnerable to diffusion across the Nafion membrane at 75 °C. After 5 hours of electrolysis of 20 mM (30 ml in volume) of guaiacol and 10 mM of phenol, only 14 mM of guaiacol and 9 mM of phenol remained in the cathode compartment. 0.6 mM of guaiacol, and 1 mM of phenol were found in the anode compartment during the beginning of the ECH but disappeared in the end. This suggests both guaiacol and phenol diffused across the membrane in the beginning and was

oxidized on the anode surface. The diffusion studies accounts for the loss of materials, and suggested Nafion membrane as a compartment separator should be reconsidered. Search for other compartment separators is currently underway to improve the material balance due to diffusion.

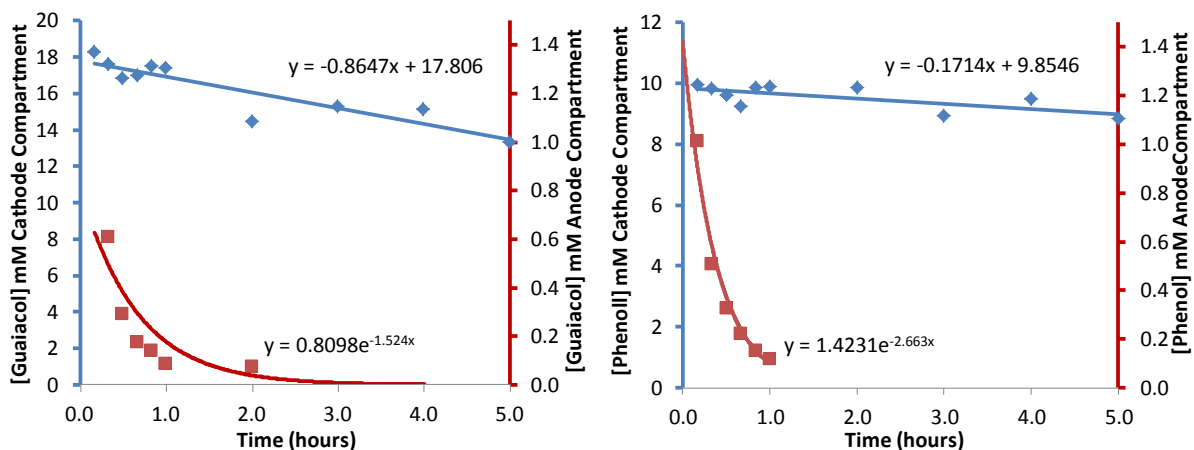


Figure 3-12: Diffusion test on guaiacol and phenol under experimental condition. Raney nickel electrode is substituted with a plain nickel bar to prevent the hydrogenation of the substrates.

3.6.3 Current Efficiency

A different approach on the Coulombic efficiency was attempted by plotting the charged (in coulomb) spent on product generation verses the amount of charged passed to the reduction shown in Figure 3-13.

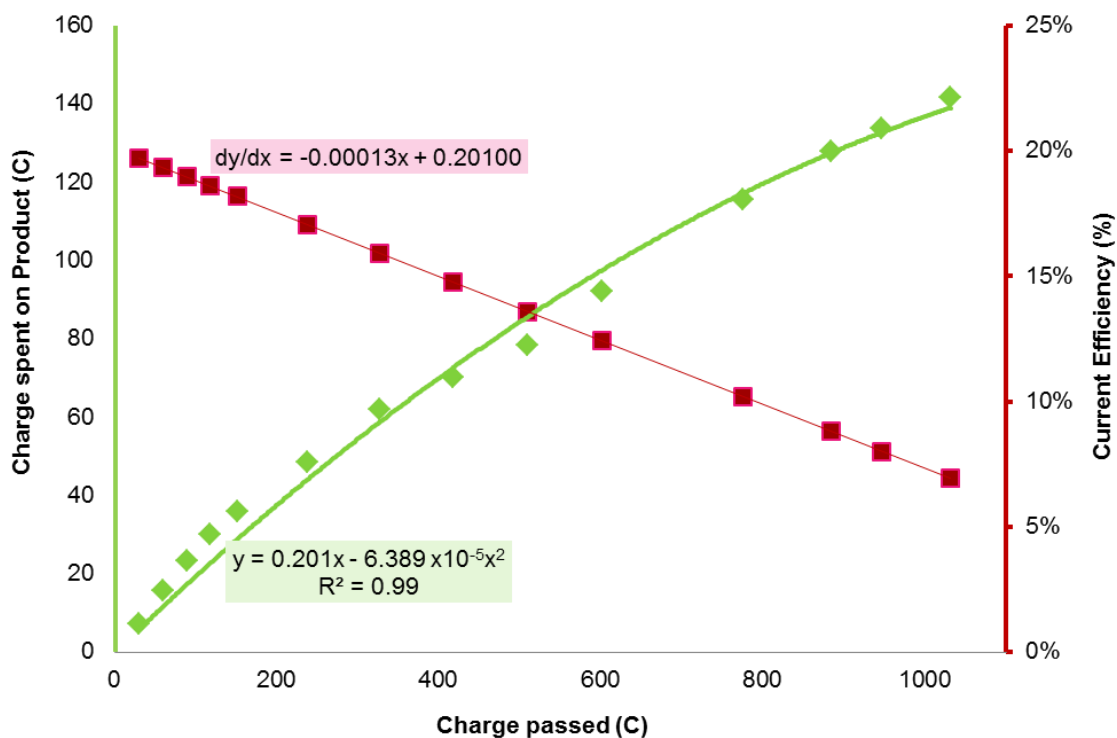


Figure 3-13: Total charged passed of the reaction vs. amount of charge spent on guaiacol reduction for the reaction shown in Figure 3-10.

Differentiation of “charge spent on product” over “charge passed” yields the function of Columbic efficiency of the guaiacol ECH reaction describes in Figure 3-10. (Note: 8 and 6 moles of electrons were consumed for each mole of cyclohexanol and phenol formed, respectively). A 2nd polynomial trend line (lime green) was applied to cover the data points of the experiment, and gave an R² value of 0.99, an excellent fitting index, and a function of $y = 0.201 - 6.389 \times 10^{-5}x^2$. Differentiating function yields: $\frac{dy}{dx} = 0.201 - 1.278 \times 10^{-4}x$. A set of data points were plotted in red with the secondary axis on the right (red) showing the highest Columbic efficiency of the process was 20.1%

3.6.4 Mechanistic Insight

The demethoxylation of guaiacol under such ambient condition was the key to the lignin model compound upgrading. To understand the process better, we postulated several schemes and conducted the study in deuterated solvent.

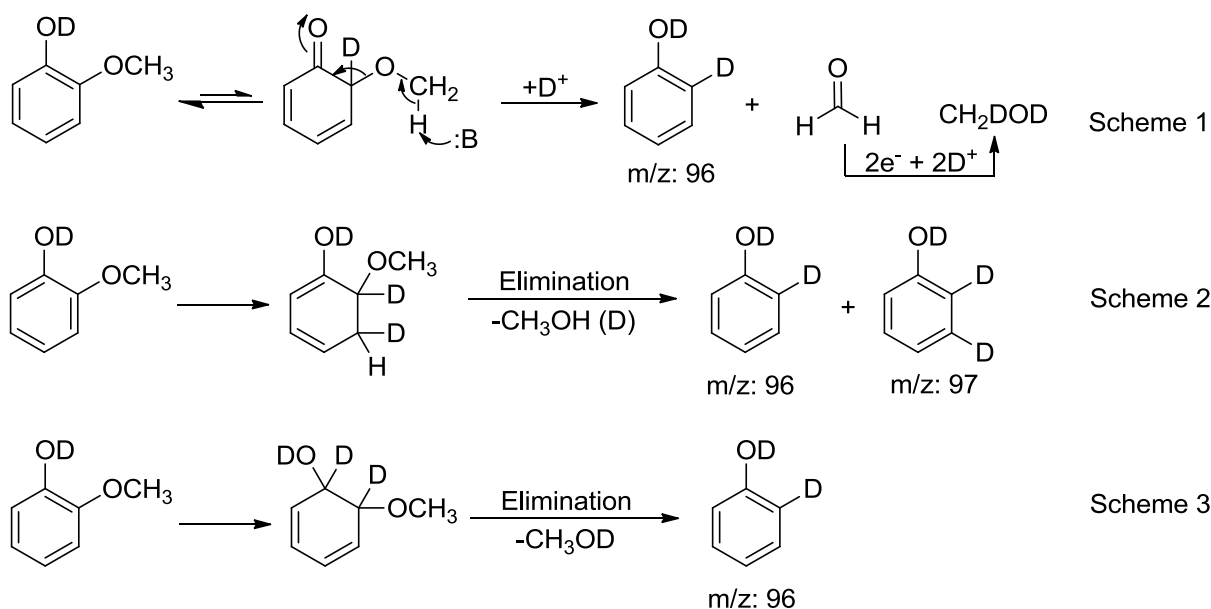


Figure 3-14: Proposed mechanism for the alkoxy-demethoxylation. Scheme 1 has been eliminated with 1H -NMR study. Scheme 2 and 3 are the probable route for the reaction.

1H -NMR showed presence of methanol, confirmed with sample spiking, with the singlet peak at 3.49 ppm in the product mixture. The presence of non-deuterated methanol suggests scheme 1 is an unlikely route as the formaldehyde produced from a basic concerted elimination would have been hydrogenated to CH_2DOD , which would show up as a triplet.¹⁸²

ECH of guaiacol was run in a similar condition as described in the experimental section using D_2O as a solvent. Reaction was only allowed to process 30 minutes instead of 6 to capture all 3 components: cyclohexanol, phenol and guaiacol. Sample was analyzed by both 1H -NMR and GC-MS to determine the possible mechanistic pathway by which guaiacol underwent demethoxylation. Control experiments, where both guaiacol and phenol independently subjected

to 75 °C in an pH 10.5 borate buffer for 6 hours, showed no deuteration on the aromatic ring in the absence of Raney nickel.

In principle, the deuterium installation on the phenol ring could provide valuable insight of the demethoxylation since phenol generated from Figure 3-14 scheme 2 would result in di- and tri-deuterated phenol in equal amount while Figure 3-14 scheme 3 will result solely di-deuterated phenol. However, it occurred the formed phenol would undergo deuterium exchange immediately at an unexpectedly high rate. The structural memory of the phenolic ring was erased by the natural H/D exchange and led us to an indecisive conclusion of the demethoxylation mechanism.

In addition to the deuterium study, we have also studied the reaction in the presence of p-cresol, as a phenol competitor. Control experiment showed p-cresol and phenol hydrogenated at approximated the same rate. 1:1 and 1:2 ratio of guaiacol to p-cresol was subjected to ECH, and we observed the formation of cyclohexanol is sensitive to the present of p-cresol, which appears to be competing with the phenol for the aromatic hydrogenation site. This indicates the formed phenol must have desorbed from the surface, and competes with p-cresol for the hydrogenation site.

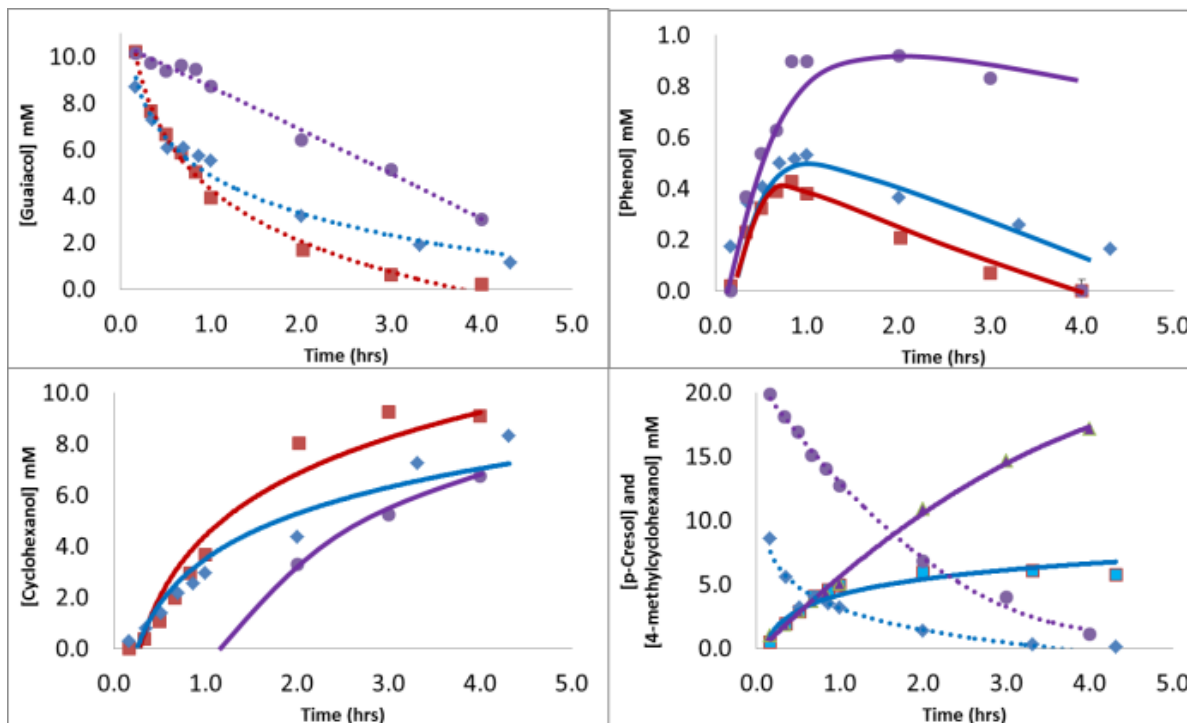


Figure 3-15: Competition study of 10 mM guaiacol in the presence of various amount of p-cresol. Upper left (a) guaiacol analysis, upper right (b) phenol analysis, lower left (c) cyclohexanol analysis and lower right (d) p-cresol and 4-methylcyclohexanol analysis: With 20 mM of p-cresol added (---), with 10mM of p-cresol added (---), and no p-cresol added (---). Legends are same across all figures, each figure focuses on the specific compound of interests specified on the vertical axis.

Interestingly, p-cresol also seems to be inhibiting guaiacol consumption as shown in Figure 3-15. This leads us to believe p-cresol could be occupying the same reaction site that achieves demethoxylation on guaiacol. If the two reactions: demethoxylation and aromatic hydrogenation were taken place at two different sites, guaiacol depletion would remain unaffected in the presence of p-cresol, and that is contrast to the evidence showed on Figure 3-15. Along with the Figure 3-14 scheme 2 on the mechanistic equations, we postulate a mechanism where guaiacol first adsorb on an active site and get partially hydrogenated, followed by the release of the partially hydrogenated ring. The desorbed product is recirculated in the solution

and goes through a basic elimination to produce the corresponding alcohol, methanol in the case of guaiacol, and restore the aromaticity to become phenol.

Cyclohexanol formation in the presence of 20 mM p-cresol formed significantly slower than other two listed condition as shown in Figure 3-15c. Together with the information from Figure 3-15b, it could be established that p-cresol was an effective phenol competitor substrate for the adsorption/desorption study. Figure 3-15d was provided to illustrate the p-cresol was converted into 4-methylcyclohexanol without reacting with other substrate in the reaction.

In further pursue of the mechanism, we have other similar substrates to explore the demethoxylation process. Anisole did not undergo demethoxylation to produce benzene but slowly goes through demethylation to produce phenol instead. and the stability of the resulting anion, phenolate or methanolate, is crucial to the reaction. Moreover, this also implies the presence of hydroxyl group is crucial to the demethoxylation process, leading to the involvement of tautomerization during the reaction.

Similar to guaiacol, o-anisidine (IUPAC: 2-methoxyaniline) also underwent demethoxylation producing aniline. However, the formed aniline was not hydrogenated to aminocyclohexane¹⁸³ as aniline is lesser favorable to hydrogenation compared to phenol with nickel catalyst.^{183, 184} To support the foreign calculation data, all the possible pathway of the guaiacol were mapped out. Base on the calculated hydroxyl-aromatic adsorption energy on the Ni (111) surface along with the possible de-alkoxylation pathway, the cresol, and syringol results, we proposal the mechanism goes through a stepwise hydrogenation sequence followed by an alkoxy elimination to form phenol as shown in the following scheme:

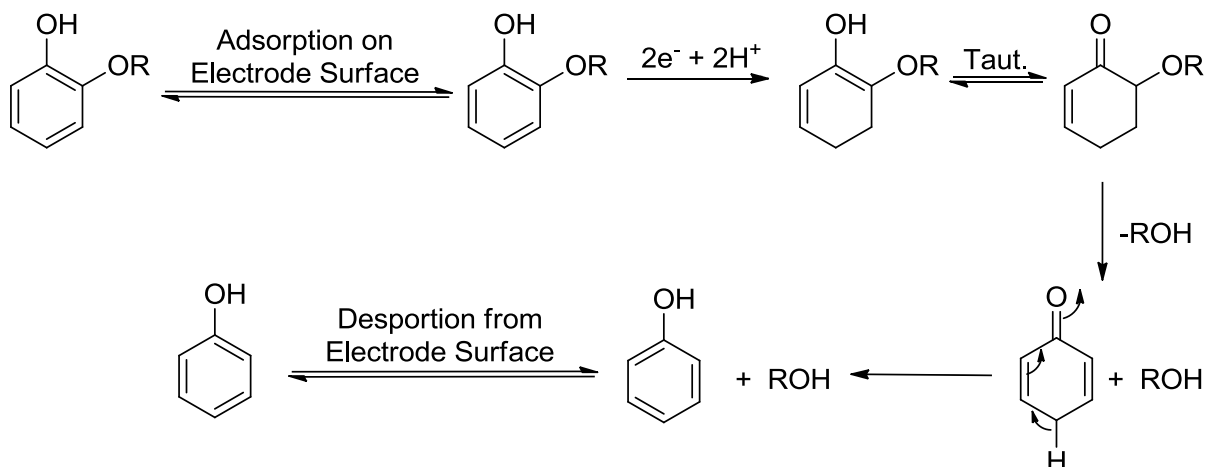


Figure 3-16: Possible mechanism for the de-alkoxylation of 2-alkoxyphenol

3.7 Summary

This chapter described a mild electrocatalytic deoxygenation/hydrogenation process for reduction of lignin model compounds in a simple, low-cost system that avoids the use of precious metal or costly molecular catalysts. Remarkably, instead of arene reduction, the first event in ECH of alkoxyphenols is the cleavage of the aryl-OR ether bond. The anode's cobalt-phosphate water oxidation catalyst selectively oxidizes water and prevents corrosion. The cobalt-phosphate system served through our typical 6-hours reactions, and the 16-hour syringol trial with no signs of degradation. Also, though Nafion is known to transport cations, no cobalt was detected by EDX on the used Raney nickel cathode. On the other hand, the Raney nickel cathodes were found to lose their catalytic hydrogenolysis activity over longer reaction runs. We will report on our efforts to stabilize the Raney nickel ECH electrodes in a separate publication.

This upgrading scheme opens a new way to maximize yields from biomass-based feedstocks via carbon-retentive energy upgrading using renewable electricity. In turn, it represents a strategy for buffering demand-mismatched production of solar or wind energy by storing it in a fungible chemical form.

To optimize efficiency and working lifetime of the system, areas of ongoing development include improvements in cell design, energy and Columbic efficiency, and cathodic electrocatalyst stability. The organic chemical transformations described here also have synthetic potential. Studies to probe selectivity and mechanism of the aryl ether cleavages, and to extend the range of substrates are also underway.

Chapter 4 Electrocatalytic Hydrogenation of Aliphatic Model Compounds in a Solid Polymer Electrolyte Electrolyzer (SPEE)

4.1 Introduction

Reduction of the bio-oil lignin monomer, guaiacol, has been demonstrated in a conventional dual compartment cell where a mildly basic borate buffer solution was employed as a supporting electrolyte. The selective aromatic ether dealkoxylation observed under nearly ambient conditions of pressure and temperature was encouraging. However, the need for added electrolyte creates a barrier to ECH implementation in large scale processing; use of electrolyte salts incurs materials and disposal costs; solubility of inorganics in bio-oil may be limiting; and organic supporting electrolyte are often expensive. In order to make ECH attractive for fuel production, the simplest process and cheapest chemicals possible should be used, while expensive electrolytes should be avoided. Moreover, the energy input for fuel production should be kept at minimum to make the processing energetically and economically favorable.

The solid polymer electrolyte electrolyzer (SPEE) project began with two thoughts: can the two electrodes be placed right on the membrane surface a) to minimize the potential needed to drive ion transport, and b) to eliminate the use of electrolyte by oxidizing water at the membrane surface, generating protons for conduction through the membrane. This latter idea was inspired in part by Professor Nocera's artificial leaf design in which the two electrodes were built on a silicon wafer to create a closed loop ion transport system for water electrolysis.

In many ways, the SPEE functions very similarly to a chemical fuel cell. In a chemical fuel cell, for instance the hydrogen fuel cell, hydrogen gas passes through an electrode that is loaded with hydrogen oxidization catalyst, typically platinum on carbon. The oxidized hydrogen (proton, H^+) then travels through a proton exchange membrane, typically Nafion, while the

electrons travel through the circuit. When the protons reach the other side, they react with oxygen plus electrons to form water. Formation of water is exothermic, which means that the reaction is thermodynamically favorable. For every water molecule that forms, four electrons are “dragged” from the anode to cathode. The demand for electrons generates voltage, and therefore, current to power electronic devices. Chemical fuel cells exploit the relative thermodynamic stability of the reaction product, water in the case of H₂ fuel cell, to power the movement of electrons. In short, chemical fuel cells harvest electrical energy from exothermic reactions. (E.g.

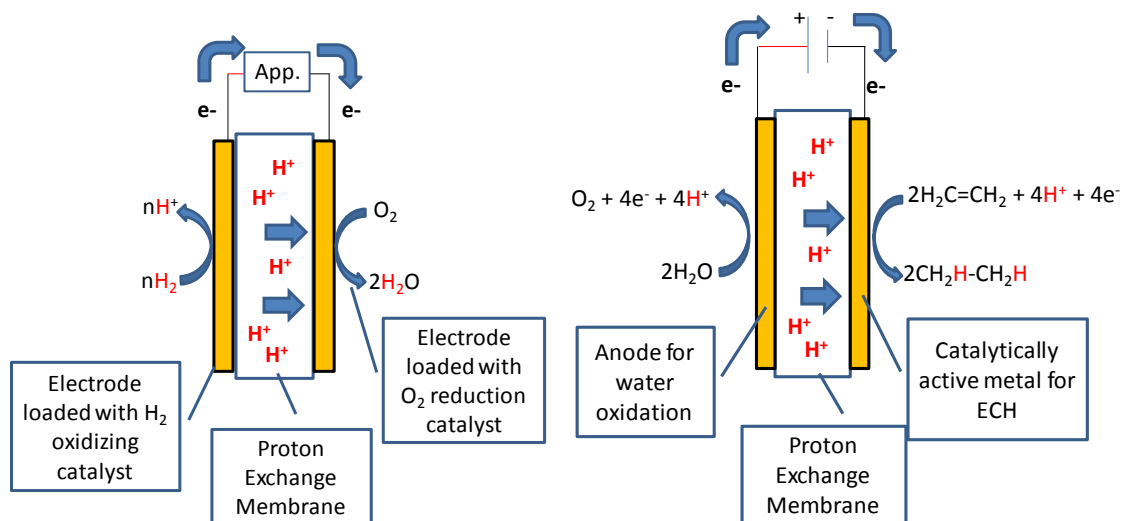
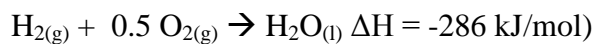


Figure 4-1: Schematic diagram to show the (Left) operating principle of a chemical (H₂) fuel cell and (Right) how the SPEE operates. Note: App. is short for electronic applications

Instead of transforming chemical bond energy into electrical energy, the SPEE takes electrical energy and in this project, stores it as chemical energy by modifying the molecules found in bio-oil via hydrogenation. The SPEE adopts the chemical fuel cell setup but uses electrical energy for electrolysis. The close proximity of both electrodes to the membrane surface allows ions to travel from anode to cathode without going through the reaction medium. This enables the reaction to happen at a moderate voltage in an ion-deficient environment.

In the past, Ogumi *et al.* published a series of reports to demonstrate the use of the solid polymer electrolyte electrolyzer (SPEE) in various organic electro-syntheses.¹⁸⁵⁻¹⁹¹ In his work, platinum was first deposited on the membrane using the Takenaka-Torika (T-T) method¹⁹² followed by electro-deposition of different metals such as gold¹⁸⁷, copper¹⁸⁹, zinc¹⁹¹, antimony¹⁹¹ and manganese¹⁹⁰. A notable success in this series is the Kolbe reaction; this oxidative decarboxylation and radical dimerization based on carboxylic acid was achievable on a platinum modified membrane in a SPEE setting.^{186, 193} Soon after, the use of the SPEE in waste water treatment such as organic dehalogenation¹⁹⁴, NO_x reduction¹⁹⁵⁻¹⁹⁹, water electrolysis²⁰⁰⁻²⁰², and organic synthesis^{191, 203-208} emerged in the literature.

The use of conventional hydrogen fuel cell membrane electrode assembly (MEA), made of platinum catalyst carbon paper, had also been reported in food hydro-processing and more.²⁰⁹⁻²¹² Recently, the SPEE has been utilized in demonstrating production of valuable chemicals from bio-oil abundant compounds.²¹³⁻²¹⁵

It must be noted, however, that all of the examples mentioned above require the use of platinum or other expensive metals for MEA construction. Seeing that the goal is to industrialize bio-fuel production using bio-oil, the use of expensive metals should be avoided if possible. Of the literature surveyed, only one example was free of precious metals; in this case, silver was deposited instead of platinum on the membrane surface before the deposition of other metal catalysts. The reaction hydrogenated benzaldehyde to benzyl alcohol with only a modest Columbic efficiency (11 – 23%).²¹⁶

Seeing the potential benefits SPEE can bring to renewable fuel production, this project seeks a low cost metal that can catalyze organic hydrogenation with good catalytic activity and longevity. The goal is to develop a scalable continuous flow style SPEE reactor that can serve as

an immediate upgrading unit at the bio-oil exhaust shown in Figure 4-2, and produce a partially saturated bio-oil stable enough to be stored and transported.²¹⁷ The primary function of the SPEE will serve as a bio-oil stabilizing unit by hydrogenating carbonyl and organic acid reduction. Catalysts capable of such reduction as well as aromatics hydrogenation should be targeted.

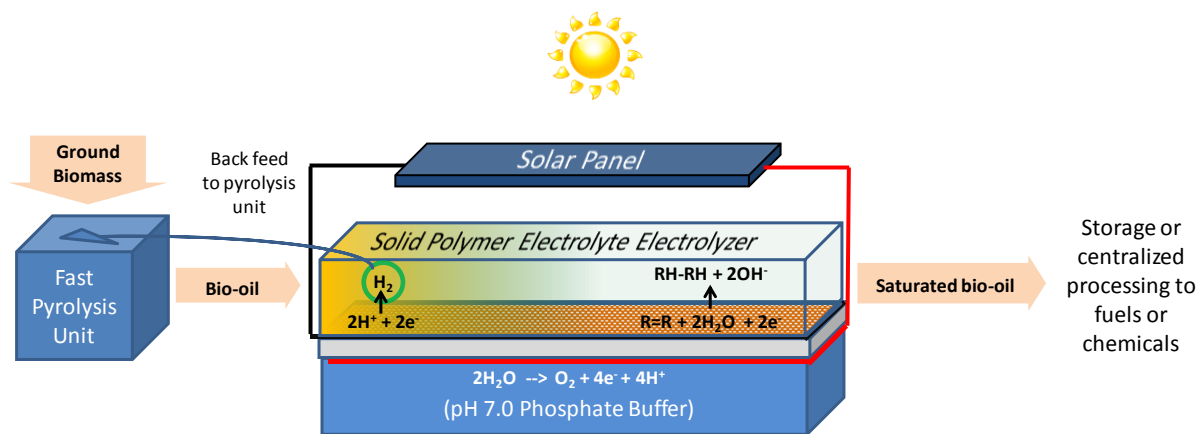


Figure 4-2: Solid Polymer Electrolyte Electrolyzer processing unit that connects to the fast pyrolysis unit. Bio-oil can be upgraded immediately upon exit.

4.2 Preliminary Experiment I – SPEE Designs and Construction

The SPEE project has been ongoing for 2 years. Different versions of reaction cells have been designed to address flaws and to optimize the Columbic efficiency of ECH. The project began without awareness of the precedents of any SPEE or related work. The term solid polymer electrolyte electrolyzer (reactor) was not known to the project until encountering the term from a chemical fuel cell review. Hence this project began with the concept of constructing a reversed fuel cell using low cost materials.

Unfortunately, all chemical fuel cells reported in the literature used research-grade chemical fuel cell equipment, which are extremely costly and time consuming to make. Moreover, these fuel cell reactors are designed to handle a small quantity of gas flow and hence it is less practical to use them for solution phase hydrogenation reaction. Due to the under-

equipped and proto-type nature of this project, a simple small glass cell was made in the chemical glass shop to serve as a proof-of-concept apparatus.

4.2.1 Preparation of the Membrane Electrode Assembly (MEA)

The MEA is the core part of the fuel cell where the reaction takes place. Hence the preparation procedures followed a reported method.²¹⁸

The MEA was prepared by the conventional paint and dry method. First a dry piece of carbon paper (2 x 2 cm, Toray, TGP-H-060) was weighed and then painted with the catalyst solution, a suspension of 1 gram of nickel or copper powder (mesh 325) per 25 ml of isopropanol. The painted carbon paper was then dried with a heat gun and reweighed. The process was repeated until 5 mg cm^{-2} catalyst was loaded onto the catalyst surface. The treated carbon paper was stored on a weighing boat inside of a dry dessicator until use.

The treated carbon paper was placed in the center of a dry Nafion N117 (2.5 x 2.5 cm) membrane, with the catalyst loaded side facing the membrane. Then, they were sandwiched between two layers of 5 x 5 cm of clean fiber glass reinforced silicon (commonly used as gas diffusion gasket in a hydrogen fuel cell setup) to provide support and prevent the Nafion membrane from melting onto the heat plates. The four sides of the gasket were carefully sealed with masking tape without distorting the membrane-carbon paper position. The resulting packet was heat-pressed at 135 °C at 1746 pounds (based on the dimension of the gasket $25 \text{ cm}^2 = 3.88 \text{ inch}^2$, approximately 450 psi) for 3 minutes on each side. After that, the packet was removed from the heat-presser, cooled to room temperature, and the carbon-Nafion composite was taken out from the gasket support. The composite served as the MEA for the reaction.

4.2.2 Construction of the 1st Generation SPEE – The Prototype

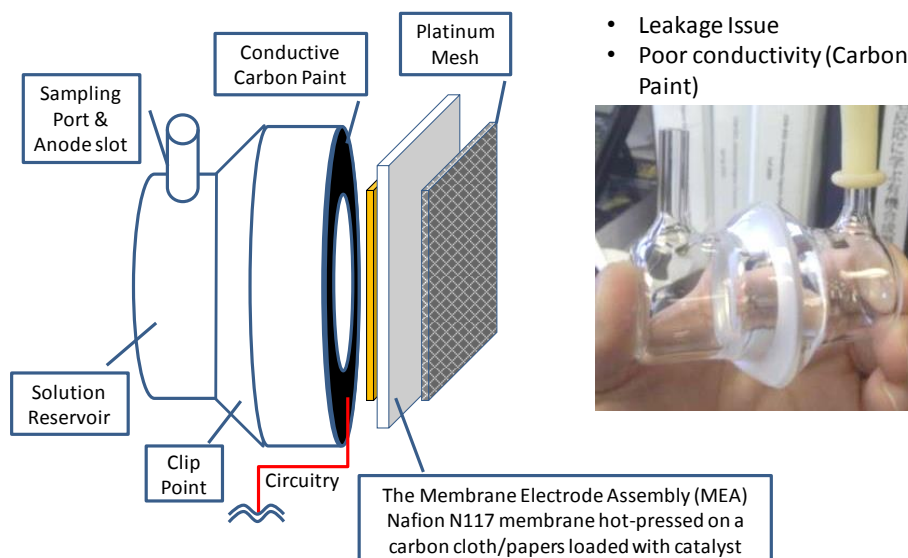


Figure 4-3: Schematic drawings of the 1st SPEE cell made of two identical pieces as shown in the figure on the right, these two halves are held together with a cell metal clip.

The prepared MEA was placed in the reaction cell shown in Figure 4-3. The carbon paper served as the cathode and its compartment was filled with 8 mL of 50 mM acetophenone dissolved in deionized water. In the anode compartment, a platinum wire was placed approximately 2 cm away from the Nafion membrane in 8 ml of 0.5 M sulfuric acid. An arbitrarily picked target current, 100 mA (actual current fluctuate at 98 ± 2 mA, and the practice is implied for the rest of the project unless it specified otherwise), was applied to the system. After 3 hours of reaction time, the cathode solution was extracted with diethyl ether which was evaporated under a N_2 flow to yield a concentrated organic residue. A small drop of the residue was then dissolved in d-chloroform and analyzed by 1H -NMR spectroscopy. The product yield was to be determined from the ratio of the aromatic hydrogens of acetophenone and the hydrogenated product, 1-phenylethanol. (Comparison between the aliphatic methyl groups is also

a viable option) Unfortunately, no reduction was observed, partly owing to the fact that the setup suffered from several flaws:

- a) Solution from both compartments leaked easily because of the heterogeneous nature of the carbon paint. The dried paint created an uneven surface which prevented effective sealing, causing leakage in the compartment.
- b) The carbon paint, which served as the current collector, lacked conductivity. While the carbon paint was good enough for SEM analysis that ran at several tens thousands volts, it was not conductive enough for the SPEE that ran at less than ten volts.
- c) The Nafion membrane swelled when it was hydrated. The swelling caused the “crispy” carbon paper to detach.
- d) The connection with alligator clips was not well considered. The cell lacked a defined location to host the alligator clip. When the alligator clip was clipped to a little exposure of the wet carbon paper during the reaction, the sharp teeth bit off the paper easily.

Summarizing the flaws, the design required several modifications. The carbon paper needed to be replaced with a more durable material such as carbon cloth. The carbon paint current collector had to be replaced with a material that was stronger, more conductive and would not enable leakage. The cell would preferably hold more than 8 mL solution so that minor leakage would not impact the experiment as much. With these ideas for improvement in mind, a new design, shown in Figure 4-4, was created.

4.2.3 Construction of the 2nd Generation SPEE

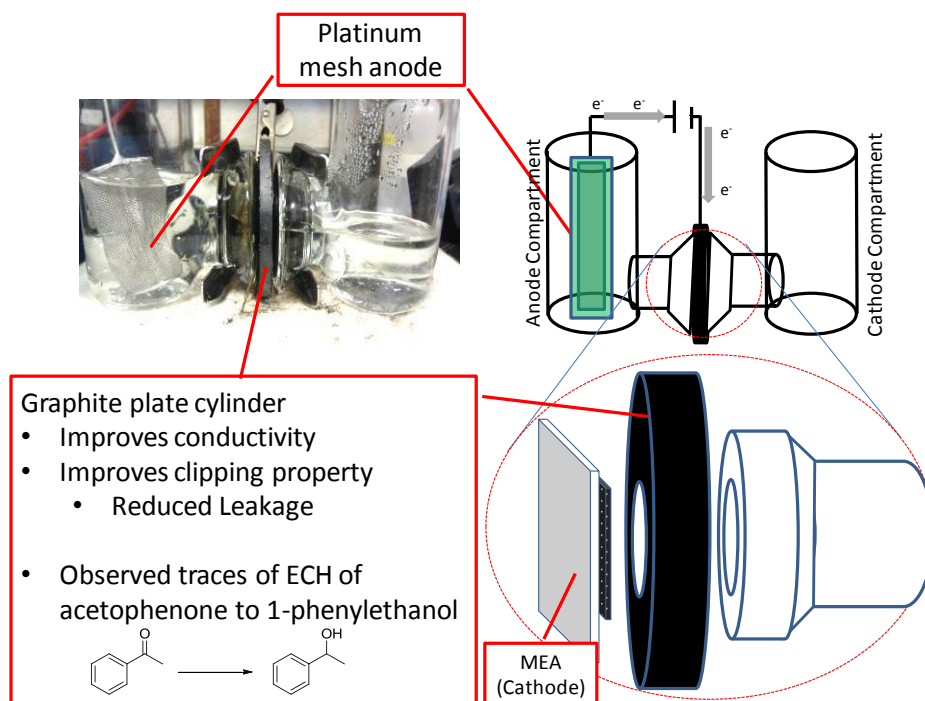


Figure 4-4: Schematic drawings of the 2nd SPEE cell which combines conventional dual compartment electrochemical cells with SPEE concepts together.

In the 2nd SPEE cell, the MEA cathode was prepared with the same procedure described above except with carbon cloth (Vendor: CST, Model #: CF11X). A platinum mesh was employed as the anode in 30 mL of 0.5 M sulfuric acid. The cathode compartment contained 30 mL of 50 mM acetophenone.

Solution leakage improved slightly with the graphite plate. The plate withstood the alligator clip bite and improved the conductivity between carbon cloth and the alligator clip. Replacing carbon paper with carbon cloth improved the durability of the MEA; however, the used MEA had to be handled with extreme care because the cloth was only loosely attached to the membrane after electrolysis again due to the membrane swelling.

In general, minor leakage at the rate of one drop every 2 – 3 minutes was observed in this setup. Even though the 2nd SPEE cell was far from ideal, traces of product, 1-phenylethanol were

observed from $^1\text{H-NMR}$ spectroscopy with the MEA prepared with copper powder. The result needed improvement, but supported the SPEE concept as a viable option for bio-oil upgrading. Even though the overall procedure was tedious and the setup in general took more than 30 minutes (as opposed to 10 minutes on the 4th SPEE cell), the observation of acetophenone reduction was encouraging.

4.2.4 Construction of the 3rd Generation SPEE

After a vigorous literature search on chemical fuel cells seeking ideas for improvement, the term “solid polymer electrolyte” came up in one of the ECH reviews. With a deeper search on the term, all the research mentioned in the introduction came to light. Combining the new knowledge and the lessons learned from the 2nd SPEE designs, the 3rd SPEE setup was created.

Two pieces of glass 5 x 5 x 0.5 cm with tracks (about 1 mm in depth created via the sand blasting technique by Scott Bancroft, an experienced chemical glassblower) was employed to host the MEA. The MEA was prepared as described above with the carbon cloth. Multiple layers of Parafilm were used as a gasket to provide a physical buffer between the MEA and the glass cell to reduce solution leakage. The platinum wire was placed inside of the anode compartment track which was connected to a reservoir (approximately 200 ml) of 0.5 M sulfuric acid solution. 10 mL of 50 mM acetophenone cathode solution was also circulated by peristaltic pump at 0.8 mL min⁻¹. The overall setup was held tightly with a carpentry clamp, which was modified with 2 holes to accommodate the inlet and outlet of the cathode and anode solutions. The whole setup was depicted in Figure 4-5.

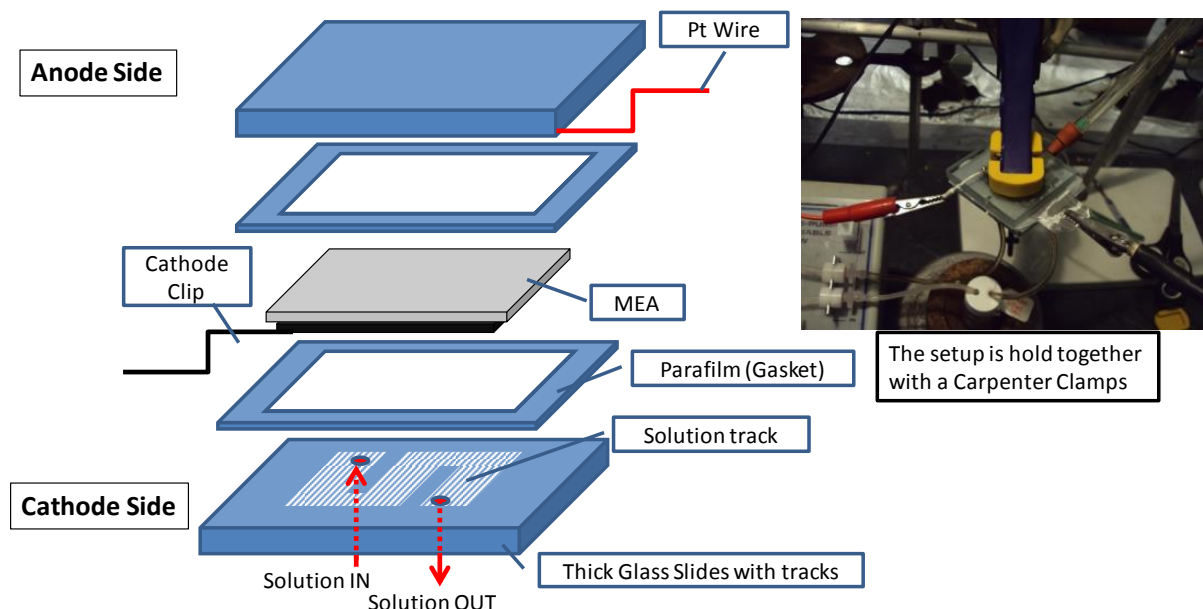


Figure 4-5: Schematic drawings of the 3rd SPEE cell – 2 pieces of glass plate that host the MEA supported by a pair of Parafilm gasket and Carpenter clamp.

The leakage issue was significantly improved compared to the previous designs. Although minor leakage occurred occasionally when the MEA and Parafilm misaligned; the setup provided a solid foundation for the SPEE project.

In an identical trial, ECH of acetophenone was conducted to compare the efficiency of 3rd cell with the 2nd cell; unfortunately there was almost no reduction of acetophenone. It was possible that the carbon cloth (0.005 inch) was too thick to allow any hydrogen ions to reach the cathode solution from the membrane's surface. Another reason could be that the hydrogen gas from water reduction generated at the cathode surface was trapped inside of the tracks, and blocked access of the cathode solution to the MEA surface. Unfortunately, when the cell was placed sideways to vent the hydrogen gas, solution from both compartments leaked. So, even

though the cell was very promising, the combination of carbon cloth MEA and SPEE had very limited success in the ECH of organic substrate.

4.3 Preliminary Experiment II – Exploring the 4thSPEE

4.3.1 Construction of the 4th Generation SPEE – The Current Version

Further searching of the literature on SPEE studies turned up an educational fuel cell company, Horizon Fuel Cell Technologies (HFCT). HFCT sold affordable grade fuel cells to teaching institutions for educational purposes. With a curious mindset and a “can’t hurt” attitude, a Solar Hydrogen Science Kit was ordered from the HFCT. The kit came with a toy-grade solar panel, a toy-grade electrical motor, measuring cylinder for the solutions, and most important of all, a palm size electrolyzer. The electrolyzer was made of two pieces of acrylic, held together by screws at the four corners. Inside of the cell, two silicone gaskets were placed between the carbon MEA and the acrylic cases to prevent leakage,

The electrolyzer housing part was ideal - another 30 of the same electrolyzers were ordered soon after, and these cells have been used for this research project since then. The 4th cell (HFCT cell) had many advantages over the first three cells. First of all, the cell rarely leaked if it was set up correctly. Second, the gaskets were held in places with the pre-implanted tracks. The screws and bolts on the corners held the cells strongly together. Most importantly, the setup typically took less than 5 minutes to assemble as opposed to almost 30 minutes for the previous designs. Also, the acrylic castings allow for easy modification if necessary.

From the literature mentioned in the introduction, the idea that Nafion membrane could be modified with deposited metals and serve as an electrode could significantly improve the overall efficiency of the SPEE. Metal deposition on the membrane surface could bypass the carbon support detachment issue due to membrane swelling. Moreover, if the metal catalyst was

deposited on the Nafion surface, it would be as intimately placed relative to the membrane surface as possible, thereby minimizing the distance for the proton ion to travel.

4.3.2 Direct Metal deposition on Nafion Membrane

There are two methods to deposit metal on a Nafion membrane surface: the internal (ion-exchange) reduction method (IR), and the Takenaka-Torika (T-T) method. For the IR method, a dry membrane is first sand blasted to increase its surface area before it is soaked in an aqueous metal ion solution. This allows the hydrogen ions from the sulfonic sites on membrane be exchanged with the metal ions in the solution. The exchanged metal ions are then reduced by soaking the membrane in a chemical reduction solution containing the reductants sodium borohydride (NaBH_4) or hydrazine (N_2H_4). Metals are reduced and deposited on both sides of the membrane but usually not in the core. Weak conductivity at several tens of mega ohm level can be observed across a face of the membrane but not through the membrane.

The T-T method only deposits metal on one side of the membrane by taking advantage of the concentration gradient and the cationic permeability nature of the Nafion membrane. For T-T deposition, a hydrated membrane is first mounted in a conventional dual compartment electrochemical cell. Then one compartment is filled with the metal ion solution, while the other is filled with the chemical reduction solution. The positively charged metal ions migrate through the membrane because of the concentration gradient, and get reduced upon arrival the other side. One precaution is that if the reductant concentration is too high, the reactant may migrate through the membrane and reduce the metal ions in the stock solution.

In Chou's work, the platinum deposited (using sodium borohydride) with the IR method was shown to be more stable than the T-T method, which the Chou paper referred to as the diffusion method. Compared to T-T method, the IR method created a more tightly bound

platinum surface was shown under SEM imaging and a higher current density was observed during C.V. analysis suggesting the surface was better at generating H₂ gas. However, when non-precious metals such as nickel, lead and copper were used in place of platinum, the MEA did not last long due to the low acid tolerance of those metals. Although reduction of benzaldehyde to benzyl alcohol was observed with the MEA prepared with the earth abundant metals, their surface erosion and resulting low conductivity necessitated exceedingly high voltage, and the experiment had to be terminated before the intended experiment time.²¹⁶

4.3.3 MEA Preparation with Different Reductants

Silver was picked to be the choice of metal foundation for the MEA preparation instead of platinum because it is cheaper and it has a lower reduction potential (a less negative E^o), which means it can be reduced easily. Although Chou's results showed silver has the lowest catalytic activity in benzaldehyde hydrogenation compared to nickel, copper and lead, the effect might be modified if other catalytic metal layers were deposited on top of the silver, as in to Ogumi's work.¹⁸⁹ Before examining the effects of different catalytic metals, it was important to prepare a well-defined silver foundation.

Silver could be reduced easily with a common reductant such as sodium borohydride or hydrazine. Though sodium borohydride (LD₅₀: 160 mg/kg) is less toxic than hydrazine (LD₅₀: 59 – 60 mg/kg), it is slightly more expensive and requires a basic environment to maintain its stability or it will be hydrolyzed by water to form H₂ gas: $\text{NaBH}_4 + 4\text{H}_2\text{O} \rightarrow 4\text{H}_2 + \text{NaB}(\text{OH})_4$. In low concentrations, hydrazine can be a safe and environmentally friendly chemical because it emits only N₂ as a by-product after it reacts. Therefore, it was reasonable to investigate the possibility of replacing sodium borohydride with hydrazine.

The results from Chou's studies suggested that the IR method preparation would give a better surface than the T-T method. Accordingly, MEA with silver surface modification was prepared by the IR method using both hydrazine and sodium borohydride. The prepared membranes were used in the acrylic cell from Horizon Fuel Cell Technologies to hydrogenate furfural, a relatively abundant compound found in bio-oil. The amount of product formed was compared to see which reductant gave a better surface for ECH of organic substrates.

4.3.4 Experimental Procedures

Preparation of the silver-based MEA began with a dry Nafion membrane, cut to the dimensions of 2.3 x 2.3 cm, which would fit the inside of the reaction cell (2.7 x 2.7 cm) after it was hydrated. The membrane was then boiled for 30 minutes in 3% hydrogen peroxide followed by 30 minutes of 50 mM sulfuric acid to remove impurities. The cleaned Nafion membrane was stored in 5 mM sulfuric acid until use.²¹⁹

The cleaned membrane was soaked in 10 mL of 5 mM silver nitrate solution overnight in a 20 ml sample vial for silver ion exchange. Glass beads were used to displace some volume if the solution could not cover the whole membrane. After that, the membrane was taken out and washed with deionized water for 1 minute before being placed in either 1% (1:99 v./v.) hydrazine solution or 0.1 M sodium borohydride solution (prepared in 0.1 M sodium hydroxide) and soaked for 4 hours. A picture on the setup is shown in Figure 4-12 later in the chapter.

The electrochemical experiment was conducted as follow: through the cathode compartment that holds about 0.2 mL, a reservoir of 10 mL of 10 mM furfural solution was circulated using peristaltic pump, and a stainless steel mesh 314 (mesh #200) was used as a current collector. For the anode compartment, a stainless steel mesh (mesh #200) was used as the anode and current collector and was placed in solution of 0.5 mM $\text{Co}(\text{NO}_3)_2$ dissolved in 0.1 M

pH 7.0 phosphate buffer (the Nocera catalyst recipe). Reactions were run for 2 hours at 100 mA at room temperature with 0.25 ml of sample taken for analysis every 30 minutes. Samples were diluted with an equal amount of deionized water prior to HPLC-UV analysis (isocratic flow at 0.5 ml ml⁻¹; 30% methanol in 0.1 M pH 7.0 water buffer; room temperature; column: Aminex HPX-87H, UV: 214 nm). The retention times for furfural and furfuryl alcohol were 37.6 and 26.0 minutes respectively.

After the experiment, the cells' compartments were flushed and stored in deionized water, and used for the same reaction the next day. Three identical experiments were run before the cells were disassembled.

4.3.5 Results and Discussion

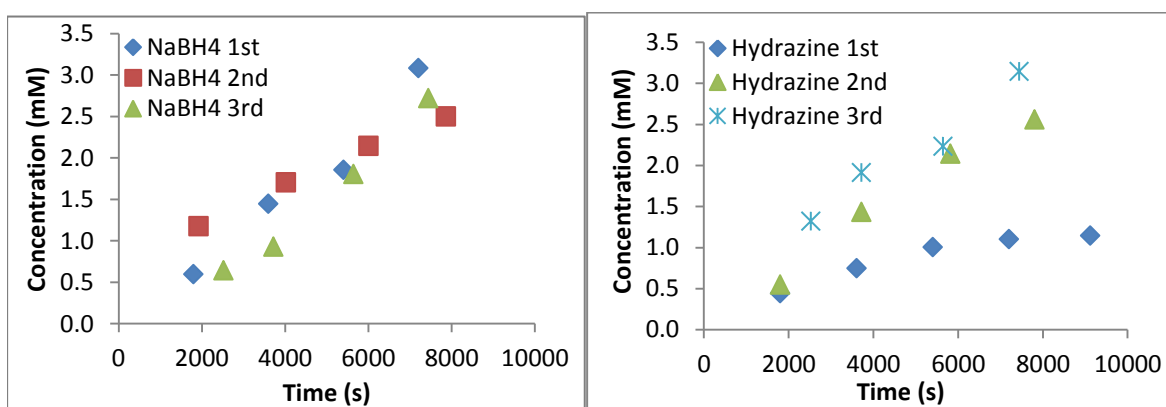


Figure 4-6: Production of furfuryl alcohol from furfural ECH in SPEE. (Left) MEA was prepared with sodium borohydride (Right) MEA was prepared with hydrazine.

Comparison between both trials in Figure 4-6, the MEA prepared with the sodium borohydride recipe was more effective in catalyzing the hydrogenation of furfural than the one prepared with hydrazine. However, interestingly, repeated use of the hydrazine-treated membrane improved the catalytic effect and the product formation rate became comparable with the borohydride membrane. This suggested that some activation process might be taking place on the surface of the silver during electrolysis on the hydrazine-reduced membrane. Control

experiments showed that hydrazine could not reduce furfural alone, and furfural could not be reduced in the absence of electricity with either one of the silver deposited membranes. In other words, the reduction could not have happened due to any traces of hydrazine or sodium hydride that might have remained in the membrane.

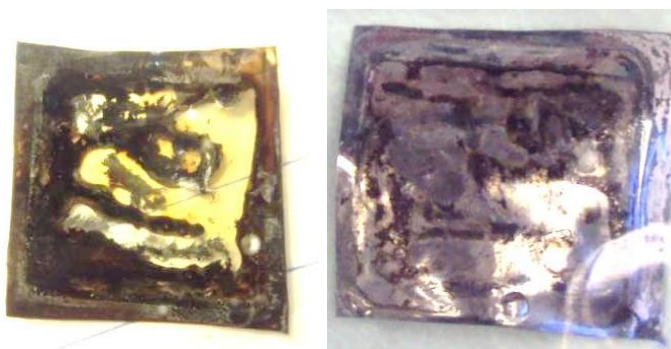


Figure 4-7: Used Ag-MEA after 3 uses of electrolysis. (Left) a used Ag-MEA prepared with sodium borohydride, and (right) a used Ag-MEA prepared with hydrazine. Conductivity measure was taken using multimeter for both membranes:

Another interesting observation was that the borohydride membrane shown in Figure 4-7 showed significant signs of erosion after the 3 trials whereas the hydrazine membrane was still looking smooth and shiny. The fact that the furfural reduction rate on the borohydride membrane was constant while the silver catalyst eroded was intriguing. One would expect the reduction rate to fall during the erosion if the silver was responsible for the reduction. This phenomenon will be examined in more detail in the next section.

In the above comparison, the membrane prepared via hydrazine reduction appeared to be more durable than the membrane prepared with sodium borohydride, and the reduction rate increase with repeated use was interesting. Even though the differences and mechanism were not fully understood, the hydrazine recipe was chosen over the borohydride method of MEA preparation because of its durability and improvement through multiple uses. Moreover, the resistance measured on the MEA prepared with hydrazine is lower than that of the MEA

prepared with sodium borohydride. $\sim 3\text{M}\Omega$ and $\sim 10\text{M}\Omega$ were measured for the hydrazine and borohydride membrane, respectively. Although both showed resistance in the mega-ohm level, this resistivity is still lower than for a cleaned membrane $\sim 16\text{M}\Omega$. The decrease in the resistance suggests silver has been deposited on the surface, but the level of deposition perhaps is not as uniform as expected. To improve the conductivity across the membrane, an additional metal was plated on top of the silver, improving reduce the cross section resistance.

4.3.6 Formation of Ag-Cu Bimetallic Layer Catalyst

In Ogumi's study, the nitro group hydrogenation of 4-bromonitrobenzene was improved by plating a layer of copper on the MEA deposited with platinum.¹⁸⁹ Compared to platinum, copper has a greater hydrogen overpotential, which makes it favor catalytic reduction of organic substrates over hydrogen evolution.⁹⁴ For this reason, a layer of copper was plated onto the Ag-MEA to see if the same effect could be achieved. The plating strategy followed Ogumi's report: 50 mM of copper sulfate solution was circulated in the cathode compartment and a 100 mA current was applied for the copper deposition. The Ag-MEA with copper deposition was denoted as Cu-Ag-MEA

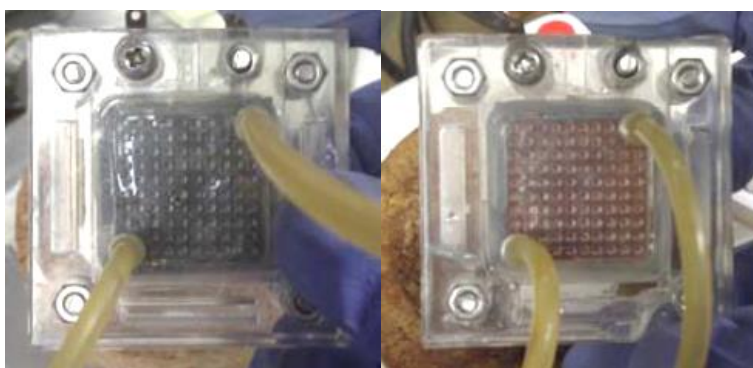


Figure 4-8: Visual comparison between (left) before, and (right) after copper plating onto the Ag-MEA

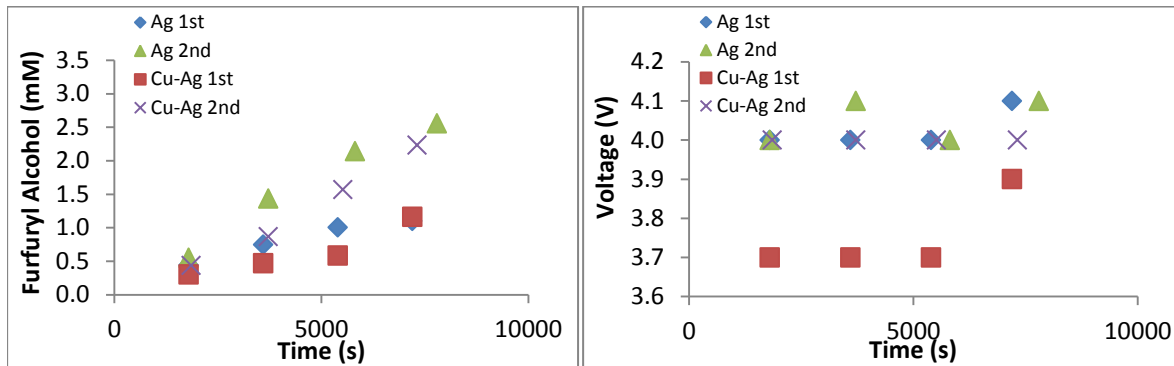


Figure 4-9: (Right) ECH of 10 ml of 10 mM furfural. Condition: Ag is deposited on Nafion using 1% Hydrazine solution. Reactions were run at 98 ± 2 mA at 1 atm at room temperature (22 ± 1 °C) for 6 hours. Note: Cu-Ag is prepared by plating copper onto the Ag-MEA electrochemically using 50 mM CuSO_4 at 98 ± 2 mA for 5 minutes. (Left) the voltage log for the reactions displayed on the right

From Figure 4-9 right, the copper plating did not have significant impact on product formation as the data points for Ag and Cu-Ag almost overlapped which suggested the copper plating had no significant effect on the reduction. With the copper plating (Cu-Ag 1st), the voltage needed for 100 mA reduced noticeably, but rises again after several hours. This rise in voltage suggests the copper may be eroded during the reaction, and interestingly, the change in copper layer does not have any effect on the reduction of furfural. Perhaps the reduction was taking place elsewhere e.g. on the current collector which would also explain why the product formation improved after the 1st use on Figure 4-6. The Ag-MEA prepared with the borohydride recipe appears to be a loose powdery surface, similar to Chou's observation for the platinum, and hence did not block the proton transport to the surface. On the other hand, the hydrazine recipe formed a smooth silver surface which blocked the proton transport. The acidic site might have been liberated due to minor erosion after the first use, which improves the proton transport and thereby increases the reduction rate. In principle the voltage log could give hints as to whether silver was blocking proton transport; blockage would be expected to result in higher voltage

during constant current electrolysis. However, the reaction area is less than 5 cm². So, with data measured to only 2 significant figures, the change may be too small to be observable. To verify the proposition, a set of control experiments were conducted to confirm where exactly did the reaction took place – the current collector or the membrane surface.

The experimental procedures in the following set of experiments evolved with minor modifications: the trials were ran for 6 hours instead of 2 to observe the reaction longer, and acetol (IUPAC: 1-hydroxypropan-2-one) was used as the model compound instead of furfural. This is because the furfural stock solution began to form dark precipitate and turn brown after 2 weeks of storage. The change in the furfural stock appeared to be resulting from furfural condensation in the aqueous environment.²²⁰ Compared to furfural, aqueous acetol was more stable. It showed no signs of polymerization or oxidation after weeks of storage. HPLC analysis of acetol and propylene glycol (hydrogenated acetol) took less time and effort compared to furfural. Hence, acetol was used as a model compound for further studies exploring the project.

To verify the importance of the current collector, current collectors with the center cut out were utilized to look for changes in the reduction rate. The area of the current collectors was reduced approximately 54.6% (1.7 x 1.7 cm was cut out from 2.3 x 2.3 cm).

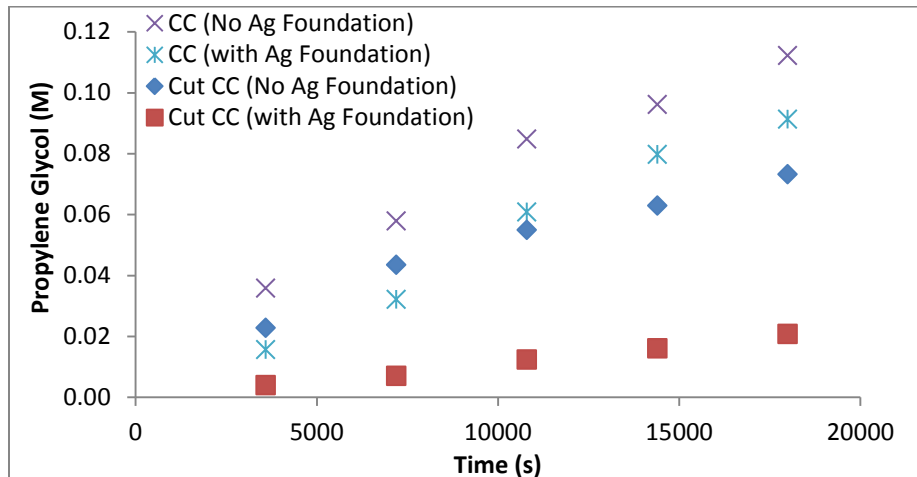


Figure 4-10: Reduction of acetol in examining the necessity of the silver foundation and the importance of the current collector.

Figure 4-10 shows that the cut current collectors have a lower reduction rate of acetol both with and without silver foundation. This is a clear indication that there is a relationship between the ECH rate and the current collector, which in turns suggests that reaction must have been happening on the current collectors rather than on the silver surface. It is interesting that these findings are somewhat in contrast to the conventional prospective, in which hydrogenation takes place on the platinum catalyst surface deposited on the membrane. It is, however, it is important to note that here, silver was used to replace platinum. Perhaps, compared to platinum, silver was less catalytically active relative to the stainless steel current collector, and hence the reduction reactions took place on the stainless steel surface instead.

The important lesson learned from the above preliminary data was that ECH can be run in the absence of a supporting electrolyte as long as the electrodes are in close contact with the membrane surface. Also, the catalyst metal does not have to be deposited on the membrane surface. In fact, metal deposition on the membrane may block proton transport. Under constant current electrolysis, the influx of proton from the anode compartment might have dissolved the silver sheet formed on the cathode surface and becomes H_2 . Protons transport improved as the

silver surface erodes; increase in proton transport led to improvement of organic reduction. This proposition is in consistence with the results displayed in Figure 4-6, where the metal modified MEA improves after the first use.

4.4 New Perspective on the SPEE and C.E. % Improvement Effort

Seeing that the silver foundation on the membrane was unnecessary, the SPEE setup was simplified to two meshes closely pressed up to the membrane surface, which resembled the setup of a micro-gap electrolyzer²⁰⁷. After this discovery, the project focused on how the cathode mesh and electrolyte environment affected the reduction rate. Current efficiency was used as a measure to evaluate the effectiveness of the system in catalyzing hydrogenation.

The first objective was to select a metal mesh that had a good catalytic effect. A literature survey found copper and nickel were the two most common low cost catalysts for electrocatalytic hydrogenation.^{98, 119, 120, 221} Unfortunately, copper and stainless steel are the only common metals available in mesh form from commercial vendors. Although nickel mesh could be made upon request, the cost was unexpectedly high and hence was not purchased.

4.4.1 Experimental Procedures

Copper meshes (mesh #200) and stainless steel 314 (mesh #200) were cut to in the dimensions of 2.3 x 2.3 cm and were stored in hexane until use. The cathode solution was 10 mL of 5% acetol with 5% acetic acid in water and the anode solution was a reservoir of 200 mL of 0.1 M pH 7.0 phosphate buffer solution. Reaction was run at room temperature.

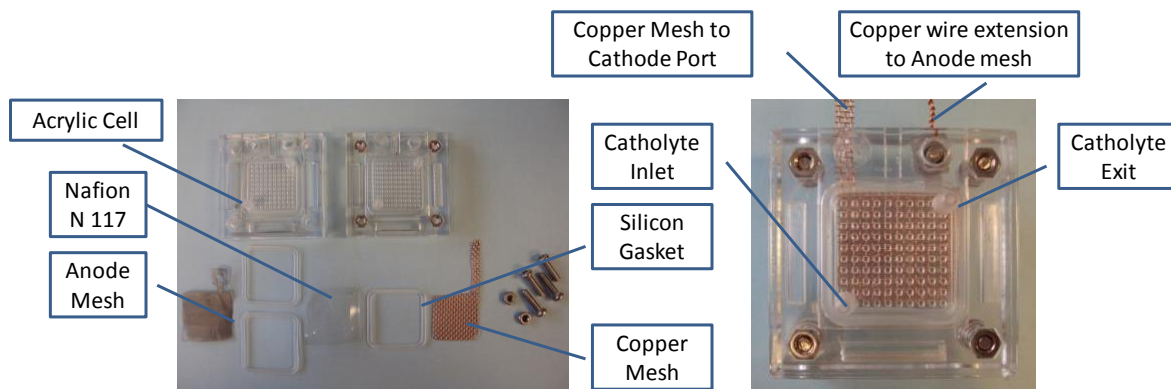


Figure 4-11: Solid Polymer Electrolyte Electrolyzer (SPEE) parts, and the setup

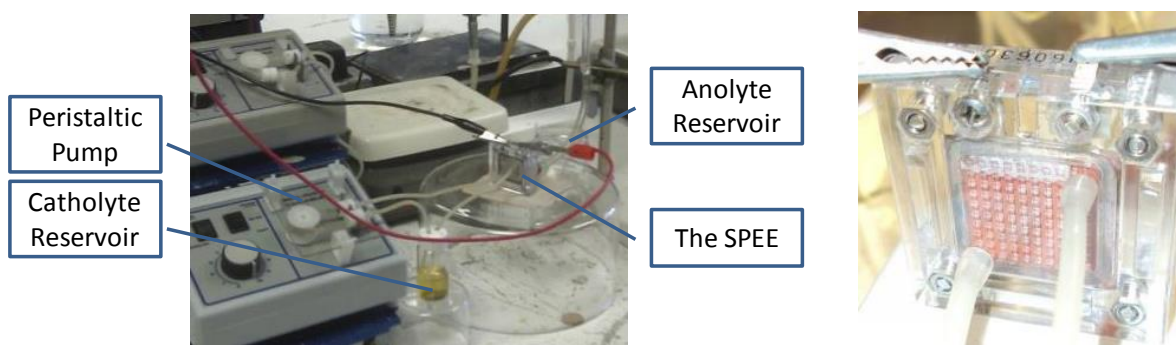


Figure 4-12: (Left) typical experimental setup of a SPEE. (Right) close-up to a SPEE with alligator clips and silicon tubing connected

The materials shown in Figure 4-11 (left) were prepared and assembled in order starting from the anode compartment (marked with a positive sign) → silicon gasket → anode mesh → silicon gasket → Nafion membrane → cathode mesh → silicon gaskets → cathode compartment (market with a negative sign).

Cathode solution was circulated by a peristaltic pump at 0.8 ml min^{-1} . 0.25 mL of sample was taken hourly from the reservoir, and was diluted with equal amounts of deionized water before HPLC-RI analysis (Isocratic flow at 0.5 mL ml^{-1} ; 5 mM of sulfuric acid; Room temperature; Column: Aminex HPX-87H, Waters 410 RI detector setting: internal temperature $35 \text{ }^{\circ}\text{C}$, Sensitivity: 128)

Table 4-1: 10 ml of 5% acetol (924.5 mM) dissolved in deionized water undergo ECH to propylene glycol after 6 hours at a constant current 98 ± 2 mA, at room temperature and ambient pressure. All current collectors are mesh 200 in size, and had been cleaned with hexane, acetone and water prior to use. Stainless steel 304 (Mesh 200) was used in a 0.1M pH 7.0 phosphate buffer as an anode for all trials. Material balance was calculated by summing acetol and propylene glycol alone. *Initial acetol concentration for the “copper with 5% acetic acid” trial was 716 mM

	Acetol remaining (mM)	Propylene glycol formed (mM)	Current efficiency (%)	Material balance (%)	End pH
Stainless Steel (Control with no e⁻ passed)	876	0	0	94.8	6.34
Stainless Steel	274	117	10.4	42.3	11.23
Nickel plated on Stainless Steel	12	319	28.4	35.8	12.28
Copper	114	398	32.9	55.4	10.88
Copper with 5% Acetic Acid*	335	152	13.8	68.0	5.23

The catalytic effect of three different metals: copper, nickel and stainless steel (SS) were compared in Table 4-1. In the absence of acetic acid, the reaction rate decreased in the following order Cu > Ni >> SS. Stainless Steel showed relatively low catalytic activity towards acetol hydrogenation, but the situation was changed when it was plated with nickel in a Watts plating bath¹.¹⁵⁵ This nickel plating confirmed the current collector mesh was the reaction surface. Copper had the highest Columbic efficiency of the three metals, and it also had the greatest material balance relative to the other two electrolysis trials. However, it must be noted that the mass balance of all the trials was surprisingly low 35.8 – 55.4%. Based on the control experiment using stainless steel, approximately 5% of the material loss was due to membrane crossover. The remaining losses were likely to be associated with the high pH of the cathode

¹ Nickel plating was done in a Watts bath at 100 mA for 5 minutes (H_3BO_3 30g L⁻¹, $NiCl_2 \cdot 6H_2O$, 45 g L⁻¹, $NiSO_4 \cdot 6H_2O$ 300g L⁻¹)

solution after 6 hours of electrolysis. The cathode solution changed from colorless to yellow which suggested acetol might have gone through aldol condensation in the increasingly basic conditions.

To verify whether acetol condensed in the basic environment, 0.1 mL of 1 M NaOH was added to the 10 ml 5% acetol solution and was left overnight at room temperature without electrolysis. The mixture turned a mild yellow color that resembled the color of the cathode solution after ECH. The sample was then analyzed by liquid phase MS (Note: no chromatography involved). Higher molecular weight compounds (presumably oligomers) were detected from the control experiment and confirmed that acetol did condense in the basic environment. The higher final pH from the nickel plated mesh trial suggested that nickel favored water reduction (Scheme 4-1, equation d) forming hydroxyl anion. Paired with the potassium ion diffusing from the anode chamber through the membrane into the cathodic chamber, it is clear that the pH increased as the reaction proceeded.

Although the condensation can lead to the formation of molecules with a greater carbon number, feature preferred for fuel purposes (typical carbon number of gasoline ranged from $C_5 - C_8$, whereas the majority of bio-oil molecules typically range from $C_2 - C_6$), uncontrollable condensation is undesirable, especially in real bio-oil where hundreds of organics are present leading to formation of unusable tar. Knowing there was already insufficient carbon to cover the US transportation sector usage from biomass, it is important to maximize the utilization and minimize losses of carbon during the upgrading process.

- a) $2\text{H}^+ + 2\text{e}^- \rightarrow \text{H}_2$
 b) $\text{Acetol} + 2\text{e}^- + 2\text{H}^+ \rightarrow \text{Propylene Glycol}$
 c) $\text{Acetol} + 2\text{H}_2\text{O} + 2\text{e}^- \rightarrow \text{Propylene Glycol} + 2\text{OH}^-$
 d) $\text{H}_2\text{O} + 2\text{e}^- \rightarrow 2\text{OH}^- + \text{H}_2$

Scheme 4-1: Possible cathodic reactions: a) Hydrogen evolution b) acetol undergoes ECH to propylene glycol using electrons and protons c) acetol undergoes ECH to propylene glycol using water and electron as a reductant. d) cathodic water reduction forming hydroxide anion.

Based on the molecular weight information gathered from direct MS analysis of the solution, the processes shown in

Figure 4-13 were proposed to explain the material losses during the ECH experiments. Understanding how condensations could lead to material loss could be helpful in deriving an upgrading strategy that maximizes carbon retention. Compound structures were proposed based on detected MS parent peaks with knowledge of aldol condensation, and estimated quantity was given based on their relative height.

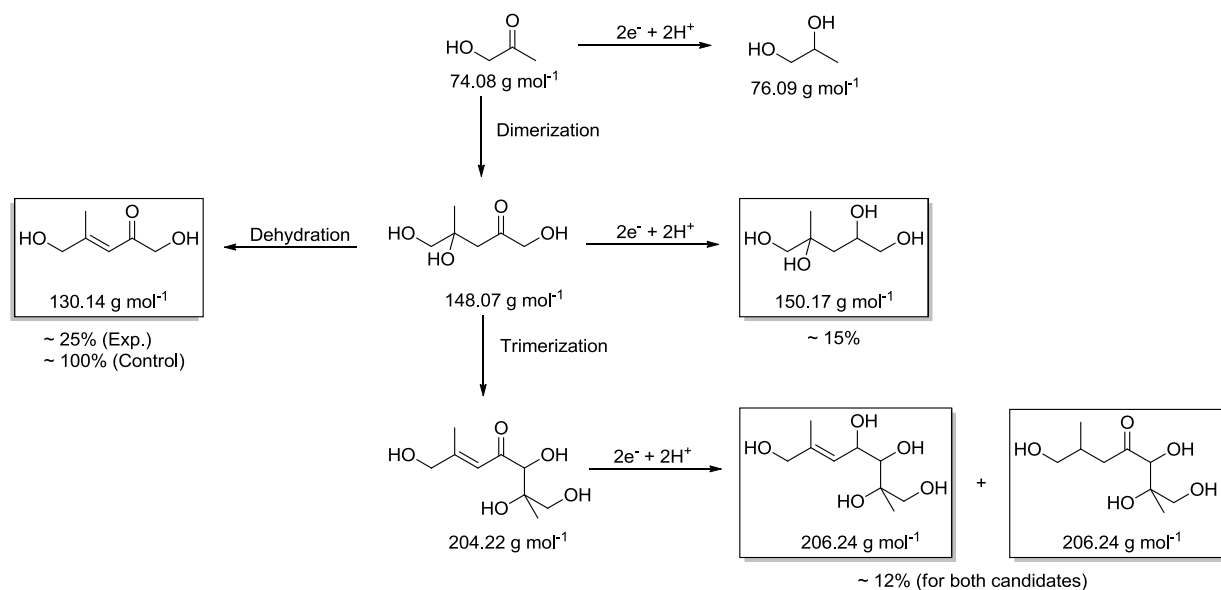


Figure 4-13: Proposed reaction pathways of acetol. Candidates are proposed based on the observed molecular weight from aqueous phase MS analysis. Percentages of the compounds are given based on the relative intensity of the peak.

Electrolysis using an ionic salt buffer as the anolyte can increase pH which can lead to material loss, but on the other hand, such phenomena may be an option in neutralizing the bio-oil's acidity. It must be kept in mind, however, that if potassium ion (from anode buffer) is the cation flowing from anode to cathode compartment, it may defeat the purpose of using the SPEE, which was proposed as a strategy to upgrade bio-oil in the absence of a supporting electrolyte. However, if the phosphate buffer is replaced with any protic solution such as sulfuric acid, the stainless steel will corrode quickly and terminate the reaction – only platinum can withstand the acidic oxidative environment in electrolysis. There was no obvious solution to the problem, either the project would proceed with an expensive platinum mesh anode to carry on with the SPEE principle, or continue to explore the possibility of using the stainless steel and see if it is possible to improve its lifetime under the anodic oxidative environment. Since platinum mesh was a costly investment for this relatively new project, investigation of stainless steel was preferred until the project matured.

4.4.2 ECH of acetol in the presence of acetic acid

Seeing that aldol condensations led to material loss, 5% (v./v.) of acetic acid was added to the acetol cathodic solution. Addition of 5% acetic acid served two purposes a) to mimic the acidic nature of bio-oil, and b) to verify whether the acidic environment could improve mass balance. A control experiment analyzed by HPLC-RI showed acetol did not undergo polymerization in the presence of 5% acetic acid over 15 hours at room temperature, and the acetol stock solution showed no signs of changes after months of storage.

When 5% (v./v.) acetic acid was added, the C.E. for propylene glycol formation dropped by almost 20% (Table 4-1, without acetic acid 32.9 % vs. with acetic acid 13.8 %). This is expected as greater H^+ concentration favors H_2 formation rather than acetol hydrogenation.

Formation of H₂ occurred at the expense of H⁺ from acetic acid, so the average pH after 6 hours of electrolysis increased from 2.89 to 5.23. On the other hand, the mass balance also improved 12.6 % (without acetic acid 55.4 % vs. with acetic acid 68 %), which is significant but still incomplete. HPLC-RI analysis showed no side products or polymerized products formed in the reaction. Therefore, the 30% loss of material may be due to membrane crossover.

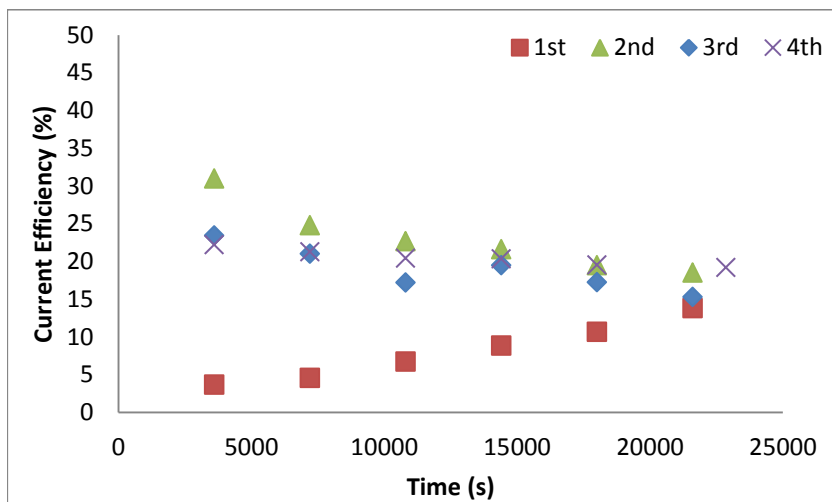


Figure 4-14: ECH of 10 ml of 5% acetol with 5% (v. /v.) glacial acetic acid added. Condition: copper mesh 200 at 98 ± 2 mA at 1 atm at room temperature (22 ± 1 °C) for 6 hours. Copper mesh is being reused multiple times and compared with the Monel 400 mesh 200 Note: reaction is evaluated using the cumulative current efficiency, each point accounts for the product accumulated previously. For equation, see Scheme 2-2

Interestingly, when the copper mesh was reused again for the same reaction, the Columbic efficiency trend changed significantly. The Columbic efficiency of new copper mesh started low at approximately 3.7% and rose to 13.8% whereas the used copper mesh started at ca. 30% then dropped slowly during the course of reaction. The trend suggested that perhaps the copper was being activated during its 1st use. Upon disassembly of the reaction cell, a black layer was found on the surface of the copper. Examination under SEM with EDX analysis revealed the black layer resulted from morphological changes on the cathode surface. As shown in Figure 4-15, nickel and copper were detected (EDX analysis: 55% Ni and 30% Cu) with minor carbon

and oxygen impurities. The nickel likely originated from the stainless steel anode mesh that was slowly undergoing anodic oxidation; this notion was confirmed by the SEM images of the used stainless steel mesh in Figure 4-15 (bottom left). Knowing stainless steel contains 8 – 10% nickel, and seeing the SEM observation of the surface erosion of the stainless steel, it is reasonable to conclude that the nickel deposition originated from the stainless steel anode.

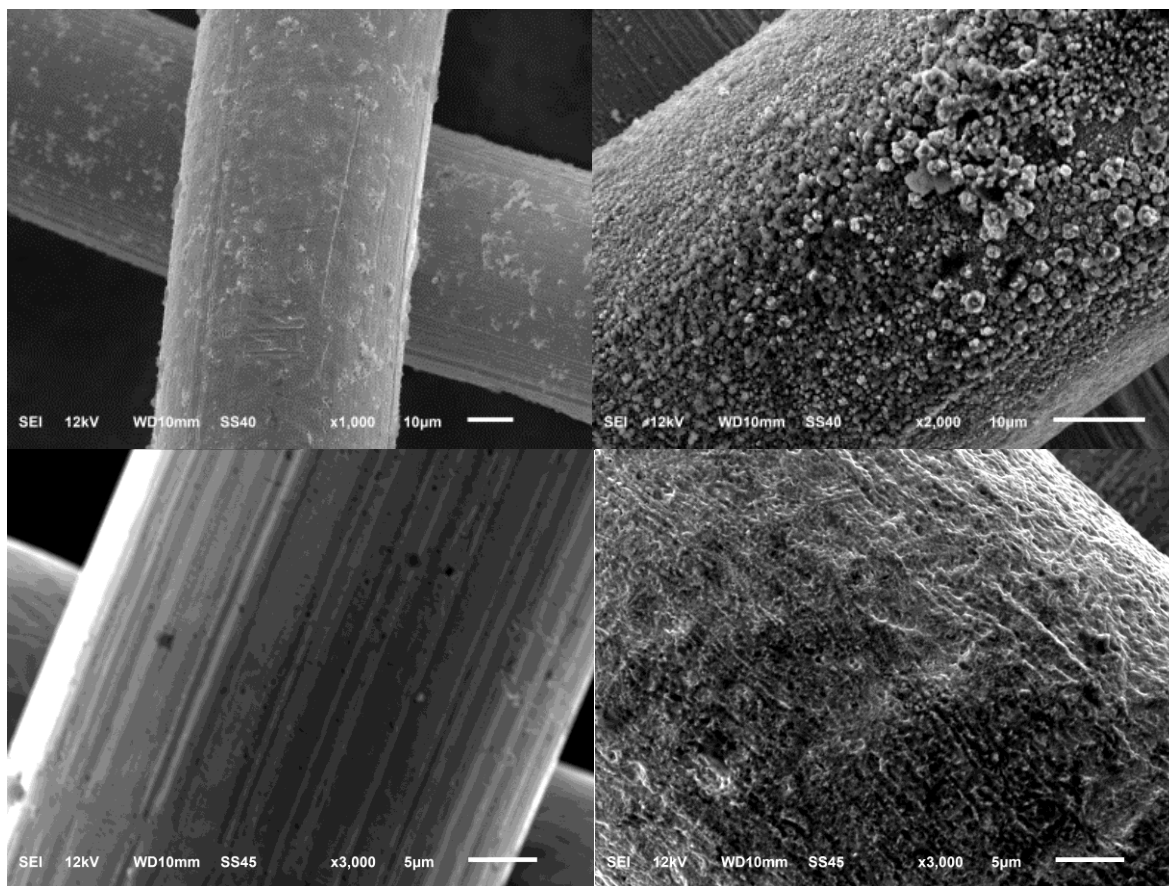


Figure 4-15: SEM examination on copper mesh before (Top, Left) and after (Top, Right) 6 hours of electrolysis. New Stainless Steel (Bottom, Left) and used stainless steel (Bottom, right). Samples were washed with water, acetone and chloroform to remove organic residues. Then they were dried in vacuum desiccator for 2 hours before SEM examination at 12kV and 10 mm working distance under ultrahigh vacuum.

The positively charged nickel ions (Ni^{2+}) presumably travelled through the membrane and re-deposited on the copper mesh. This newly formed nickel-copper surface may be catalytically active towards organic hydrogenation. Moreover, it appears rough as seen in Figure

4-15 (top right) which would have increased the surface area thereby improving the ECH rate. Interestingly, even though the stainless steel anode mesh was undergoing oxidation, it lasted for 30 hours, 5 trials of 6 hours, of electrolysis without obvious macroscopic signs of degradation.

4.4.3 Effect of Anolyte on Current Efficiency Improvement

Given the improvement in Columbic efficiency triggered by the nickel re-deposition, it was proposed that a nickel-copper alloy might possess a special advantage towards catalytic hydrogenation. Hence, Monel 400², a commercially available nickel-copper alloy mesh, was purchased to test out the effect of acetol hydrogenation.

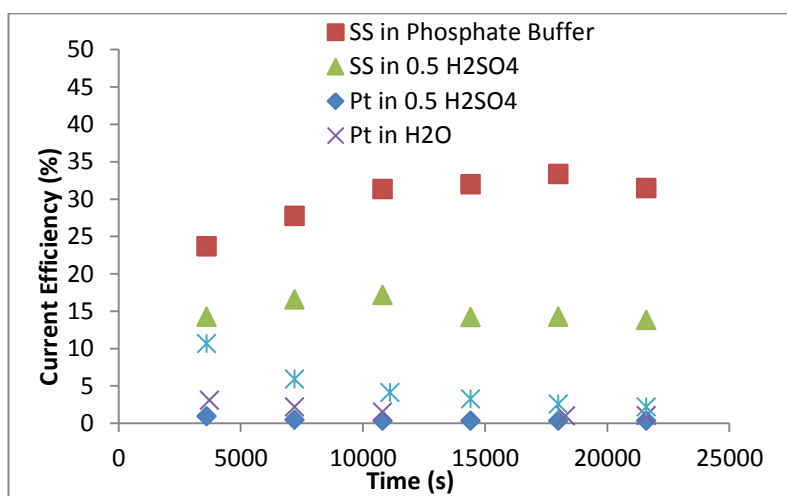


Figure 4-16: ECH of 10 ml of 5% acetol with 5% (v./v.) glacial acetic acid added. Condition: Monel 400 at 98 ± 2 mA at 1 atm at room temperature (22 ± 1 °C) for 6 hours. The anode compartment conditions are listed in the legend

When the copper mesh cathode was replaced with the Monel 400 mesh, the efficiency reached the well over 30% (Figure 4-16 - [SS in phosphate buffer]), which seemed like that nickel-copper alloy was responsible for the catalytic enhancement. However, when the Monel 400 mesh was used in conjugation with platinum mesh, which gave no nickel ions, the efficiency

² Monel 400 is an alloy consisting of 63% Ni min., 28 – 34 % Cu, 2.5% Fe, and 2% Mn. Note: the 400 associated with Monel describes its composition, and is not a mesh number. The mesh number for the Monel 400 was 200, same as other meshes used.

decreased dramatically to less than 5% (Figure 4-16 – [Pt in H₂O]). Therefore, the re-deposition of the nickel ions, which were leached from the stainless steel anode, must have been a contributing factor towards the catalytic enhancement. To verify the importance of nickel, in a separate trial of 10 mM of nickel chloride was added to the catholyte with platinum used as the anode. As expected, the initial efficiency improved (Figure 4-16, [Pt in H₂O with 10 mM NiCl₂], 10.6% vs. [Pt in H₂O] 3.1%). The fall of the efficiency is likely owing to the small quantity of nickel ions that were then plated out in the 10 ml electrolyte. In 10 ml of 10 mM of nickel ion solution, there is only 0.1 mmol of nickel ions, which would require 19.3 coulombs to plate out. Given a 6 hours electrolysis would supply roughly of 2000 coulombs, and assuming of 30% went into acetol hydrogenation, there is still 70% of the 2000 coulombs (2000 x 70% = 1400 C) going towards H₂ formation and nickel plating. Thus it is reasonable to understand the 10 ml of 10 mM nickel solution does not have enough nickel ions for test its effect. When the solution volume increased to 100 mL, there was 10 times more nickel ions in the solution to improve the supply of nickel ions. In a sufficient nickel supply environment, the reaction gave a Columbic efficiency trend became more steady as shown in Figure 4-17.

The effect of anolyte pH on Columbic efficiency was also examined. When the stainless steel anode was used with 0.5 M H₂SO₄, the Columbic efficiency dropped significantly compared to the trials with the potassium phosphate buffer. Apparently, when there was a high influx of protons from the anode compartment, the cathode surface concentration of protons increases, favoring H₂ formation which in turn decreased the Columbic efficiency. In other words, a non proton flux would improve the Columbic efficiency by lowering the proton concentration on the cathode surface. This model was supported by the high Columbic efficiency boost using potassium phosphate buffer anolyte. When the stainless steel mesh anode was used

in phosphate buffer solution, the initial Columbic efficiency was 9.5% higher than using it in 0.5 M sulfuric acid. The differences increased to 17.6% after 6 hours of electrolysis shown in Figure 4-16. In the beginning, the influx of potassium ions decreased the proton concentration on the cathode surface, and reduced the rate of H₂ formation. The higher efficiency after 6 hours of electrolysis may result from the potassium ion influx replacing H⁺ ions and thus increasing the pH of the cathode solution; higher pH disfavors H₂ formation, and forces reaction to favor organic ECH under the constant current electrolysis setting.

4.4.4 Influence of Metal Ion Re-deposition

Aside from nickel, the Columbic efficiency improvement due to other metals that could have been leached from the stainless steel mesh was also examined. Stainless steel (314) mesh is made of 0.03% sulfur, 0.05% phosphorus, 0.08% carbon, 0.10% of nitrogen, 0.75% silicon, 2.0% Manganese, 8 – 10% nickel, 18 – 20% chromium, and (remaining) 67.3 – 71.8% of iron. Of the listed composition, only nickel, chromium and iron could be re-deposited on the cathode. Therefore, chromium (II) acetate²²² and chromium (III) acetate (from air oxidation of chromium (II) acetate) and iron (III) chloride and several different concentrations of nickel (II) chloride were tested and compared for their improvement on Columbic efficiency. The chloride salts were preferred over nickel acetate because of their high solubility in the aqueous electrolyte. The presence of 5% acetic acid made the choice of counter ion, chloride or acetate, unimportant.

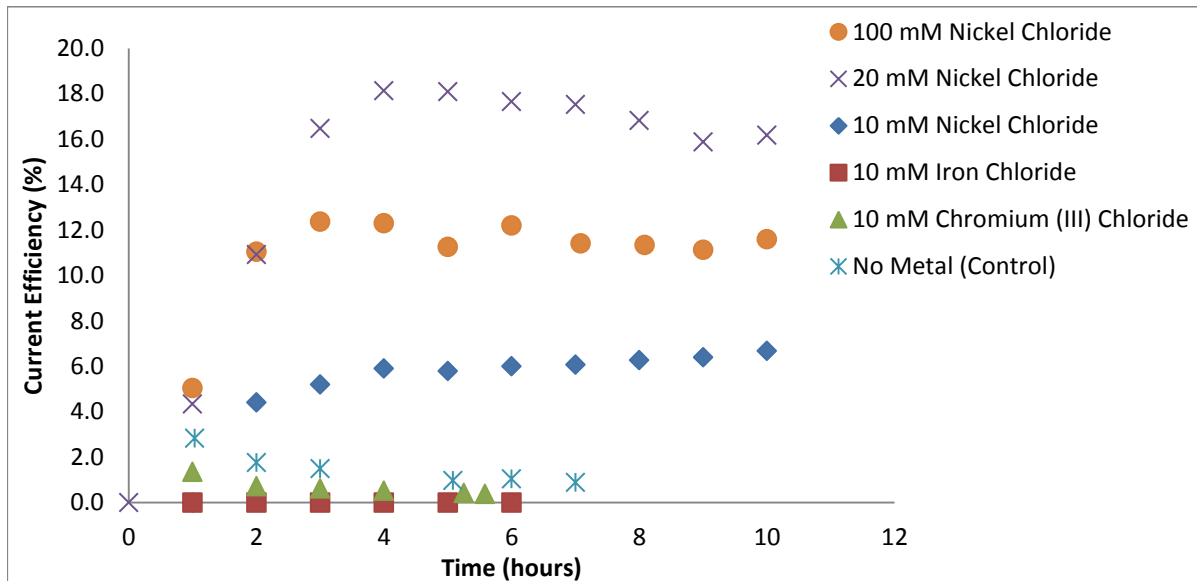


Figure 4-17: ECH of **100 ml** of 5% acetol with 5% (v. /v.) glacial acetic acid added. Condition: Monel 400 mesh 200 at 98 ± 2 mA at 1 atm at room temperature (22 ± 1 °C) with a platinum mesh anode in deionized water for 6 – 12 hours. Metal salts were added at the beginning of the experiment.

Only the nickel salts had a positive impact on the Columbic efficiency. Of the three concentrations tested 10, 20, and 100 mM, the 20 mM of nickel chloride trial reached its highest Columbic efficiency to 18%, and declined slowly. The 10 and 100 mM trial maintained a reasonable flat line after reaching its plateau. The increases in efficiency between 10 to 20 mM of nickel chloride is reasonable, double the concentration led to approximately 2.5 times greater efficiency. However, when the nickel ion concentration got too high in the 100 mM trial, the efficiency was lower than that of 20 mM, this probably resulted from competition between nickel ions and the organic substrate for reduction.

Compared to the nickel (II) ions, chromium (III) and iron (III) ions decreased the Columbic efficiency. This can be rationalized through the concept of standard reduction potential of these metals. Chromium (III) (+0.74v vs. SHE.) and iron (III) (+0.44v vs. SHE) have greater positive potential compared to nickel (+0.25v vs. SHE) which means they are more likely to stay

in an oxidized form under mildly reducing environment. Hence, EDX surface analysis showed only nickel was deposited on the copper mesh, but not the other two metals. The lack of plating of iron and chromium supports the nickel deposition was indeed the key factor towards catalytic improvement on acetol hydrogenation. Similar observation was made by Navarro in his conventional two undivided cell, in which a sacrificial nickel enhanced the efficiency of carbonyl groups hydrogenation. The constant nickel deposition was proposed to have a positive effect on organic substrate hydrogenation.^{98, 120}

Knowing that potassium ions influx and nickel plating were responsible for the Columbic efficiency enhancement, the two factors were tested together to see if they could be used to improve the Columbic efficiency further.

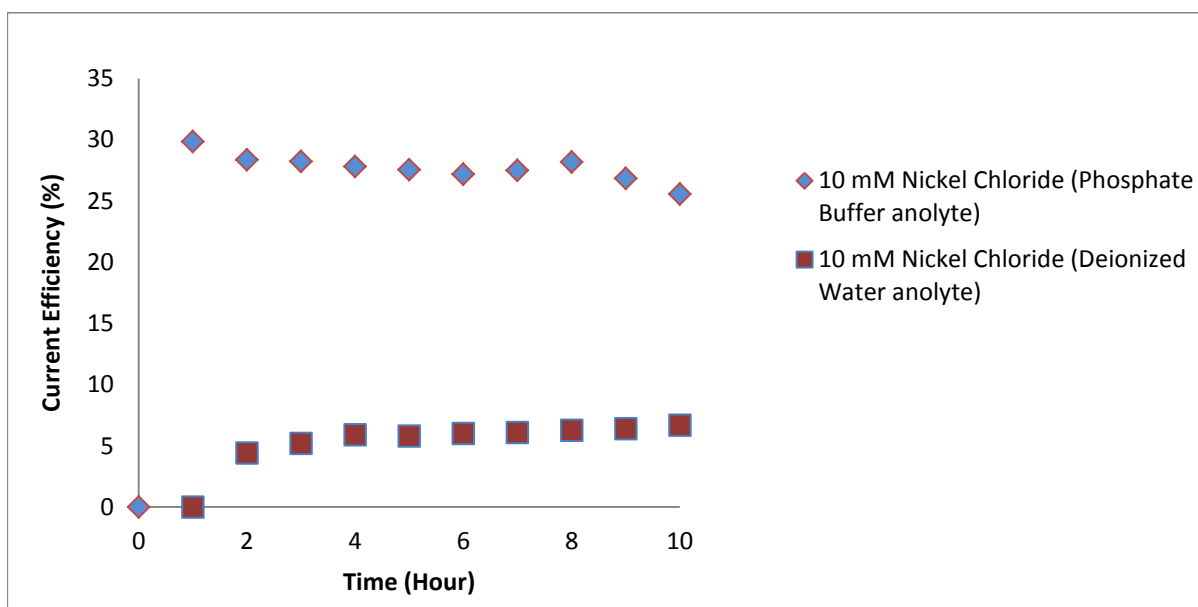


Figure 4-18: ECH of **100 ml** of 5% acetol with 5% (v. /v.) glacial acetic acid added. Condition: Monel 400 mesh 200 at 98 ± 2 mA at 1 atm at room temperature (22 ± 1 °C) with a platinum mesh anode in different anolytes for 12 hours.

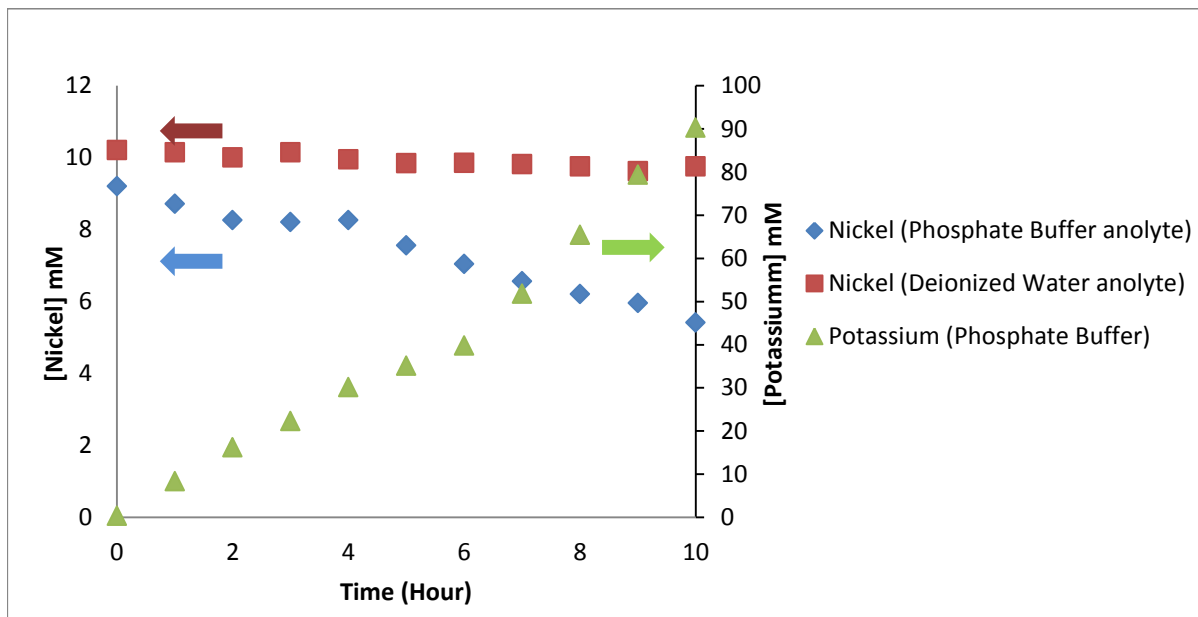


Figure 4-19: ICP-OES analysis of nickel and potassium in the cathode solution for trials described in Figure 4-18. Samples were diluted 125 times with 2% nitric prior analysis (0.2 ml of sample in 25 ml of 2% nitric acid).

From Figure 4-18, the use of phosphate buffer anolyte had a significantly higher Columbic efficiency compared to deionized water anolyte – a boost of almost 25%. With phosphate buffer, the efficiency started at above 30% and declined slowly, whereas the Columbic efficiency for the deionized water trial slowly rose. The difference in these trends could be explained by combining the information from Figure 4-18 and Figure 4-19. Compared to the water anolyte, the nickel ion concentration dropped quicker in the presence of phosphate buffer anolyte. This suggests that a high influx of protons, generated via water splitting, from the anolyte was discouraging the nickel deposition and thus decreasing the Columbic efficiency.

The fact that the Columbic efficiency did not correlate with the steady rise of potassium ion concentration, shown in Figure 4-19, suggests the potassium ion has no direct effect in aiding the reduction. Thus, the rise in conductivity, due to the potassium influx, had no effect on the reduction. The constant influx of potassium might have created a steady state concentration of

potassium ions near the cathode mesh surface which reduced the local proton concentration, and in turns favored nickel deposition. In other words, the potassium influx made the cathode surface less acidic and so did not favor H₂ formation as much. In short summary, the combination of potassium influx and nickel ion deposition are the two major factors in boosting the Columbic efficiency.

4.4.5 Mesh Size Effect on Current Density

Table 4-2: ECH of 10 ml of 5% acetol with 5% (v/v) glacial acetic acid added. Condition: copper mesh with various mesh size at 98 ± 2 mA at 1 atm at room temperature (22 ± 1 °C) for 6 hours. Note: mesh size 2.3×2.3 cm = 5.29 cm²

Copper Mesh Size	Wire Thickness (inch)	% Open Area	Nafion Exposure (mesh open area) (cm ²)	Copper Exposure (cm ²)	Copper / Nafion Exposure ratio	Acetol Remaining (mM)	Propylene glycol Formed (mM)	Current Efficiency (%)	Material Balance (%)
16	0.011	67.9	3.59	1.7	0.47	178	154	13.2	47.1
22	0.012	51.47	2.72	2.57	0.94	43	197	17.3	34.0
100	0.0045	30.25	1.60	3.69	2.31	418	162	14.5	72.2
200	0.0022	31.36	1.66	3.63	2.19	214	244	21.9	69.1

The effect of mesh size was also examined. Based on Table 4-2 there was no simple correlation between mesh number and C.E. found. However, the mesh size had some impact on the material balance – the lower the mesh number, the greater the open area (the Nafion exposure), which increases the area for organic diffusion through the Nafion membrane. Mesh 16 and 22 only have 34% and 47% material balance respectively while mesh 100 and 200 have 72.2% and 69.1% respectively. Note: the copper exposure of mesh 100 and 200 are same, 0.27 cm², the wire from mesh 200 was half as thick as that of mesh 100. The result suggests lower mesh number (with greater opening) leads to lower material balance because of membrane crossing of organic substrates.

4.4.6 The Effect of Current Density on Current Efficiency

Table 4-3: ECH of 10 ml of 5% acetol with 5% (v/v) glacial acetic acid added. Condition: Monel 400 mesh 200 at different current density (mA cm^{-2}) 1 atm at room temperature (22 ± 1 °C). Note: charge passed was calculated by the summation of multiplying current level (recorded hourly) with the time interval between sampling time. Note: current density was calculated based on the cut dimension of $2.3 \times 2.3 \text{ cm} = 5.29 \text{ cm}^2$

Average Applied Current (mA)	Current Density (mA cm^{-2})	Time (s)	Charge passed (C)	Average applied potential (V)	Acetol remained (mM)	P.G. formed (mM)	C.E. (%)	Material Balance (%)
48.7	9.21	29280	1422.9	2.67	429	49	6.7	67.9
99.8	18.87	14400	1438.7	2.72	214	244	21.9	69.1
195.0	36.86	7200	1404.0	3.85	420	121	16.7	76.9

Two other current settings were attempted to explore the effect of current density using the Monel 400 mesh 200 and the results are summarized in Table 4-3. 200 mA has a lower Columbic efficiency, might be due to the higher current density was favoring H_2 formation over the ECH of organics. The average applied voltage for 200 mA was 3.85 (average of initial and final voltage); 41.5 % higher than the average applied voltage of the 100 mA trial. The increase in voltage is required to drive the higher current which means in turn, that more reactions must take place on the electrode surface and hence a higher voltage is required to generate a thicker double layer. The material balance was also higher for the 200 mA trial. This is most likely due to a higher concentration of H_2 gas formed on the surface, and the bubbles increase the shielding between the cathodic solution and the membrane. In short, the 200 mA trial gave an 8% improvement on the material balance compared to the 100 mA; but required a 41.5% greater voltage. Hence, 98 ± 2 mA (targeted at 100 mA) was a better current setting for the reaction.

When 50 mA was applied to the reaction, the applied potential got slightly lowered but the C.E. % decreased dramatically down to 6.7%. From the standpoint of the current, a lower applied current would lead to less adsorbed hydrogen on the surface and the adsorbed organics would be less likely to encounter an adsorbed hydrogen atom to achieve hydrogenation. From the perspective of voltage, a lower current led to lower applied voltage, which means a decrease in cathodic voltage. When the cathodic voltage gets too low (or too high), the electron energy level does not match with the LUMO of the substrate pi orbital: this causes an inefficient transfer of the electron to the π^* orbital of the organics substrate.

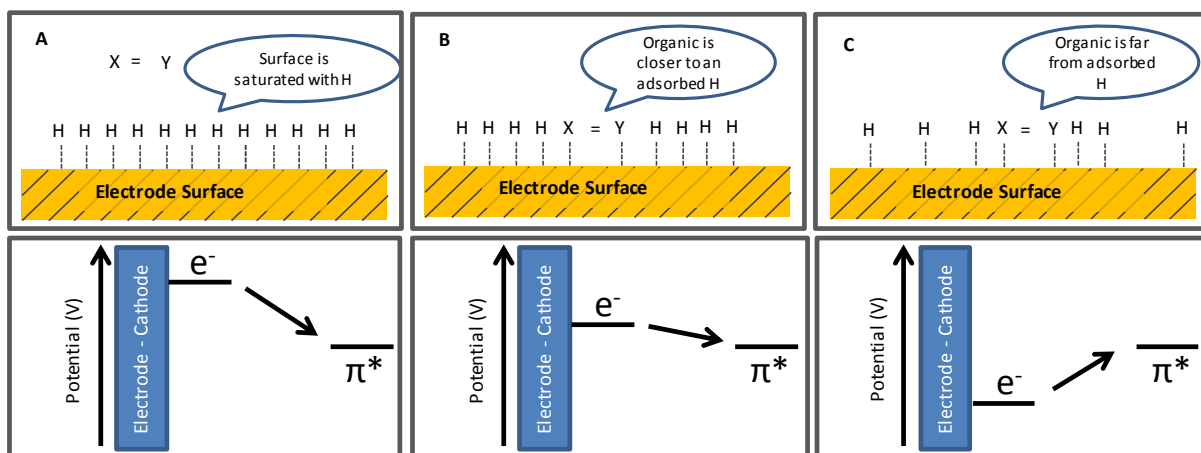


Figure 4-20: graphical interpretation of A) at low current, hydrogen adsorption is low, resulting in low hydrogenation efficiency. when the applied potential is too low (or too high), energy of the electron and the LUMO is mismatched, causing an inefficient transfer and lower the C.E. B) at moderate level of current, surface is filled with enough adsorbed hydrogen and can fit in organics to achieve hydrogenation. C) at high current, surface is saturated with adsorbed hydrogen and disfavors organic adsorption. H_2 formation becomes dominated result. energy of the transfer electron matches the LUMO of the pi bond to give an efficient electron(s) transfer

4.4.7 Isopropyl Alcohol Study

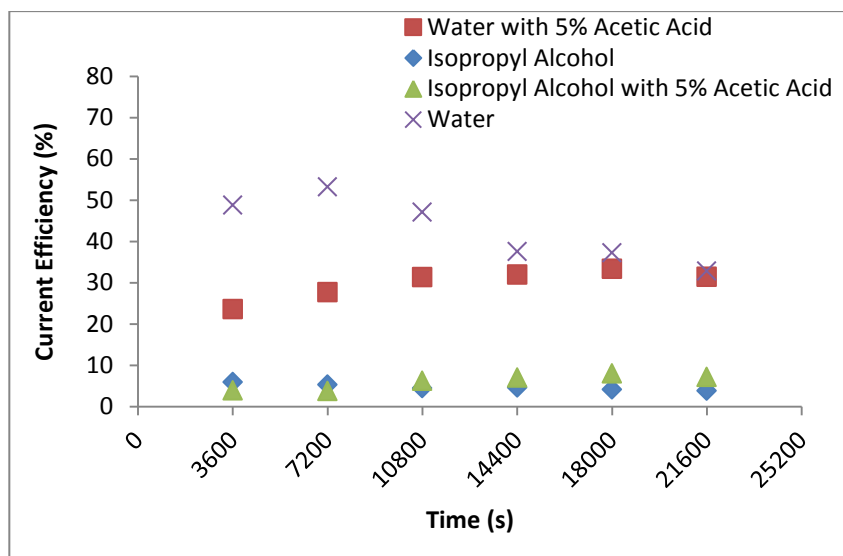


Figure 4-21: ECH of 10 ml of 5% acetol in water or isopropanol, with and without acetic acid. Condition: Monel 400 mesh 200 at 98 ± 2 mA at 1 atm at room temperature (22 ± 1 °C) for 6 hours.

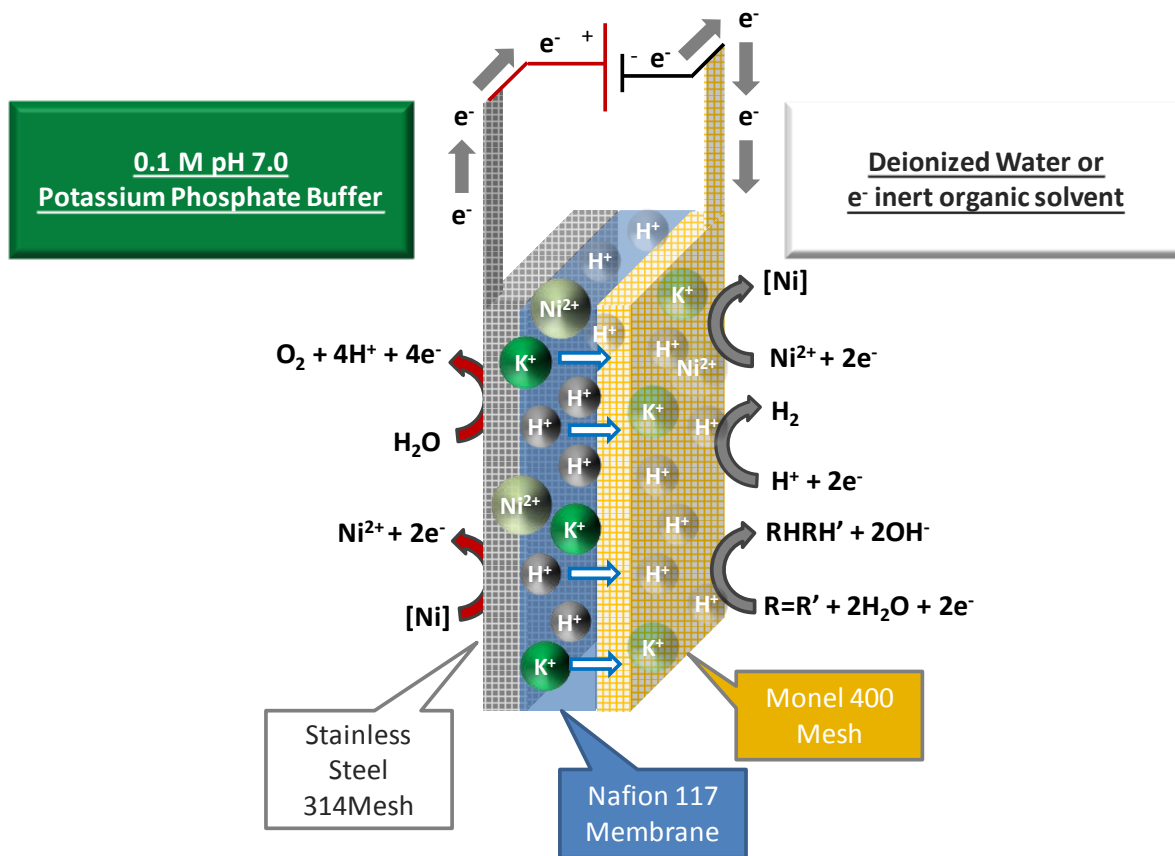
Despite the fact that the cell could operate in the absence of supporting electrolyte, the SPEE required water to achieve ECH (equation c in Scheme 4-1). When water was replaced with isopropanol in the cathode compartment, the C.E. dropped to less than 10 % and the C.E. was the same with and without addition 5% glacial acetic acid. In the absence of water, the nickel ion leached from stainless steel could not be plated on the surface of the cathode mesh, and the potassium ion was not soluble in isopropanol. The combination of these two factors resulted in near-zero Columbic efficiency. Interestingly, gas evolution was still observed from the cathode mesh for both isopropanol trials, suggesting H^+ might have diffused through the Nafion membrane, and been immediately reduced to H_2 on the mesh. At the same time, it might be possible that IPA ($pK_a \sim 15$, which is roughly same as water) assisted the H^+ transportation from the Nafion surface for hydrogen evolution. The important lesson from this part of the study is that an aqueous environment is critical to the hydrogenation efficiency, because it is central to

the metal ions transportation. The lack of metal ion replenishment on the cathode surface, as discussed in the previous section, will disfavor organic substrate hydrogenation, and H₂ evolution the dominant reaction.

4.5 Summary

After almost 3 years of work, the mechanism of the SPEE system is finally understood. The ongoing deposition of nickel and the mildly basic environments in the catholyte are the two most important factors in boosting the Columbic efficiency. Admittedly, the use of the stainless steel mesh anode started out with a different purpose; it was supposed to support the cobalt phosphate water oxidation catalyst as an ongoing water oxidizing anode similar to the guaiacol reduction. Unfortunately, the optimal current density for the cobalt phosphate catalyst was 1.17 mA cm⁻² while the SPEE operates at almost 20 mA cm⁻², a difference of almost 20 times. In a long run, a non-oxidizable anode of a high surface materials for the water oxidation catalyst is desirable. After all, stainless steel would be a costly replacement on a large scale.

In summary, the anode surface is first oxidized and releases nickel ions. The nickel ions, potassium ions, and hydrogen ions travel through the Nafion membrane to reach the cathode surface. The influx of potassium ions created a less acidic catholyte solution which favors the deposition of nickel. Freshly deposited nickel in turn favors organic hydrogenation and improves the Columbic efficiency. Although the SPEE functions in the absence of aqueous electrolyte, it offers a low Columbic efficiency because organic solvents disfavor ion transport. The overall mechanistic scheme is depicted in Scheme 4-2.



Scheme 4-2: Revised mechanism for the SPEE cell that accounts for all observed reactions. Reaction mechanism is proposed based on the conditions described in the diagram.

The current density also has impact on the Coulombic efficiency; an optimal current density for acetol is approximately 20 mA cm^{-2} .

Although cyclic voltammetry (CV) could be used to determine the reduction potential on high H_2 overpotential metals, mercury for instance, copper and nickel cannot benefit from CV analysis because the H_2 evolution peak current will over shadow the organic reduction peak. And, unfortunately, the reduction potential values of organic substrates are different between metals, and so there is no direct way to probe the optimal reduction voltage for copper or nickel but through experimentation.

From an energy standpoint, the SPEE is a better system than the conventional electrolyzer because it has a much smaller internal resistance. The classical dual compartment

cell requires a minimal 5.5 volts to run at 50 mA at 75 °C (almost 9 volts at room temperature in 0.1 M borate buffer supporting electrolyte) whereas a SPEE cell needs less than 3 volts to run at 100 mA at room temperature in a supporting electrolyte free environment. The energy aspect definitely makes the SPEE system more appealing for catalytic hydrogenation in fuel production. Although the nickel ion deposition and use of the potassium ion influx for Columbic efficiency enhancement defeated the initial purpose of SPEE, the trace quantity of nickel ion dopant is consumed by the cathode and the potassium salt can be removed easily with aqueous extraction. So SPEE is still arguably an efficient and cost effective strategy for bio-oil upgrading.

The important aspects of Columbic efficiency enhancement are summarized in Table 4-4. Estimations are given based on comparison between trials that have only one changed variable.

Table 4-4: Factors that enhance current efficiency towards organic substrate hydrogenation

	K ⁺ influx to lower surface acidity	Presence of acetic acid	Nickel ion re-deposition	Acidic anolyte	Mesh Size	Current Density
Enhance C.E.%	Yes	No	Yes	No	N.A.	Depends
Qualitative Estimate	High	High	Moderate	Moderate	N.A.	Moderate
Estimate %	20 – 25	20	10 - 15	15 – 20	N.A.	Depends
Sources	Figure 4-16 (p.113) Figure 4-18 (p.117)	Table 4-1 (p.107) Figure 4-21 (p.122)	Figure 4-16 (p.113) Figure 4-17 (p.116)	Figure 4-16 (p.113)	Table 4-2 (p.119)	Table 4-3 (p.120)

The percentage values are only given as a crude estimation on the efficiency because the precise influence may depend on the actual condition. In general, the surface acidity appears to have the greatest impact; lower pH tends to favor more H₂ formation than organic hydrogenation as expected. The situation can be averted with salted anolyte to provide an aprotic cation influx

to discourage H₂ formation. However, the presence of acetic acid is a great challenge toward hydrogenation; the formation of H₂ gas will not only “waste” electrons but it also creates a thin gas layer that may shield the catholyte from the membrane surface. Although, technically, the formation of H₂ is not entirely wasteful, because H₂ is a valuable commodity that carries high fuel value, which can be used to fuel the pyrolysis process shown in Figure 4-2.

4.5.1 Miscellaneous Ideas and Future Directions

Plating strategies are being developed to create a ruthenium surface which opens to the pathway towards aromatic hydrogenation. In the past, several thoughtful attempts on incorporating the guaiacol Raney-nickel chemistry, which is presented in chapter 4, has been tried but to no avail. The Raney-nickel plating strategy creates a thick fragile surface that cannot be fitted in to the small compartment of the current SPEE design. Packing Raney-Nickel powder in the compartment either led to powder leakage or high pressure that the peristaltic pump cannot withstand. An innovative Raney-nickel deposition strategy is required to achieve the aromatic hydrogenation the SPEE. Lessard et al reported a different Raney-nickel deposition strategy, in which mixture of the powder ingredients were pressed in an electrode shape before activation.¹⁵¹ The electroless preparation perhaps gives control for the size and shape of the electrode and is worth a try. At the same time, the ruthenium catalyst deposition on the copper mesh has also been attempted, and the proto-type results are reported in the final chapter. The simplicity of SPEE opens limitless opportunities for modifications. The flexibility can be another advantage of in bio-oil hydrogenation aside from electrolyte free catalysis; the SPEE components can be modified easily to tailor the specific needs for bio-oil, a complex mixture whose composition varies depending on feedstocks and upgrading. Furthermore, easy implementations and parts

substitutions are great advantage in industrial synthesis as these processes often require regular part replacement.

Although acetol is the only model compound tested and it may not reflect the overall hydrogenation chemistry happening during the upgrading process, understanding the mechanism of SPEE marks the critical first step towards an efficient and effective hydrogenation. Aside from developing a new mesh surface for aromatic hydrogenation, other abundant molecules such as furfural and 2,3-butanedione will soon be examined in the SPEE system. The Columbic efficiency data of reducing these molecules will be helpful to understand ECH of different functional groups, and lead to better predictions on how bio-oil will behave during the upgrading reaction.

Chapter 5 Pedagogy: Electrocatalytic Hydrogenation of Acetol with US. Coins

5.1 Introduction

The addition of hydrogen across pi-bonded systems is a category of transformation central to organic synthesis. But textbook alkene hydrogenations involve costly noble metal catalysts, H₂ gas handling, and often elevated pressures and temperatures.²²³ Catalytic hydrogenations are thus relatively unattractive as pre-college or undergraduate classroom experiments. However, organic hydrogenation has existed for over a century and is one of the most widely applied reactions in the history of organic syntheses. For carbonyl pi systems, hydrogenations are usually effected with hydride delivery reagents such as NaBH₄ or LiAlH₄. Such reactions are easy and quick and therefore readily adapted to use in a teaching lab. On the other hand, the reagents can be hazardous and costly, they have poor atom economy, and the required post-reaction workups generate substantial waste streams.

Compared to H₂ molecular hydrogenation (MH) and carbonyl reduction by hydride reagents (HR), electrocatalytic hydrogenation (ECH) is a relatively uncommon technique. With a direct current at modest voltage, hydrogenation of organic substrates can be readily achieved on the surface of a cathode of suitably chosen catalytic metal. ECH typically runs at ambient pressure and modest temperatures, conditions mild enough to make it straightforward to implement as a pre-college or undergraduate laboratory experiment.^{97, 221}

This experiment is designed for students equipped with entry level of organic chemistry. Participants should be made aware of the harsh condition of conventional H₂ hydrogenation so they may appreciate ECH as be a mild alternative. We believe this experiment can be a good complementary study to the introduction of catalytic H₂ hydrogenation or pi-bond addition. Or, it

can serve as an extra laboratory activity to help student appreciate chemical transformations that can happen with ambient objects such as battery, coins and filter papers.

Since ECH is outside of the usual coverage of the ACS bachelor's degrees program, instructors should introduce this exercise where they see fit. In our case, we introduced this experiment to students as seeking the part of their "honors option" during their sophomore organic chemistry class. Some high school students from local institutions also tested it. A total of 30 undergraduate sophomore and 2 high school students participated in teams of 2 – 3; all participants completed the experiment within 2 hours under supervision of a graduate assistant.

A typical setup for ECH can be as simple as a container of conductive solution with two electrodes coupled with a direct current power supply. Building on this simplicity, we demonstrate herein that ECH can be practiced even with ordinary familiar materials: coins and batteries!

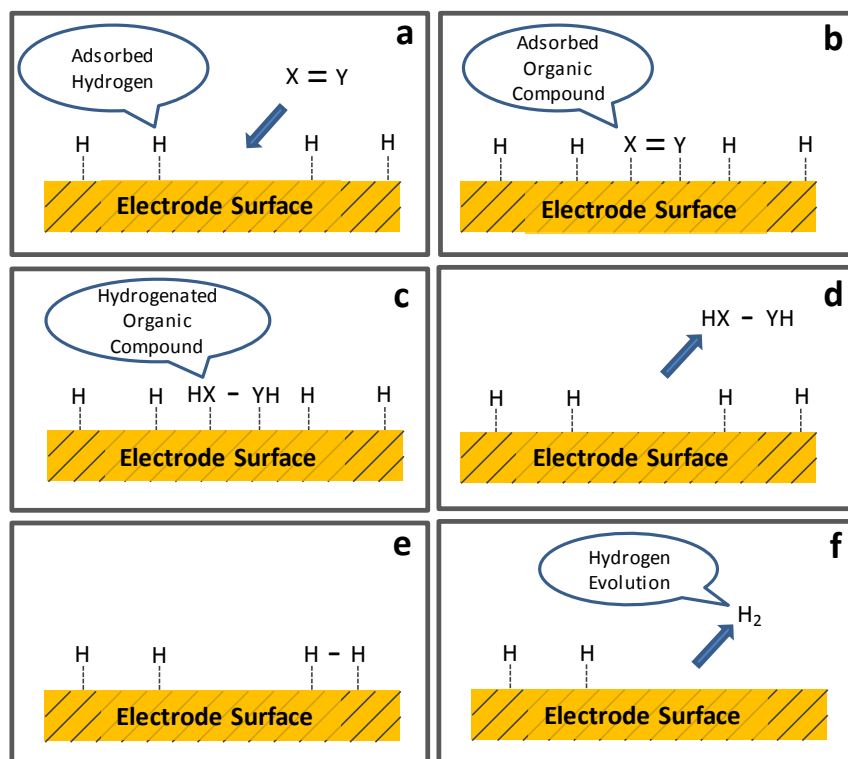


Figure 5-1: Schematic diagram of ECH of unsaturated organic molecules (a-d) and hydrogen evolution (e-f)

On a catalytic metal cathode in aqueous electrolyte, reduction of protons from solution forms surface-bound hydrogen atoms. When an unsaturated organic molecule is adsorbed nearby, it can undergo hydrogenation by bonding with these hydrogens (Figure 5-1a). However, hydrogen gas may also form via either the Tafel reaction, in which two adsorbed hydrogen atoms come together, bond and desorb (Figure 5-1b), or the Heyrovski reaction, where a solution proton reacts with a surface-bound hydride. With more than one reaction consuming the delivered current, it is important to quantify the electrochemical selectivity for formation of the desired product, a measure known as *Coulombic efficiency*.

As shown in Scheme 5-1, Acetol, a bio-derived substrate, can undergo ECH to propylene glycol without an external hydrogen supply, using batteries and coins with modest heating. The purpose of this exercise is to show how catalytic chemical transformations can be performed

with familiar household objects, highlighting the idea that chemistry is not just the province of experts with access to specialized resources. Properly probed, chemical behavior can be found and easily understood in everyday things.

5.2 Hazards and Disposals

Reagents used or formed in this study--acetol, propylene glycol, and ammonium chloride--are generally harmless and non-corrosive, making it suitable for undergraduate or high school students. The Benedict's solution requires neutralization for disposal, but is otherwise non-hazardous. Nevertheless standard safety protections such as lab coat safety gloves should be worn at all times during experiments. After the experiments, the used coins should be cleaned with de-ionized water and gently brushed to remove any surface residue before being returned to circulation.

5.3 Experimental Procedures

5.3.1 Materials and Preparations

All procedure in the manuscript is written for instructor preview, student should be working with the stepwise procedure found in the supporting info section.

Preparation from the instructor:

Recommended quantities of supplies for each team (2-3 students): 2 x 1.5 v batteries, multimeter, 5-6 plastic bags, 4-5 electrical wires with banana clips and alligator clips, 12 test tubes, 10 pennies and 6 nickels and 8 office binder clips.

Quantitative Benedict's (QB) solution²²⁴ can either be purchased or made from common reagents: Solution 1: Dissolve 100 g of sodium citrate, 32.5 g of anhydrous sodium carbonate, and 62.5 g of potassium thiocyanate in 400 ml of de-ionized water. Solution 2: Dissolve 9 g of copper sulfate pentahydrate in 50 ml of deionized water. Add solution 2 to solution 1 with rapid stirring. Add 0.13 g potassium hexacyanoferrate to the mixture, then dilute to 500 ml. Dilute 35 ml of the resulting solution to

100 ml with water. The stock solution does not require a hazard warning label, but its final disposal calls for a labeled hazardous waste container.

Preparation from the Students



Figure 5-2: (left) Experimental setup of ECH of acetol with coins. A copper coin anode is clipped with red wire, and the nickel coin cathode is clipped with the black wire. An extra coin is added on each side to act as a current collector and provide enough pressure for the clamp (right). Setup is in a small sample bag to prevent filter paper drying.

Standards preparation for analysis: cut out ten 1" x 2" rectangles of filter paper; fold each into a 0.5" x 0.5" square. Prepare 20 ml each of 5% v/v acetol (0.67 M) and 5% v/v propylene glycol (0.67 M) in 0.25 M of ammonium chloride electrolyte. Use these stocks to make standard 5 ml solutions of 5:0, 4:1, 3:2, 2:3, 1:4, and 0:5 acetol: propylene glycol ratios. In each standard, soak one filter paper for 5 minutes, then remove and squeeze out the excess electrolyte with 2 clean coins. Clamp each of the soaked filter papers as shown in Figure 5-2 without passing electricity through them. These control experiments are to be left in a sealed bag for 10 minutes (or time equivalent to actual experimental runs). Then submerge each filter paper in a separate 10 ml aliquot of QB solution, and proceed with the experimental trials.

5.3.2 Experiment

Clean the coins by boiling them in 5% CH_3COOH solution for 10 minutes and rinse them thoroughly with distilled water. Prepare 10 mL of 1 M acetol in 0.25 M NH_4Cl electrolyte solution. Cut out a 1" x 2" filter paper and fold it into a 0.5" x 0.5" square and measure its weight,

then soak it in the prepared electrolyte for 5 minutes. Squeeze out the excessive electrolyte with the dried, cleaned coins and reweigh the filter paper. The amount of acetol absorbed into filter paper can be calculated from the weight difference and known concentration of the solution. Sandwich the filter paper between the cathode coin and anode coin with a binder clip carefully insulated with masking tape to prevent a short circuit. To minimize electrolyte evaporation, enclose the coin and filter paper assembly in the bag as shown in Figure 5-2.

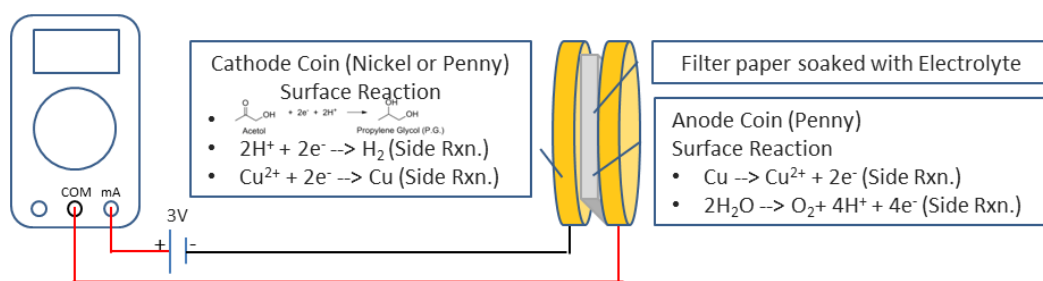


Figure 5-3: Electronic setup of the experiment. Note: Drawing is not to scale

Connect the setup with a pre-configured power supply set at 3 V or a pair of 1.5 V batteries connected in series, as shown in Figure 5-3. Be sure to connect multimeter in ammeter mode. Upon closing the circuit, record the current reading every 10 seconds for the first five minutes. After that, take the current reading at 1 minute intervals until the reaction time reaches 10 minutes. The amount of charge passed through the circuit can be computed from the area under the curve in a current vs. time plot. After reaction, take out and separate the coins, put the filter paper into a test tube, and pour in 10 ml of QB solution. Heat the set of QB-treated standards prepared earlier along with these experiment sets for 20 minutes in a boiling water bath. Be sure the solution is loosely capped with a rubber stopper to minimize evaporation during heating. The resulting change of color of the solutions should approximately resemble Figure 5-4. Allow solutions to cool to room temperature, filter them individually through Pasteur pipettes packed with a small piece of cotton at the tip to remove the light-scattering particles, and

then analyze them spectrophotometrically. Calibrate spectrophotometer, Spec 20 or equivalent, with the standard solutions at $\lambda = 670$ nm using de-ionized water as a 100% transmittance calibrant. Plot the absorbance (y) vs. percent acetol (x) in a standard plot (Figure 5-5), which can be used to determine the concentration of the remaining acetol from experimental samples.



Figure 5-4: Color changes of Q.B. solution in response to concentration of acetol. From left

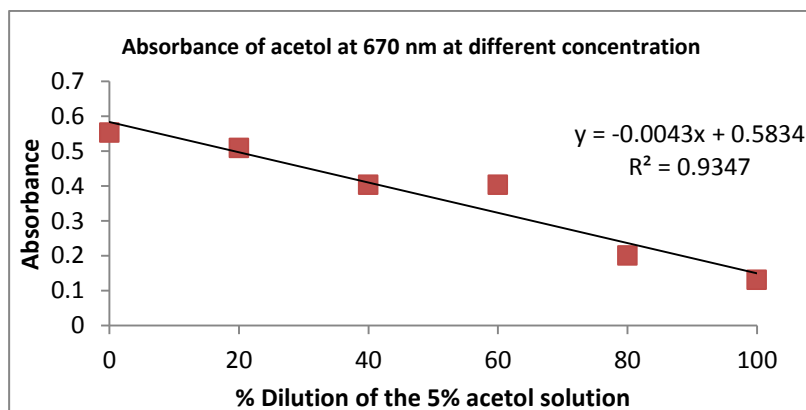
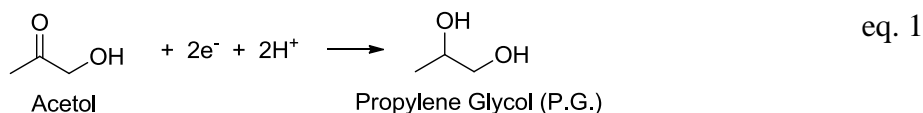


Figure 5-5: Change in absorbance of QB solution in response to % of acetol in standard solution. Note: students can take readings in transmittance and calculate the absorbance using the equation: $A = 2 - \log (\% T)$

5.4 Current Efficiency Analysis



Scheme 5-1: Acetol hydrogenation to propylene glycol electrocatalytically, and hydrogen evolution

Table 5-1: Results of ECH of acetol in various conditions. All trials were run using a penny as the anode at room temperature. Note: results were determined by ^1H -NMR peak integration to verify the formation of propylene glycol (See Figure 5-6). 1) 3 V d.c. power supply; 2) 3 V (two AA cells in series) batteries; 3) 3 V d.c. power supply with bag/coins in an ice bath.

	Cathode	Charge Passed (mC)	Mole of P.G. formed (μmol)	% C.E.
1	Penny	4.95	3.5	13.5
	Nickel	4.99	7.9	30.6
2	Penny	5.97	5.8	18.9
	Nickel	7.97	12.8	31.0
3	Penny	4.83	3.0	12.2
	Nickel	7.02	9.7	26.5

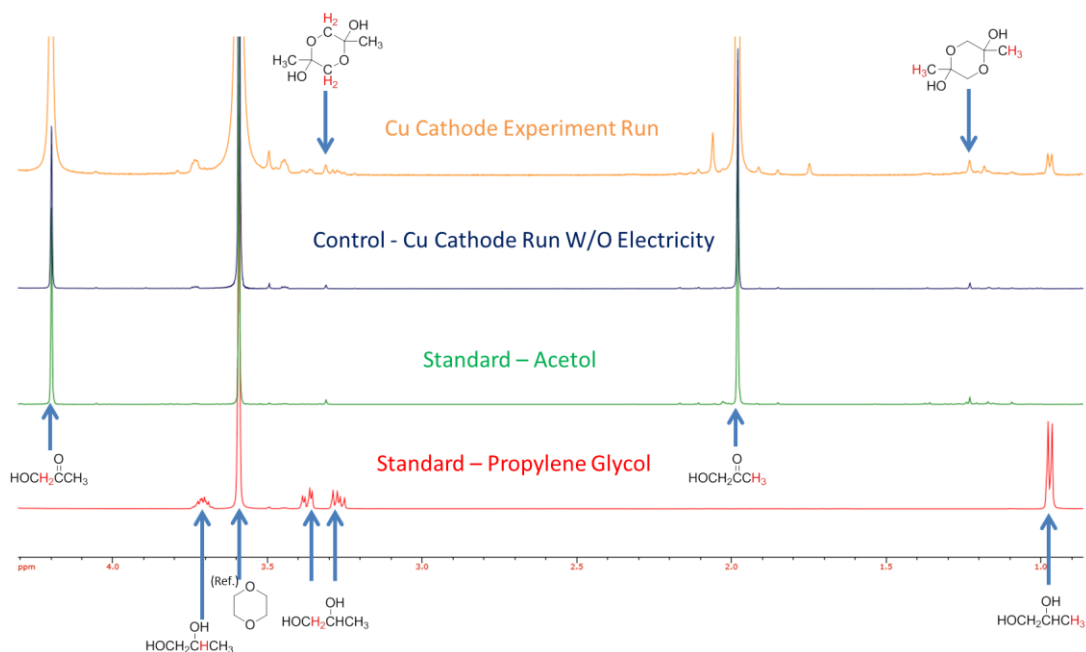


Figure 5-6: ^1H -NMR spectrum (Red) propylene glycol standard (Orange) ECH of acetol with penny for 10 minutes; low resolution of the orange spectrum was due to Cu^{2+} ion contamination. (Green) acetol standard (Blue) experiment 10 minutes with no electricity passed

The fraction of electrons passed that are spent in the desired reaction is termed “Columbic efficiency”. Two reactions occur on the cathode surface as shown in equations 1 and 2. The total charge passed can be estimated by integrating the current vs. time plot shown in Figure 5-7. The Columbic efficiency is calculated as follows:

$$C.E. (\%) = \left(\frac{Mol. \times F \times n}{C_{total}} \right) \times 100\%$$

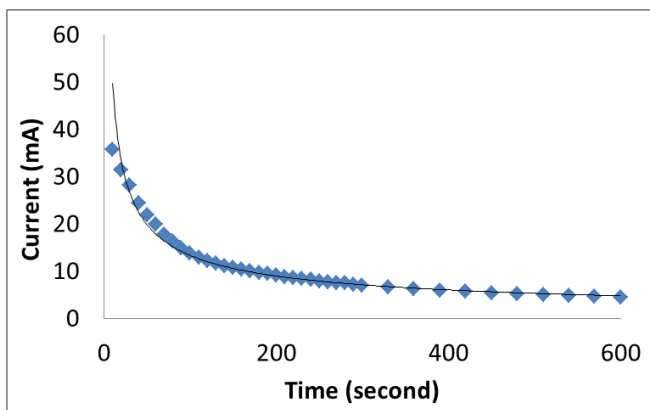


Figure 5-7: An example of current-time profile. Total charge passed (C_{total}) can be estimated by calculating area of the curve. Area under the curve can be estimated by simple summing of the trapezoidal areas.

5.5 Results and Discussion

A layer of copper black can be seen on the cathode coin surface after the reaction; Figure 5-8 shows analyses of this surface by SEM and EDX spectroscopy. The copper black layer was generated by re-deposition of copper ions that came from the surface of the sacrificial penny anode³

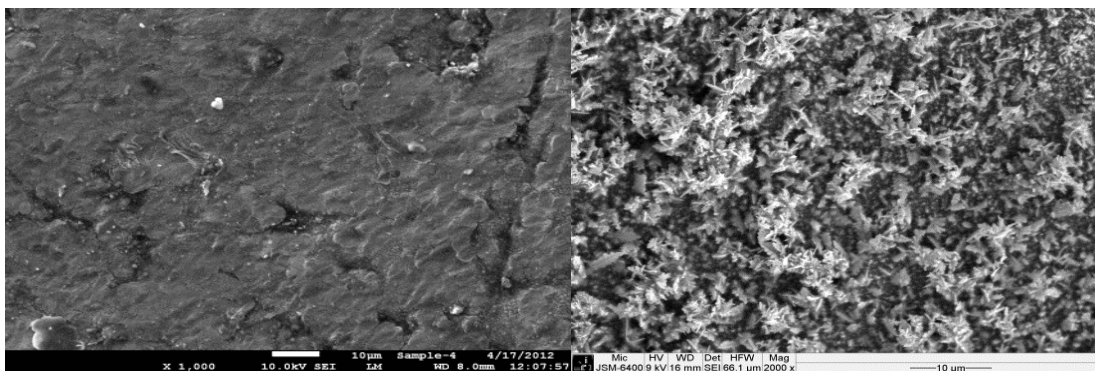


Figure 5-8: (left) SEM spectroscopic analysis of plain penny surface, and (right) the black copper layer after reaction

In general, the nickel cathodes show greater Columbic efficiency for ECH than the penny. The nickel coin surface is an alloy of copper and nickel metal,²²⁵ so the results suggest that the catalytic effect of nickel metal doped in copper is greater towards ECH than that of copper alone. In an ice bath (trial 3), the Columbic efficiency of the run does not change significantly at low temperature. The 3 V battery trial (trial 2) shows a lower conversion with the penny cathode and greater conversion with nickel cathode; these variations may reflect slightly different battery voltages, but the Columbic efficiency agrees fairly well with the other trials, suggesting that catalytic function remains constant.

The analytical method was designed to accommodate laboratory that have limited access to analytical instruments such as GC, LC and ¹H-NMR. Noting that the Beer's law related experiment are very common among entry level analytical chemistry courses, we proposed a non-instrument intensive analytical scheme that only requires Benedict's solution and a Spec 20 UV-vis spectrophotometer. Admittedly, this scheme does not measure the formation of propylene glycol and student should be focusing on the formation of product (P.G.) rather than disappearance of acetol. However, to the best of our knowledge, there is no simple means to determine small quantities of propylene glycol without employing sophisticated instruments.

Despite the success and simplicity of the above organic conversion, there are a few potential issues worth mentioning. a) A relatively high concentration of acetol, 5% v./v. (0.67 M) is needed to ensure extraction efficiency for analysis. Volume to volume type concentration is chosen specifically to minimize students waiting time at a balance to weigh reagents. b) Excessive electrolyte must be squeezed out as much as possible to prevent alternative conduction paths that could short circuit the cell. Consistency in the squeezing is crucial to the results as it determines the amount of acetol left in the filter paper. As the same time, filter paper should not

be too dried out for the electrochemical reaction. Admittedly, hand squeezing of the electrolyte may seem subjective. However, this error can be avoided via determining the weight of the liquid (electrolyte) absorbed into the filter paper.

As for the reference standards preparation, the weighing part can be omitted because the line of best fit (Figure 5-9) compensates for the uncertainty due to filter paper squeezing, assuming the filter paper squeezing process is consistent throughout the preparation.

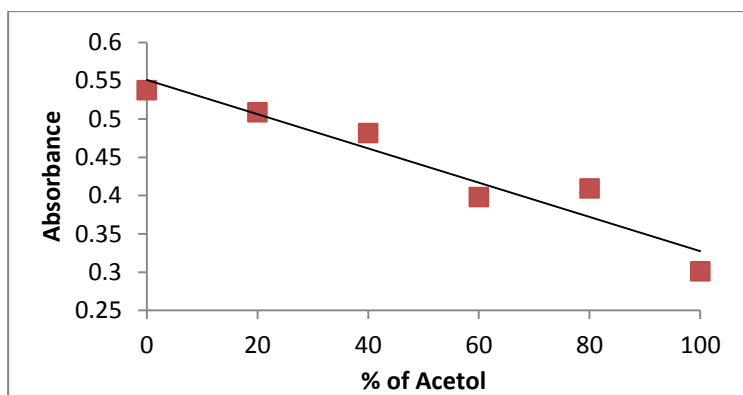


Figure 5-9: Change in absorbance of QB solution in response to % of acetol in standard solution.

Also, the reaction should be run at room temperature or below: higher temperatures lead to filter paper dehydration and changes in the resistance of the system. c) Teams of 2-3 students are highly recommended. d) A short reaction time (10 minutes) is recommended to minimize oxidative damage to the coin surfaces. e) Accuracy of the 10 ml QB solution addition is crucial to the experiment results; small changes in the observed transmittance can result in large variations in the Coulombic efficiency calculations. A mechanical pipette, which we used, is recommended to maximize the consistency of each aliquot transfer. f) Absorbance measured digitally on typical modern UV-vis instruments can help minimize variability from transmittance or absorbance conversion. g) The amount of current passed during the reaction depends on the

cleanness of the wires and alligator clips. Though Columbic efficiency is an intrinsic property of the reaction, it is best to keep all equipment as clean as possible to maximize reproducibility.

This experimental procedure was tested by a group of undergraduate students (class of 30) in groups of 2-3. Average lab times ranged from 150-180 minutes. Lab time can be shortened to 2 hours if QB solution, filter papers, boiling water bath, and coins are prepared by the instructor in advance. Special care should be taken to ensure consistency of the QB solution preparation and addition, Spec 20 calibration, amount of electrolyte carried in filter paper (hand squeezed as hard as possible), electronic connections of the electrodes, and multimeter setup. For consistency and time efficiency, the instructor may prepare the standard mixtures, QB solutions, data sheet templates, pre-calibrated spectrophotometry, and pre-cleaned coins in advance. In general, reproducibility problems are typically due to variations in preparation of the filter paper (saturation with electrolyte) and addition of QB solution.

The aim of this experiment is to introduce the concept that organic transformations can be performed electrochemically with familiar objects, even with coins. Unlike molecular hydrogenation (H_2) or chemical hydrogenation (CH), Electrocatalytic Hydrogenation (ECH) does not require harsh conditions, purchase or preparation of a specific reducing reagent or handling of H_2 gas, making it attractive for entry level laboratory experiments. The use of U.S. coins in this experiment highlights the point that organic chemistry does not necessarily require elaborate setups or reagents. In addition, acetol is an oxygenate like many bio-based organic compounds of relevance to future technologies in which refineries will make chemicals and fuels from renewable plant-derived carbon compounds instead of fossil petroleum.

5.6 Summary

We have reported a simple electrochemical experiment that employs only common abundant objects and harmless chemicals. This experiment is designed to introduce mild electrochemical hydrogenation to students as a complimentary reaction to the conventional H_2 hydrogenation. Though electrocatalytic hydrogenation (ECH) of acetol to propylene glycol (PG) may seem trivial but one should be reminded that PG (the product) is vital product that impact our daily lives heavily. PG can be found in antifreeze reagent, plastic precursor, preservatives in food and tobacco products. Although the current industrial production of propylene glycol is achieved differently, Acetol is an environmentally friendly reagent that is formed in biomass fast pyrolysis, which converts biomass to bio-oil. In other words, production of propylene glycol, can be achieved from biomass via electrocatalysis, a method potentially powered by renewable electricity source such as solar and wind. In summary, this experiment was designed to demonstrate a “green” chemical transformation that can be achieved with daily used objects. As a bonus, we hope this work can also raise the awareness on sustainability.

Chapter 6 Conclusions

6.1 Project I - ECH of Bio-oil Model Compound, Guaiacol to Chemicals and Fuel

Stabilization and energy upgrading of the model bio-oil components, guaiacol and its congeners, has been achieved electrocatalytically. Hydrodeoxygenation of guaiacol to phenol and cyclohexanol was demonstrated using a Raney-nickel electrocatalyst under ambient conditions. Although cyclohexanol still requires further deoxygenation before it reaches the fuel level energy, it is far more stable than guaiacol in the presence of other organic substrates. The phenolic ring of guaiacol can easily be oxidized or undergo polymerization whereas the saturated ring of cyclohexanol is stable under reasonable storage condition. With this technique developed, it is possible to envision bio-oil getting stabilized in a local electrocatalytic upgrading station, stored, and transported to a centralized refinery for deoxygenation (via dehydration) before it is distributed as fuel. Ideally, of course, it would be better if the final deoxygenation (e.g. cyclohexanol to cyclohexane) could be achieved electrocatalytically.

Improving Columbic efficiency remains a major future challenge. Although Raney-nickel was an excellent low cost substitution for platinum group metals, it preferentially generated hydrogen on its surface leading to low Columbic efficiency during organic hydrogenation. Doping Raney Nickel with low hydrogen activity metals (See Chapter 2, volcano plot) to create new catalyst surface may improve the situation. Furthermore, the stability of Raney-nickel is far from satisfactory – its reactivity decreased significantly after use or exposure to air. Doping the Raney-nickel with foreign metals such as chromium, similar to stainless steel manufacture, might be a good strategy to improve its stability. Following up on the material described above, several experiments are proposed to provide a good starting point for the next project participant.

6.1.1 Improvement I – Electrode Material Synthesis

Raney Nickel electrodes have been a good catalyst towards aromatic bonds hydrogenation, which is usually done with platinum group metal. In Chapter 4, aromatic alkoxy-cleavage occurred in a mildly basic environment using a Raney-Nickel cathode prepared with the Lessard electro co-deposition method. Guaiacol to phenol conversion was followed by aromatic hydrogenation to yield cyclohexanol. Raney-nickel catalyzed the reaction with moderately good Columbic efficiency and excellent selectivity shown in Figure 6-1.

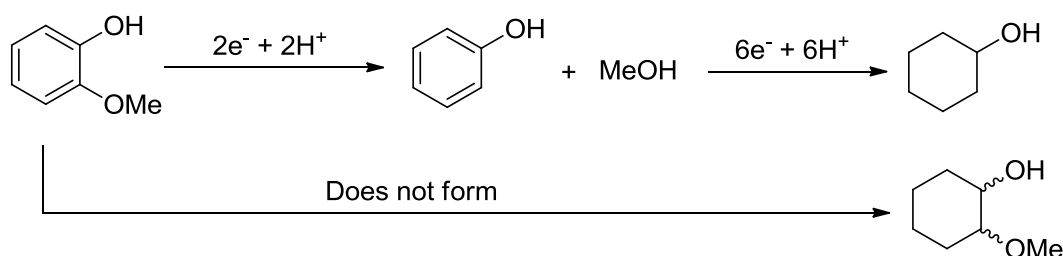


Figure 6-1: ECH of guaiacol using Raney-Nickel cathode. Reaction proceeds with excellent selectivity to form cyclohexanol as the sole product, and does not form the planar 2-methoxycyclohexanol

However, compared to precious platinum, Raney-Nickel is sensitive to air oxidation and acidic environments because nickel can be easily oxidized and dissolved in acid. Seeing the acidic nature of bio-oil, it is important to develop a skeletal catalyst that can tolerate mild acidity while still giving good catalytic effect towards hydrogenation. Moreover, the skeletal catalyst would preferably be air-stable to minimize the storage precautions. Hence, the following three starting directions are proposed to develop an improved skeletal metal.

Nickel-Aluminum-[Metal] synthesis: a significant number of studies have explored the dopant effects of other transition metals such as chromium, molybdenum, tin, lanthanum²²⁶ into the nickel aluminum alloy. These studies are typically conducted to improve the catalytic effect on hydrogen oxidation for H₂ fuel cell application. There is yet to be a modified skeletal nickel

study specifically focused on organic ECH. The natural approach would be to synthesize alloys of known composition from literature and examine their catalytic effects in organic ECH. Separately, cyclic voltammetry (CV) can be used to probe the effects of the dopant on the oxidative potential of the modified skeletal metal catalyst. Successful development of an acid resistant skeletal metal catalyst would be a valuable asset to the bio-oil hydrogenation.

“Skeletalize” known acid resistive alloy: a large number of metal alloys are known to have acid resistive property, such as Monel 400, Hasteloy C, Inconel 600, stainless steel 304 (316), and many more. If aluminum could be fused to the surface of these alloys followed by basic solution treatment to create a porous surface, this could revolutionize the fundamental preparation technique for creating high surface area catalyst.

This strategy is fairly promising, because in his first publication, Murray showed Ni-Al alloy can be synthesized by simply dissolving nickel (mp 1453 °C) into molten aluminum (mp 660 °C) under coal fire heating. In other words, the vast difference in melting point is not an impediment to the synthesis, which therefore should allow a wide substrate survey range. Success of this approach would allow any individual to create a porous highly active catalyst of a well-studied metal alloy with desired properties.

Electroless metal coating on Raney-Nickel electrode: freshly activated Raney-Nickel comes with excellent reducing power on its surface owing to the aluminum leaching. In principle, treating a freshly activated Raney-Nickel catalyst in a metal ion salt solution should achieve electroless deposition of a thin metal coating on the catalyst surface. This thin coating technique has several merits: a) the preparation procedure is simple, b) the amount of coating will automatically be thin and uniform because the reducing power will be gone once the metal is

plated, and c) a precious metals skeletal electrode could take advantage of this strategy because the technique requires minimal electrolyte for plating.

6.1.2 Improvement II – Substrate Scope and Mechanistic Studies

Being able to hydrogenate guaiacol to cyclohexanol is an encouraging step in upgrading similar aromatic compounds found in bio-oil. Syringol (2,6-dimethoxyphenol) reacted similarly to guaiacol to produce cyclohexanol as the final product. The current step is to expand the substrate scope to other aromatics such as eugenol, vanillin, sinapyl alcohol and many more. Understanding how mixtures of different substrates hydrogenate is critical to address the complexity of bio-oil during its upgrading – the mechanism of hydrogenation may change in the presence of multiple substrates.

The current proposed mechanism for guaiacol demethoxylation is informative but not yet conclusive. Although some proposals have been ruled out by designed experiments, the exact mechanism (e.g. how guaiacol adsorbs on the nickel surface) is not clear. Probing guaiacol adsorption on the electrode surface may explain and enable control over the poor selectivity seen in the 3- and 4-methoxyphenol reactions, which showed only partial ether cleavage, leading to similar quantities of the corresponding methoxycyclohexanol and cyclohexanol itself.

6.2 Project II – Development of SPEE system for Bio-oil Hydrogenation

The success of the SPEE cell in ECH of simple aliphatic compounds in the absence of electrolyte was encouraging. However, bio-oil contains a fair number of aromatic compounds that require a more active catalyst for hydrogenation. Ideally, it would be feasible to merge the Raney-nickel chemistry with the SPEE cell setup, using a Raney-nickel cathode to hydrogenate the guaiacol or aromatic compounds. So far, several attempts in this direction have been unsuccessful as discussed in the conclusion section of chapter 5.

Ruthenium has been employed frequently in various research projects in the Jackson Group. It is a natural idea to develop a strategy to deposit a ruthenium surface which opens a path towards aromatic hydrogenation in the SPEE cell. As a prototype experiment, a multiple layer plating scheme was developed to deposit ruthenium onto the stainless mesh surface to carry out phenol hydrogenation. Starting from the support, layers were as follows: Stainless Steel --> Nickel --> Palladium --> Ruthenium. Although the deposition of these multiple layers seems cumbersome, the resulting system did reduce phenol, an aromatic molecule in low yield, in the absence of electrolyte at slightly elevated temperature (75 °C). The use of ruthenium has great potential in the bio-oil upgrading project, and it is a priority to improve the current plating strategy to ensure reproducibility as much as efficiency for the deposition.

6.2.1 Improvement I – Deposition of Ruthenium on Stainless Steel Mesh

Procedures: a 2.5 x 2.5 cm stainless steel was cleaned with hexane to remove wiring oil residue prior the plating. First, the cleaned stainless steel mesh surface was activated by anodic oxidation in 30 °C 10% H₂SO₄ for 30 seconds at 500 mA using a RVC carbon as cathode. After that, the mesh was rinsed briefly with deionized water and plated with nickel in a Watts Strike bath for 2 minutes at 75 mA using a nickel bar as anode. After the Watts Strike bath plating, the mesh is immediately soaked into a 60 °C Woods plating bath and is plated for 15 minutes at 200 mA using a nickel bar as anode. The resulting mesh is denoted as SS-Ni.

The SS-Ni was activated with palladium by placing in contact for 2 minutes in a 5% PdCl₂ solution that was prepared in 2M Hydrochloride acid. The resulting mesh was denoted as SS-Ni-Pd. Then the SS-Ni-Pd mesh is electrocatalytically plated with ruthenium in a dual compartment cell, where the catholyte was prepared with 0.1236 g of RuCl₃.xH₂O in 50 ml of

solution while the analyte was 0.1 M HCl. The plating took take for an hour for 100 mA using a platinum wire as anode.

Each stage of the plating processing, nickel, palladium and ruthenium, was imaged with SEM for surface morphology changes examination, and the results are shown below:

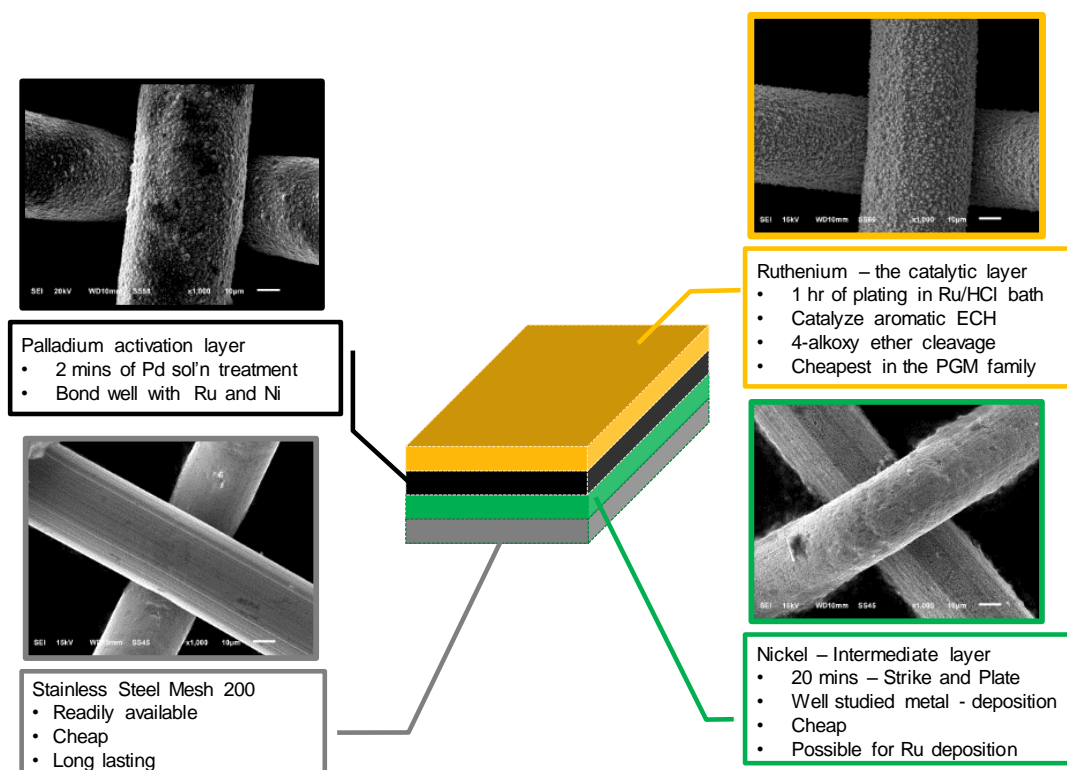


Figure 6-2: Multiple layers of metals plated onto stainless steel to support the deposition of ruthenium.

The complexity of this plating procedure arises from the lack of direct electrochemical deposition of ruthenium onto stainless steel surface. Nickel is a common metal that can be plated on stainless steel after the Woods and Watts bath treatment,²²⁷ and can alloy well with palladium because they belong to the same group.²²⁸ Ruthenium has been reported to deposit on palladium chemically, but this strategy requires elaborate preparation of the reagent solution²²⁹, and hence electrochemical plating was attempted. Fortunately, ruthenium deposition was successful as shown in SEM images, and the EDX analyses.

Table 6-1: atomic % from EDX analysis on the surface of the electrodes, SS-Ni-Pd and SS-Ni-Pd-Ru, showing palladium and ruthenium were deposited onto the surface. Note: the remaining percentage is made of nickel and chloride.

Catalyst Surface	Ruthenium	Palladium
SS-Ni-Pd	Not detected	38.755 ± 5.082
SS-Ni-Pd-Ru	13.680 ± 1.653	4.452 ± 2.078

Both SS-Ni-Pd and SS-Ni-Pd-Ru were used as the electrode for ECH of 10 ml of 50 mM of guaiacol in SPEE at 75 °C for hours at 100 mA. Preliminary results showed 22.1% Columbic efficiency for cyclohexanol formation and no signs of 2-methoxycyclohexanol, an unprecedented hydrogenation of aromatic substrate in an electrolyte free environment.

6.2.2 ECH of Aqueous Bio-oil using Ru-SPEE

Seeing the excitement in aromatic reduction, an aqueous fraction of bio-oil was attempted. An aqueous fraction of bio-oil samples preparation was prepared as earlier published.²¹⁷ Bio-oil is an organic mixture comprising hundreds of organic components, and so it is easier to address a portion at a time in the beginning. The aqueous portion was chosen the groups had earlier studied hydrogenation of bio-oil in a conventional cell using ruthenium on active carbon cloth, and 0.1 M sodium chloride was used as a supporting electrolyte.

A 10 ml sample of aqueous bio-oil fraction was circulated in the cathode compartment at 0.8 ml min⁻¹ in the SPEE cell equipped with the SS-Ni-Pd-Ru cathode and a stainless steel anode in 0.1 M pH 7.0 phosphate buffer. Reaction was run for 6 hours at 75 °C at 100 mA, and the results are shown in Figure 6-4.

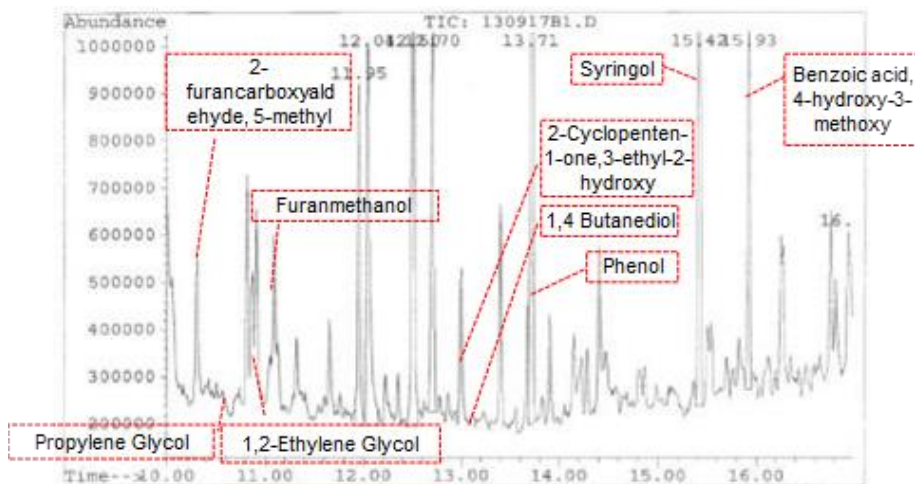


Figure 6-3: GC-MS results on the aqueous fraction of bio-oil before hydrogenation in SPEE cell. Temperature program: 50 °C hold for 3 minutes, then 15 °C/minute until 270 °C and hold for 5 minutes

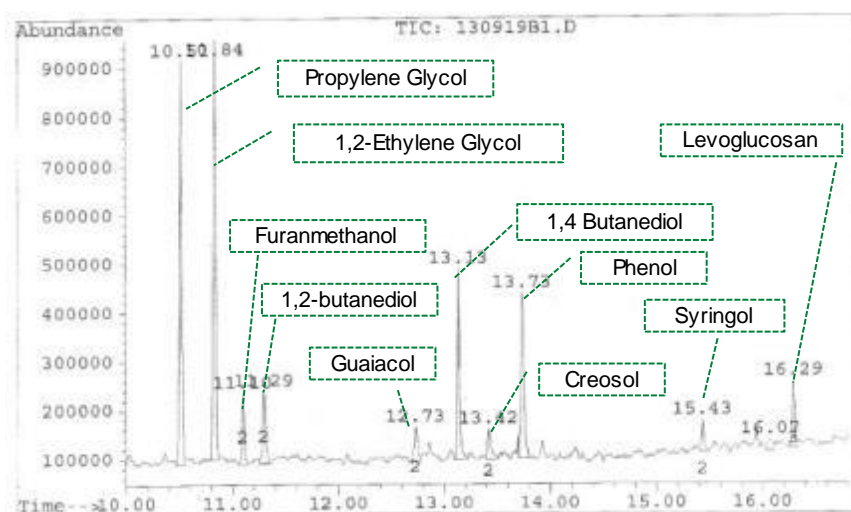


Figure 6-4: GC-MS results on the aqueous fraction of bio-oil after hydrogenation in SPEE cell. Temperature program: 50 °C holds for 3 minutes, then 15 °C/minutes until 270 °C and hold for 5 minutes

After 6 hours of electrolysis, the pH rose from 2 to 11, as tested by universal pH paper. The color of the bio-oil changed from clear light yellow to clear dark brown, and no precipitation was observed. Another distinctive change was that the barbecue smell of the bio-oil disappeared after the electrolysis. Presumably the rise in basicity caused bio-oil components to polymerize which accounts for the darkened color and more importantly, the disappearance of many peaks in

Figure 6-4. From Figure 6-4, formation of various diols and furanmethanol proved organic hydrogenation happened during the electrolysis as expected. However, there were still noticeable amounts of aromatic substrate remaining. The greatest concern is the disappearance of the many peaks compared to the starting spectrum shown in Figure 6-3 due to basic polymerization, similar to the acetol condensation. For these reasons, two strategies were proposed to resolve the basicity issue: a) the use of an anion exchange membrane, and b) use of platinum to supply protons via water splitting. The use of an anion exchange membrane allows the hydroxide formed during cathodic reduction to be transported away and hence maintaining the cathodic acidity constant. In the case of acetol hydrogenation in SPEE: $\text{Acetol} + 2\text{H}_2\text{O} + 2\text{e}^- \rightarrow \text{Propylene Glycol} + 2\text{OH}^-$. Although the use of platinum mesh in deionized water can provide H^+ to neutralize the basicity, the use of platinum would raise the cost of the system, and so it should be considered as the last resort.

An important consideration for this project is to decrease the acidity of bio-oil by converting acetic acid to neutral organics such as ethanol. So far, there is yet to be a reported reaction in literature demonstrating reduction of acetic acid, however, acetic acid oxidative condensation (Kolbe reaction) has been in an SPEE setup and is worth to consider. Otherwise, addition of ammonium hydroxide would be required to neutral the acetic acid before it can be transported or stored.

6.3 New Cell Design – The High Pressure Tube Reactor

Sparked by the continuous flow nature of the SPEE cell, another cell design came to light – the HPLC-like flow tube reactor.

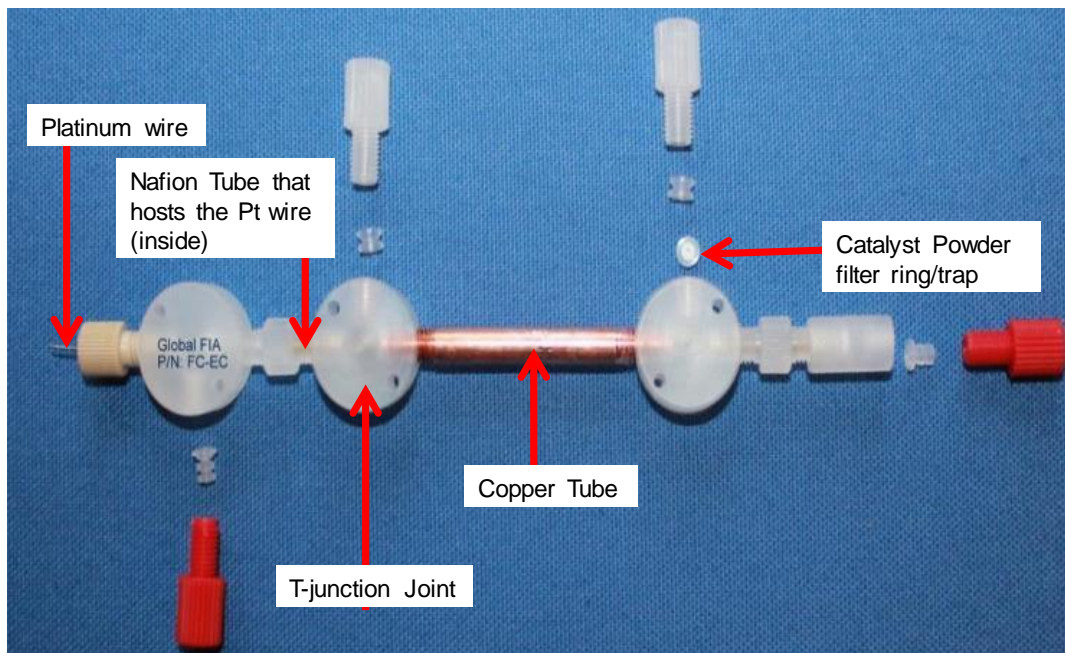


Figure 6-5: HPLC-Flow style cell anatomy

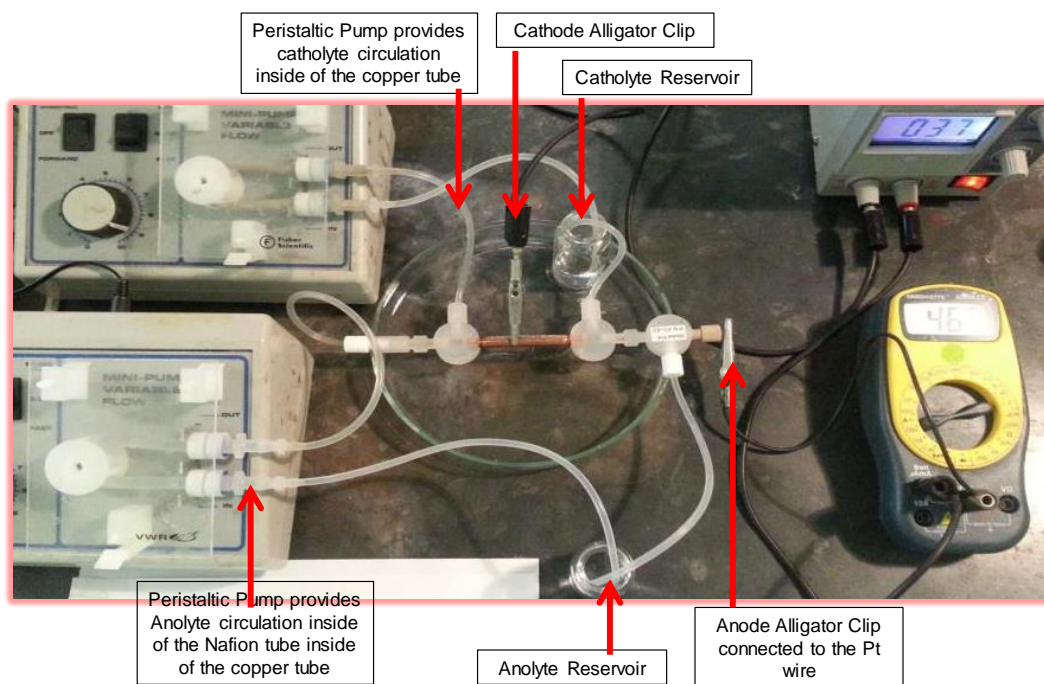


Figure 6-6: the general overall setup of the Flow cell reactor

The flow cell reactor is designed to explore if a higher pressure environment could improve the efficiency of ECH. There is only one study published regarding the effect of

elevated pressure in ECH of phenanthrene using Raney-Nickel with N₂ as an inert gas.²³⁰ The result showed elevated pressure had a negative impact on the Columbic efficiency under constant current electrolysis, evidently due to immobilization of the formed hydrogen in the pores of the electrode. However, when the current is switched to periodic mode, elevated pressure at 20.4 atm has a positive effect. The positive effect could be due to a pressure of hydrogen in the pores insuring by reversal of reaction, a higher concentration of chemisorbed hydrogen and the replenishment of the chemisorbed hydrogen consumed in the hydrogenation reaction.

In the flow cell reactor, the copper tube body serves as a high pressure electrolyte container and the cathode. Inside the copper tube, a Nafion membrane tube houses a platinum wire that serves as the anode. During the reaction, an HPLC pump is employed to circulate the catholyte at moderate flow rates from 0.1 – 1 ml min⁻¹. The end tiny pores trap shown in Figure 6-5 serves as a catalyst powder trapper (future direction – high surface with trapped catalyst powder) and creates back pressure. The higher pressure may boost the absorption for both hydrogen and organics, thereby improving the Columbic efficiency. So far, standard pressure electrolysis has been performed to ensure the functionality of the tube flow cell. In the flow cell, 10 ml of 5% acetol solution dissolved in 0.25 M of ammonium acetate (as a supporting electrolyte) catholyte was circulated in the flow system at 1.0 ml min⁻¹ at room temperature. A 50 mA constant current (estimated current density 117.9 mA cm⁻², based on inner cylinder area of 0.424 cm²) was applied to the system for 6 hours. The anode was a platinum wire inside of a Nafion tube hold a reservoir of 0.1 M H₂SO₄ solution. In addition, an identical experiment was also performed in a non-circulated mode in which 800 ml of cathode was pumped in a “single-pass” motion to simulate the actual industrial style. The comparison was shown in Figure 6-7.

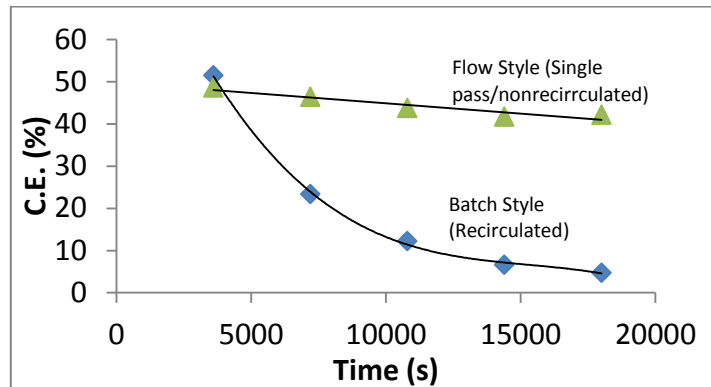


Figure 6-7: Prototype testing of the flow cell reactor. Reaction condition: 5% of acetol dissolved in 0.25 M of ammonium acetate, 50 mA (117.9 mA cm^{-2}), room temperature, 1 ml min^{-1} . Analyte was the platinum wire inside of 0.1 M H_2SO_4 solution. 0.01 ml of sample was taken hourly and was mixed with 0.75 ml of D_2O for H-NMR analysis. The absolute concentration of product was calculated by the internal concentration reference, 1,4-dioxane, that was pre-dissolved in the D_2O solvent. Note: the current efficiency is calculated based on the charge passed and product formed hourly, NOT accumulatively.

In general, the reaction proceeded with good efficiency, forming propylene glycol as the sole product. A single pass experiment showed a small decline in Coulombic efficiency suggesting the cathode surface, inside of the copper tube, was slowly deactivating during the reaction. The batch style flow system started out at a higher Coulombic efficiency (extrapolating the line back to zero), but reached the same level as the single pass reactor after an hour, and the decreased substantially. This was likely due to the lack of reactant on the electrode surface, and in turns forced the electrode surface to form hydrogen, which is not included in the Coulombic efficiency calculation.

An elevated pressure may benefit the electrocatalytic hydrogenation by having the formed H_2 gas potentially be incorporated into the molecules through catalytic hydrogenation. Furthermore, a higher pressure allows the system to reach a higher temperature which may improve the Coulombic efficiency. Several attempts on increasing the pressure of the system led

to catholyte leakages, and current effort is being spent on modifying seals and pressure valves to ensure consistent system performance.

6.4 Overall Progress Summary

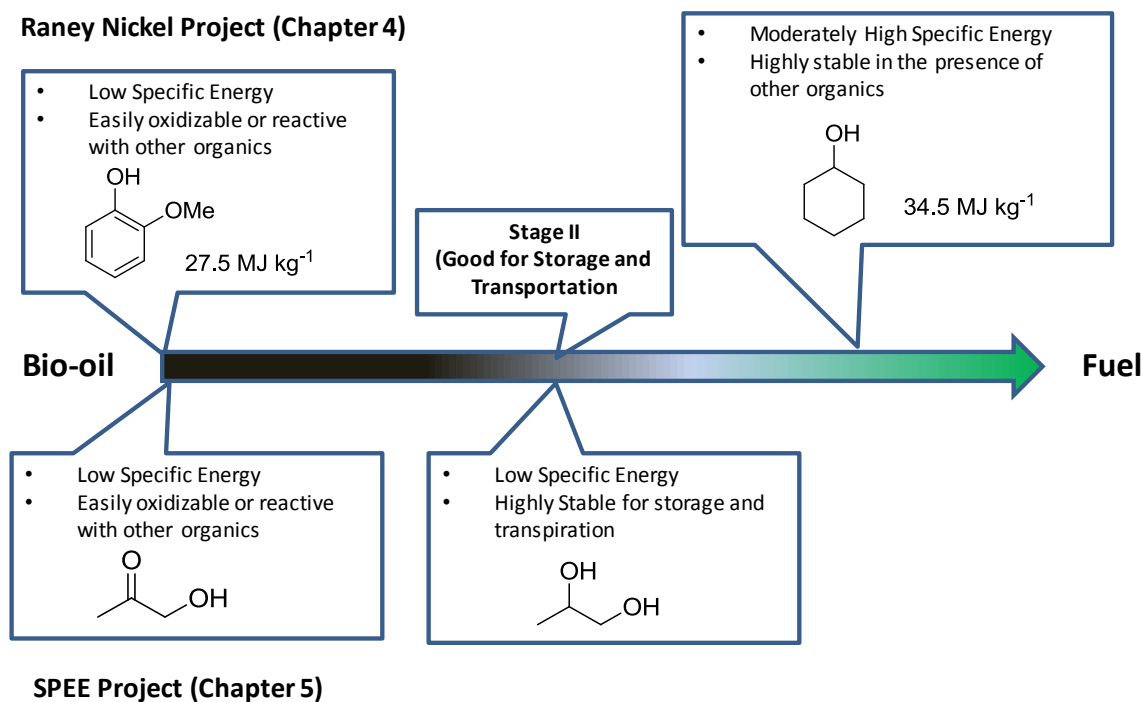


Figure 6-8: Overall time summary of the progress of this research project.

Compared to the SPEE project, the Raney nickel project is relatively closer to the fuel stage because of the guaiacol demethoxylation. Unfortunately, the mechanism of this process is not applicable to cyclohexanol, which typically requires dehydration to deoxygenate. In this context, dehydration is unlikely because ECH typically runs in an aqueous environment, and even if an organic solvent were available (neglecting the expensive cost of organic electrolyte), the acidic environment would favor H₂ evolution and perhaps worse, dissolve the electrode. Therefore, cyclohexanol dehydration would be more readily achieved in a centralized location. However, an acid tolerant catalytically active metal should still be pursued; bio-oil is acidic due to the large quantity of acetic acid. Another improvement would be to find other water splitting

catalysts also made of earth abundant materials but effective at higher current density. The simplicity of cobalt phosphate and the neutral pH performance range are remarkably attractive, but the low current density (1.17 mA cm^{-2}) demands a huge surface area support for adequate current output. Furthermore, use of phosphate buffer will decrease acidity for bio-oil which is good at first but will induce polymerization in the long run beyond neutral pH. Neutralization of bio-oil should be achieved via hydrogenation of the acetic acid, not introducing aprotic cations.

6.5 Final Remarks – The Carbon Balance

Both projects, bio-oil aromatic model compounds upgrading and the SPEE systems, have been studied extensively to understand the mechanism of how the reaction occurred. Various side projects have been devised to advance the fuel production of the project. It is important however, to remember that even with perfect Columbic efficiency and perfect biomass carbon conversion to fuel, there is still not enough carbon by 2030 to address the carbon demand solely for the transportation sector today. Therefore, in order to make biomass fuel sustainable, bio-oil conversion to fuel cannot be the only effort; an alternative fuel consumption strategy is critically needed to maximize the energy extraction from hydrocarbon fuel. The current internal combustion engine (ICE) can, at best, be 40% energy efficient. However, fuel cell technology could boost the energy extraction efficiency to 80%. If ICE could be replaced by hydrocarbon fuel cell, it would effectively reduce the US fuel dependence by half.

This section is not meant to discuss hydrocarbon or related chemical fuel cell in detail, but to keep readers reminded that creating a sustainable renewable fuel cycle will require more than just making hydrocarbons. Renewable fuel production is only the first half of the sustainable fuel cycle; the other half is the development of a more efficient energy extraction system to lower fuel demand. As noted, the projected 2030 non-food grade biomass will only

have enough carbon to cover approximately $2/3$ of the current consumption today. Hence a different approach for extracting hydrocarbons' energy is needed to complete the overall equation. It need not be a fuel cell, though that appears most promising today. As much as a world free from fossil carbon use would be wonderful, hydrocarbon will still be needed as the primary energy carriers that are safe, well-established, and high in specific energy. Until a new energy source is identified with equal or greater merits, hydrocarbons will still be the primary fuels for transportation. By replacing fossil with biomass carbon and a devising more energy efficient extraction systems, a future that travels using a truly sustainable renewable fuel recycle can be envisioned.

REFERENCES

REFERENCES

1. BTS Table 1-11: Number of U.S. Aircraft, Vehicles, Vessels, and Other Conveyances. http://www.rita.dot.gov/bts/sites/rita.dot.gov.bts/files/publications/national_transportation_statistics/html/table_01_11.html (accessed 12 Mar 2014).
2. EIA How many alternative fuel and hybrid vehicles are there in the U.S.? <http://www.eia.gov/tools/faqs/faq.cfm?id=93&t=4> (accessed 1 Mar 2014).
3. Thomas, G. Overview of Storage Development DOE Hydrogen Program. <http://www1.eere.energy.gov/hydrogenandfuelcells/pdfs/storage.pdf> (accessed 1 Mar 2014).
4. Musk, E.; Straubel, J. B. Model S Efficiency and Range. <http://www.teslamotors.com/blog/model-s-efficiency-and-range> (accessed 1 Mar 2014).
5. EERE Ethanol Fueling Station Locations. http://www.afdc.energy.gov/fuels/ethanol_locations.html (accessed 1 Mar 2014).
6. Tesla Tesla Charging | Tesla Motors. <http://www.teslamotors.com/charging#/calculator> (accessed 1 Mar 2014).
7. Sherif, S. A.; Barbir, F.; Veziroglu, T. N., Wind energy and the hydrogen economy—review of the technology. *Solar Energy* **2005**, *78* (5), 647-660.
8. DeLuchi, M. A., Hydrogen vehicles: an evaluation of fuel storage, performance, safety, environmental impacts, and cost. *Int. J. Hydrogen Energy* **1989**, *14* (2), 81-130.
9. Winkler, W.; Nehter, P., Thermodynamics of Fuel Cells. In *Modeling Solid Oxide Fuel Cells*, Bove, R.; Ubertini, S., Eds. Springer Netherlands: 2008; pp 13-50.
10. O'Garra, T.; Mourato, S.; Pearson, P., Analysing awareness and acceptability of hydrogen vehicles: A London case study. *Int. J. Hydrogen Energy* **2005**, *30* (6), 649-659.
11. Stopher, P.; Stanley, J., *Introduction to Transport Policy: A Public Policy View*. 1st ed.; Edward Elgar Publishing Limited: Cheltenham, UK, 2014; p 360.
12. Cadwallader, L. C.; Herring, J. S. *Safety Issues with Hydrogen as a Vehicle Fuel*; Idaho National Engineering and Environmental Laboratory: Idaho Falls, 1999; p 78.
13. Kikukawa, S.; Yamaga, F.; Mitsuhashi, H., Risk assessment of Hydrogen fueling stations for 70MPa FCVs. *Int. J. Hydrogen Energy* **2008**, *33* (23), 7129-7136.
14. Bockris, J., A Hydrogen Economy. *Science* **1972**, *176* (4041), 2.

15. Peplow, M. Hydrogen's False Economy. <http://www.rsc.org/chemistryworld/2013/03/hydrogen-economy-clean-energy> (accessed 1 Mar 2014).
16. EERE Benefits and Challenges. https://www.fueleconomy.gov/feg/fcv_benefits.shtml (accessed 1 Mar 2014).
17. Dillich, S. Hydrogen Production & Delivery. http://www.hydrogen.energy.gov/pdfs/review12/pd_plenary_dillich_2012_o.pdf.
18. Siler, S. Pump it Up: We Refuel a Hydrogen Fuel-Cell Vehicle. <http://www.caranddriver.com/features/pump-it-up-we-refuel-a-hydrogen-fuel-cell-vehicle-hydrogen-filling-stations-are-still-rare-page-3> (accessed 2 Mar 2014).
19. Bossel, U.; Eliasson, B. *Energy and the Hydrogen Economy*; Alternative Fuels Data Center - U.S. Department of Energy: 2003.
20. Çengel, Y. A.; Boles, M. A., *Thermodynamics: An Engineering Approach*. McGraw-Hill Professional Publishing: 2004.
21. EERE Ethanol Production and Distribution. http://www.afdc.energy.gov/fuels/ethanol_production.html (accessed 27 Mar 2014).
22. Nopmongcol, U.; Griffin, W. M.; Yarwood, G.; Dunker, A. M.; MacLean, H. L.; Mansell, G.; Grant, J., Impact of dedicated E85 vehicle use on ozone and particulate matter in the US. *Atmos. Environ.* **2011**, *45* (39), 7330-7340.
23. Yang, Y.; Bae, J.; Kim, J.; Suh, S., Replacing Gasoline with Corn Ethanol Results in Significant Environmental Problem-Shifting. *Environmental Science & Technology* **2012**, *46* (7), 3671-3678.
24. Hill, J.; Nelson, E.; Tilman, D.; Polasky, S.; Tiffany, D., Environmental, economic, and energetic costs and benefits of biodiesel and ethanol biofuels. *Proceedings of the National Academy of Sciences* **2006**, *103* (30), 11206-11210.
25. Donner, S. D.; Kucharik, C. J., Corn-based ethanol production compromises goal of reducing nitrogen export by the Mississippi River. *Proceedings of the National Academy of Sciences* **2008**, *105* (11), 4513-4518.
26. Fargione, J.; Hill, J.; Tilman, D.; Polasky, S.; Hawthorne, P., Land Clearing and the Biofuel Carbon Debt. *Science* **2008**, *319* (5867), 1235-1238.
27. Kim, S.; Dale, B. E., Life cycle assessment of various cropping systems utilized for producing biofuels: Bioethanol and biodiesel. *Biomass Bioenergy* **2005**, *29* (6), 426-439.

28. Steynberg, A. P.; Espinoza, R. L.; Jager, B.; Vosloo, A. C., High temperature Fischer–Tropsch synthesis in commercial practice. *Appl. Catal., A* **1999**, *186* (1–2), 41-54.
29. de Klerk, A., Fischer–Tropsch Process. In *Kirk-Othmer Encyclopedia of Chemical Technology*, John Wiley & Sons, Inc.: 2000.
30. Espinoza, R. L.; Steynberg, A. P.; Jager, B.; Vosloo, A. C., Low temperature Fischer–Tropsch synthesis from a Sasol perspective. *Appl. Catal., A* **1999**, *186* (1–2), 13-26.
31. Demirbas, A., Biorefineries: Current activities and future developments. *Energy Conversion and Management* **2009**, *50* (11), 2782-2801.
32. Fatih Demirbas, M., Biorefineries for biofuel upgrading: A critical review. *Applied Energy* **2009**, *86*, *Supplement 1* (0), S151-S161.
33. Jitaru, M., Electrochemical Carbon Dioxide Reduction - Fundamental and Applied Topics (Review). *Journal of the Univeristy of Chemical Technology and Metallurgy* **2007**, *42* (4), 12.
34. Azuma, M.; Hashimoto, K.; Hiramoto, M.; Watanabe, M.; Sakata, T., Electrochemical Reduction of Carbon Dioxide on Various Metal Electrodes in Low-Temperature Aqueous KHCO₃ Media. *J. Electrochem. Soc.* **1990**, *137* (6), 1772-1778.
35. Hori, Y., Electrochemical CO₂ Reduction on Metal Electrodes. In *Modern Aspects of Electrochemistry*, Vayenas, C.; White, R.; Gamboa-Aldeco, M., Eds. Springer New York: 2008; Vol. 42, pp 89-189.
36. Haynes, L. V.; Sawyer, D. T., Electrochemistry of carbon dioxide in dimethyl sulfoxide at gold and mercury electrodes. *Anal. Chem.* **1967**, *39* (3), 332-338.
37. Bewick, A.; Greener, G. P., The electroreduction of CO₂ to glycollate on a lead cathode. *Tetrahedron Lett.* **1970**, *11* (5), 391-394.
38. Bewick, A.; Greener, G. P., The electroreduction of CO₂ to malate on a mercury cathode. *Tetrahedron Lett.* **1969**, *10* (53), 4623-4626.
39. Kuhl, K. P.; Cave, E. R.; Abram, D. N.; Jaramillo, T. F., New insights into the electrochemical reduction of carbon dioxide on metallic copper surfaces. *Energy Environ. Sci.* **2012**, *5* (5), 7050-7059.
40. Gattrell, M.; Gupta, N.; Co, A., A review of the aqueous electrochemical reduction of CO₂ to hydrocarbons at copper. *J. Electroanal. Chem.* **2006**, *594* (1), 1-19.
41. Kondratenko, E. V.; Mul, G.; Baltrusaitis, J.; Larrazabal, G. O.; Perez-Ramirez, J., Status and perspectives of CO₂ conversion into fuels and chemicals by catalytic, photocatalytic and electrocatalytic processes. *Energy Environ. Sci.* **2013**, *6* (11), 3112-3135.

42. Gibbins, J.; Chalmers, H., Carbon capture and storage. *Energy Policy* **2008**, *36* (12), 4317-4322.
43. Metz, B.; III., I. P. o. C. C. W. G., *IPCC Special Report on Carbon Dioxide Capture and Storage*. Cambridge University Press for the Intergovernmental Panel on Climate Change: 2005.
44. Rochon, E.; Bjureby, E.; Johnston, P.; Oakley, R.; Santillo, D.; Schulz, N.; Goerne, G. v. *False Hope - Why Carbon Capture and Storage won't save the climate*; The Netherlands, 2008.
45. Pires, J. C. M.; Martins, F. G.; Alvim-Ferraz, M. C. M.; Simões, M., Recent developments on carbon capture and storage: An overview. *Chem. Eng. Res. Des.* **2011**, *89* (9), 1446-1460.
46. EIA Petroleum & Other Liquids.
http://www.eia.gov/dnav/pet/pet_cons_psup_dc_nus_mbbldpd_a.htm (accessed 26 Mar 2014).
47. Tverberg, G. Why is US Oil Consumption Lower? Better Gasoline Mileage?
<http://ourfiniteworld.com/2013/01/31/why-is-us-oil-consumption-lower-better-gasoline-mileage/> (accessed 2 Mar 2014).
48. EIA How much petroleum does the United States import and from where?
<http://www.eia.gov/tools/faqs/faq.cfm?id=727&t=6> (accessed 1 Mar 2014).
49. James.H.Butler The NOAA Annual Greenhouse Gas Index.
<http://www.esrl.noaa.gov/gmd/aggi/> (accessed 25 Apr 2011).
50. Tans, P. ESRL Global Monitor Division - Global Greenhouse Gas Reference Network.
<http://www.esrl.noaa.gov/gmd/ccgg/trends/> (accessed 4 Mar 2014).
51. EPA Overview of Greenhouse Gases.
<http://www.epa.gov/climatechange/ghgemissions/gases/co2.html> (accessed 1 Mar 2014).
52. Statistics, B. o. T. National Transportation Statistics.
http://www.bts.gov/publications/national_transportation_statistics/ (accessed 20 Apr 2011).
53. Downing, M.; Eaton, L. M.; Graham, R. L.; Langholtz, M. H.; Perlack, R. D.; Turhollow Jr, A. F.; Stokes, B.; Brandt, C. C. *U.S. Billion-Ton Update: Biomass Supply for a Bioenergy and Bioproducts Industry*; ORNL/TM-2011/224; Other: BM0102030; CEBM007; TRN: US201118%%1083 United States10.2172/1023318Other: BM0102030; CEBM007; TRN: US201118%%1083Thu Jun 06 09:43:04 EDT 2013ORNLEnglish; 2011; p Medium: ED.
54. Joosten, J.; Gross, P.; Kydes, A.; Maples, J. D. *The Impact of Increased Use of Hydrogen on Petroleum Consumption and Carbon Dioxide Emissions*; National Energy Information Center: 2008; p 20.

55. Zhu, X.-G.; Long, S. P.; Ort, D. R., What is the maximum efficiency with which photosynthesis can convert solar energy into biomass? *Curr. Opin. Biotechnol.* **2008**, *19* (2), 153-159.
56. Govindjee; Govindjee, R. What is Photosynthesis? <http://www.life.illinois.edu/govindjee/whatisit.htm> (accessed 26 Mar 2014).
57. Blaikie, D. Most Efficient Solar Panels. <http://sroeco.com/solar/most-efficient-solar-panels>.
58. Bridgwater, A. V.; Meier, D.; Radlein, D., An overview of fast pyrolysis of biomass. *Org. Geochem.* **1999**, *30* (12), 1479-1493.
59. Elliott, D. C.; Beckman, D.; Bridgwater, A. V.; Diebold, J. P.; Gevert, S. B.; Solantausta, Y., Developments in Direct Thermochemical Liquefaction of Biomass - 1983-1990. *Energy Fuels* **1991**, *5* (3), 399-410.
60. Bridgwater, A. V., Production of high grade fuels and chemicals from catalytic pyrolysis of biomass. *Catal. Today* **1996**, *29* (1-4), 285-295.
61. Bridgwater, A. V., Principles and practice of biomass fast pyrolysis processes for liquids. *J. Anal. Appl. Pyrolysis* **1999**, *51* (1-2), 3-22.
62. Bridgwater, A. V.; Peacocke, G. V. C., Fast pyrolysis processes for biomass. *Renew. Sust. Energ. Rev.* **2000**, *4* (1), 1-73.
63. Bridgwater, A. V., *Fast Pyrolysis of Biomass 2: A Handbook*. CPL Scientific Publishing Services, Limited: 2002.
64. Czernik, S.; Bridgwater, A. V., Overview of Applications of Biomass Fast Pyrolysis Oil. *Energy Fuels* **2004**, *18* (2), 590-598.
65. Nowakowski, D. J.; Bridgwater, A. V.; Elliott, D. C.; Meier, D.; de Wild, P., Lignin fast pyrolysis: Results from an international collaboration. *J. Anal. Appl. Pyrolysis* **2010**, *88* (1), 53-72.
66. Bridgwater, A. V., Review of fast pyrolysis of biomass and product upgrading. *Biomass Bioenergy* **2012**, *38* (0), 68-94.
67. Campbell, M. M.; Sederoff, R. R., Variation in lignin content and composition - Mechanism of control and implications for the genetic improvement of plants. *Plant Physiol.* **1996**, *110* (1), 3-13.
68. Mosier, N.; Wyman, C.; Dale, B.; Elander, R.; Lee, Y. Y.; Holtzapple, M.; Ladisch, M., Features of promising technologies for pretreatment of lignocellulosic biomass. *Bioresour. Technol.* **2005**, *96* (6), 673-686.

69. Elliott, D. C., Historical Developments in Hydroprocessing Bio-oils. *Energy Fuels* **2007**, *21* (3), 1792-1815.
70. Elliott, D. C.; Hart, T. R., Catalytic Hydroprocessing of Chemical Models for Bio-oil. *Energy Fuels* **2008**, *23*, 631-637.
71. Singh, S. K.; Mukherjee, A. K.; Singh, M. M., Corrosion characteristics of mild steel in aqueous solution of formic acid containing some acetic acid. *Indian J. Chem. Technol.* **2008**, *15* (2), 174-179.
72. Dickerson, T.; Soria, J., Catalytic Fast Pyrolysis: A Review. *energies* **2013**, (6), 25.
73. Driveclean Ethanol (E85) Flex Fuel.
[http://www.driveclean.ca.gov/Search_and_Explore/Technologies_and_Fuel_Types/Ethanol_\(E85\)_Flex_Fuel.php](http://www.driveclean.ca.gov/Search_and_Explore/Technologies_and_Fuel_Types/Ethanol_(E85)_Flex_Fuel.php) (accessed 27 Mar 2014).
74. Zhao, C.; Kou, Y.; Lemonidou, A. A.; Li, X.; Lercher, J. A., Highly selective catalytic conversion of phenolic bio-oil to alkanes. *Angew. Chem.* **2009**, *121*, 4047-4050.
75. Zhao, C.; Kou, Y.; Lemonidou, A. A.; Li, X.; Lercher, J. A., Hydrodeoxygenation of bio-derived phenols to hydrocarbons using RANEY® Ni and Nafion/SiO₂ catalysts. *Chem. Commun.* **2010**, *46*, 412-414.
76. Song, C., An overview of new approaches to deep desulfurization for ultra-clean gasoline, diesel fuel and jet fuel. *Catal. Today* **2003**, *86* (1-4), 211-263.
77. Babich, I. V.; Moulijn, J. A., Science and technology of novel processes for deep desulfurization of oil refinery streams: a review. *Fuel* **2003**, *82* (6), 607-631.
78. Brunet, S.; Mey, D.; Pérot, G.; Bouchy, C.; Diehl, F., On the hydrodesulfurization of FCC gasoline: a review. *Appl. Catal., A* **2005**, *278* (2), 143-172.
79. Grange, P., Catalytic Hydrodesulfurization. *Catalysis Reviews* **1980**, *21* (1), 135-181.
80. Lee, J.; Kim, Y. T.; Huber, G. W., Aqueous-phase hydrogenation and hydrodeoxygenation of biomass-derived oxygenates with bimetallic catalysts. *Green Chem.* **2014**, *16* (2), 708-718.
81. Talmadge, M. S.; Baldwin, R. M.; Bidy, M. J.; McCormick, R. L.; Beckham, G. T.; Ferguson, G. A.; Czernik, S.; Magrini-Bair, K. A.; Foust, T. D.; Metelski, P. D.; Hetrick, C.; Nimlos, M. R., A perspective on oxygenated species in the refinery integration of pyrolysis oil. *Green Chem.* **2014**, *16* (2), 407-453.
82. Zacher, A. H.; Olarte, M. V.; Santosa, D. M.; Elliott, D. C.; Jones, S. B., A review and perspective of recent bio-oil hydrotreating research. *Green Chem.* **2014**, *16* (2), 491-515.

83. Mortensen, P. M.; Grunwaldt, J.-D.; Jensen, P. A.; Jensen, A. D., Screening of Catalysts for Hydrodeoxygenation of Phenol as a Model Compound for Bio-oil. *ACS Catalysis* **2013**, *3* (8), 1774-1785.
84. Mortensen, P. M.; Grunwaldt, J. D.; Jensen, P. A.; Knudsen, K. G.; Jensen, A. D., A review of catalytic upgrading of bio-oil to engine fuels. *Appl. Catal., A* **2011**, *407* (1-2), 1-19.
85. Pstrowska, K.; Walendziewski, J.; Luzny, R.; Stolarski, M., Hydroprocessing of rapeseed pyrolysis bio-oil over NiMo/Al₂O₃ catalyst. *Catal. Today* **2014**, *223*, 54-65.
86. Saidi, M.; Samimi, F.; Karimipourfard, D.; Nimmanwudipong, T.; Gates, B. C.; Rahimpour, M. R., Upgrading of lignin-derived bio-oils by catalytic hydrodeoxygenation. *Energy Environ. Sci.* **2014**, *7* (1), 103-129.
87. Ruddy, D. A.; Schaidle, J. A.; Ferrell, J. R.; Wang, J.; Moens, L.; Hensley, J. E., Recent advances in heterogeneous catalysts for bio-oil upgrading via "ex situ catalytic fast pyrolysis": catalyst development through the study of model compounds. *Green Chem.* **2014**, *16* (2), 454-490.
88. Popov, A.; Kondratieva, E.; Mariey, L.; Goupil, J. M.; El Fallah, J.; Gilson, J. P.; Travert, A.; Mauge, F., Bio-oil hydrodeoxygenation: Adsorption of phenolic compounds on sulfided (Co)Mo catalysts. *J. Catal.* **2013**, *297*, 176-186.
89. Wisniak, J.; Hershkowitz, M.; Stein, S., *Ind. Eng. Chem. Prod. Res. Dev.* **1974** *13*, 232-236.
90. Zhang, Z.; Jackson, J. E.; Miller, D., *J. Appl. Catal. A* **2001**, *219*, 89-98.
91. Dalavoy, T. S.; Jackson, J. E.; Swain, G. M.; Miller, D. J.; Li, J.; Lipkowski, J., Mild electrocatalytic hydrogenation of lactic acid to lactaldehyde and propylene glycol. *J. Catal.* **2007**, *246*, 15-28.
92. Iikiti, H.; Rekik, N.; Thomalla, M., *J. Appl. Electrochem.* **2002**, *32*, 603-609.
93. Iikiti, H.; Rekik, N.; Thomalla, M., *J. Appl. Electrochem.* **2004**, *34*, 127-136.
94. Lund, H., A Century of Organic Electrochemistry. *Journal of Electrochemical Society* **2002**, *149*, 21-33.
95. White, H. L., *Introduction to Industrial Chemistry*. Wiley: 1986.
96. Vilar, M.; Oliveira, J. L.; Navarro, M., *Appl. Catal., A* **2010**, *372*, 1-7.
97. Navarro, D. M. A. F. N.; Navarro, M., Catalytic Hydrogenation of Organic Compounds without H₂ Supply: An Electrochemical System. *J. Chem. Educ.* **2004**, *81*, 1350-1352.

98. Santana, D. S.; Melo, G. O.; Lima, M. V. F.; Daniel, J. R. R.; Areias, M. C. C.; Navarro, M., Electrocatalytic hydrogenation of organic compounds using a nickel sacrificial anode. *J. Electroanal. Chem.* **2004**, *569* (1), 71-78.
99. Iikti, H.; Rekik, N.; Thomalla, M., Electrocatalytic hydrogenation of alkyl-substituted phenols in aqueous solutions at a Raney nickel electrode in the presence of a non-micelle-forming cationic surfactant *J. Appl. Electrochem.* **2004**, *34*, 127-136.
100. Iikti, H.; Rekik, N.; Thomalla, M., Electrocatalytic hydrogenation of phenol in aqueous solutions at a Raney nickel electrode in the presence of cationic surfactants. *J. Appl. Electrochem.* **2002**, *32* (6), 603-609.
101. Anderson, M. T.; Martin, J. E.; Odinek, J. G.; Newcomer, P. P., Effect of Methanol Concentration on CTAB Micellization and on the Formation of Surfactant-Templated Silica (STS). *Chem. Mater.* **1998**, *10* (6), 1490-1500.
102. Shi, Z.; Zhou, Y.-H.; Cha, C.-S., Influence of perfluorinated surfactants on the electrochemical behaviour of a lead electrode in sulfuric acid solution. *J. Power Sources* **1998**, *70* (2), 214-221.
103. Beraud, V.; Thomalla, M.; Lessard, J., The influence of a non-micelle-forming surfactant on the electrocatalytic hydrogenation of carvone and limonene in aqueous medium at Raney nickel electrodes. *Can. J. Chem.* **1997**, *75* (11), 1529-1535.
104. Chambrion, P.; Roger, L.; Lessard, J.; Béraud, V.; Mailhot, J.; Thomalla, M., The influence of surfactants on the electrocatalytic hydrogenation of organic compounds in micellar, emulsified, and hydroorganic solutions at Raney nickel electrodes. *Can. J. Chem.* **1995**, *73* (6), 804-815.
105. Cifuentes, A.; Bernal, J. L.; Diez-Masa, J. C., Determination of Critical Micelle Concentration Values Using Capillary Electrophoresis Instrumentation. *Anal. Chem.* **1997**, *69* (20), 4271-4274.
106. Swann, S.; Nelson, G. H., The Electrolytic Reduction of Acetophenone. *Transactions of The Electrochemical Society* **1935**, *67* (1), 201-207.
107. Laursen, A. B.; Varela, A. S.; Dionigi, F.; Fanchiu, H.; Miller, C.; Trinhammer, O. L.; Rossmeisl, J.; Dahl, S., Electrochemical Hydrogen Evolution: Sabatier's Principle and the Volcano Plot. *J. Chem. Educ.* **2012**, *89* (12), 1595-1599.
108. de Chialvo, M. R. G.; Chialvo, A. C., Hydrogen evolution reaction: Analysis of the Volmer-Heyrovsky-Tafel mechanism with a generalized adsorption model. *J. Electroanal. Chem.* **1994**, *372* (1-2), 209-223.
109. Schmickler, W.; Santos, E., *Interfacial Electrochemistry*. Springer: 2010.

110. Cleghorn, S. J. C.; Pletcher, D., Investigations of the electrocatalytic hydrogenation of organic molecules at palladium on nickel cathodes. *Electrochim. Acta* **1993**, *38* (18), 2683-2689.
111. Antonietta Casadei, M.; Pletcher, D., The influence of conditions on the electrocatalytic hydrogenation of organic molecules. *Electrochim. Acta* **1988**, *33* (1), 117-120.
112. Cleghorn, S. J. C.; Pletcher, D., The mechanism of electrocatalytic hydrogenation of organic molecules at palladium black cathodes. *Electrochim. Acta* **1993**, *38* (2-3), 425-430.
113. Polcaro, A. M.; Palmas, S.; Dernini, S., Electrochemical reduction of carbonyl compounds at modified carbon felt electrodes. *Electrochim. Acta* **1993**, *38* (2-3), 199-203.
114. Gulyai, V. P.; Strelets, V. V., Electrochemical hydrogenation of citral. *Russian Chemical Bulletin* **1999**, *48* (1), 202-204.
115. Schwientek, M.; Pleus, S.; Hamann, C. H., Enantioselective electrodes: stereoselective electroreduction of 4-methylbenzophenone and acetophenone. *J. Electroanal. Chem.* **1999**, *461* (1-2), 94-101.
116. Brennan, M. P. J.; Brown, O. R., Mechanism of the cathodic reduction of acetophenone in acidic aqueous-methanolic media. *Journal of the Chemical Society, Faraday Transactions 1: Physical Chemistry in Condensed Phases* **1973**, *69* (0), 132-142.
117. Chapuzet, J. M.; Lasia, A.; Lessard, J., *Electrocatalysis*. Wiley-VCH: New York, 1998.
118. Couper, A. M.; Pletcher, D.; Walsh, F. C., Electrode materials for electrosynthesis. *Chemical Reviews* **1990**, *90* (5), 837-865.
119. Santana, D. S.; Lima, M. V. F.; Daniel, J. R. R.; Navarro, M., Electrocatalytic hydrogenation of organic compounds using current density gradient and sacrificial anode of nickel. *Tetrahedron Lett.* **2003**, *44*, 4725-4727.
120. Vilar, M.; Oliveira, J. L.; Navarro, M., Investigation of the hydrogenation reactivity of some organic substrates using an electrocatalytic method. *Appl. Catal., A* **2010**, *372* (1), 1-7.
121. Raney, M., Method of preparing catalytic material. Google Patents: 1925.
122. Raney, M., Method of producing finely-divided nickel. Google Patents: 1927.
123. Krupp, H.; Rabenhorst, H.; Sandstede, G.; Walter, G.; McJones, R., Raney Type Transition Metals as Fuel Electrode Catalysts. *J. Electrochem. Soc.* **1962**, *109* (7), 553-557.
124. Augustine, R. L., *Heterogeneous Catalysis for the Synthetic Chemist*. Marcel Dekker, Inc.: New York, 1995.

125. Fouilloux, P., The nature of raney nickel, its adsorbed hydrogen and its catalytic activity for hydrogenation reactions (review). *Applied Catalysis* **1983**, 8 (1), 1-42.
126. Mazingo, R.; Spencer, C.; Folkers, K., Hydrogenation by Raney Nickel Catalyst without Gaseous Hydrogen. *J. Am. Chem. Soc.* **1944**, 66 (11), 1859-1860.
127. Besson, M.; Djaouadi, D.; Bonnier, J. M.; Hamar-Thibault, S.; Joucla, M., Structure and Catalytic Properties in Hydrogenation of Valeronitrile of Raney Nickel Prepared from Cr and Mo Doped Ni₂Al₃ Alloys. In *Stud. Surf. Sci. Catal.*, M. Guisnet; J. Barrault; C. Bouchoule; D. Duprez; G. Pérot R. Maurel; Montassier, C., Eds. Elsevier: 1991; Vol. Volume 59, pp 113-120.
128. Birry, L.; Lasia, A., Studies of the Hydrogen Evolution Reaction on Raney Nickel—Molybdenum Electrodes. *J. Appl. Electrochem.* **2004**, 34 (7), 735-749.
129. Robin, D.; Comtois, M.; Martel, A.; Lemieux, R.; Cheong, A. K.; Belot, G.; Lessard, J., The electrocatalytic hydrogenation of fused poly cyclic aromatic compounds at Raney nickel electrodes: the influence of catalyst activation and electrolysis conditions. *Can. J. Chem.* **1990**, 68, 1218-1227.
130. Kokes, R. J.; Emmett, P. H., The Role of Hydrogen in Raney Nickel Catalysts. *J. Am. Chem. Soc.* **1959**, 81 (19), 5032-5037.
131. Filippov, D. V.; Ulitin, M. V.; Korosteleva, P. O., The thermodynamic characteristics of processes in Raney nickel surface layers with the participation of adsorbed hydrogen forms. *Russ. J. Phys. Chem.* **2008**, 82 (5), 835-840.
132. Endoh, E.; Otouma, H.; Morimoto, T.; Oda, Y., New Raney nickel composite-coated electrode for hydrogen evolution. *Int. J. Hydrogen Energy* **1987**, 12 (7), 473-479.
133. Choquette, Y.; Brossard, L.; Lasia, A.; Menard, H., Study of the Kinetics of Hydrogen Evolution Reaction on Raney Nickel Composite-Coated Electrode by AC Impedance Technique. *J. Electrochem. Soc.* **1990**, 137 (6), 1723-1730.
134. Smith, H. A.; Chadwell, A. J.; Kirslis, S. S., The Role of Hydrogen in Raney Nickel Catalyst. *The Journal of Physical Chemistry* **1955**, 59 (9), 820-822.
135. Freel, J.; Robertson, S. D.; Anderson, R. B., The structure of Raney nickel: III. The chemisorption of hydrogen and carbon monoxide. *J. Catal.* **1970**, 18 (3), 243-248.
136. Renouprez, A. J.; Fouilloux, P.; Coudurier, G.; Tocchetti, D.; Stockmeyer, R., Different species of hydrogen chemisorbed on Raney nickel studied by neutron inelastic spectroscopy. *Journal of the Chemical Society, Faraday Transactions 1: Physical Chemistry in Condensed Phases* **1977**, 73 (0), 1-10.
137. Konvalinka, J. A.; Van Oeffelt, P. H.; Scholten, J. J. F., Temperature programmed desorption of hydrogen from nickel catalysts. *Applied Catalysis* **1981**, 1 (3-4), 141-158.

138. Kokes, R. J.; Emmett, P. H., Adsorption Studies on Raney Nickel. *J. Am. Chem. Soc.* **1961**, 83 (1), 29-31.
139. Tétényi, P.; Babernics, L., Investigations on the chemisorption of benzene on nickel and platinum. *J. Catal.* **1967**, 8 (3), 215-222.
140. Hauptmann, H.; Walter, W. F., The Action of Raney Nickel on Organic Sulfur Compounds. *Chemical Reviews* **1962**, 62 (5), 347-404.
141. Hochard, F.; Jobic, H.; Massardier, J.; Renouprez, A. J., Gas phase hydrogenation of acetonitrile on Raney nickel catalysts: reactive hydrogen. *J. Mol. Catal. A: Chem.* **1995**, 95 (2), 165-172.
142. Kleiderer, E. C.; Kornfeld, E. C., Raney Nickel as an Organic Oxidation-Reduction Catalyat. *J. Org. Chem.* **1948**, 13 (3), 455-458.
143. Bawane, S. P.; Sawant, S. B., Hydrogenation of p-nitrophenol to metol using Raney nickel catalyst: Reaction kinetics. *Appl. Catal., A* **2005**, 293 (0), 162-170.
144. Mozingo, R.; Wolf, D. E.; Harris, S. A.; Folkers, K., Hydrogenolysis of Sulfur Compounds by Raney Nickel Catalyst. *J. Am. Chem. Soc.* **1943**, 65 (6), 1013-1016.
145. Anantharaman, V.; Pintauro, P. N., The Electrocatalytic Hydrogenation of Glucose: I . Kinetics of Hydrogen Evolution and Glucose Hydrogenation on Raney Nickel Powder. *J. Electrochem. Soc.* **1994**, 141 (10), 2729-2741.
146. Fouilloux, P.; Martin, G. A.; Renouprez, A. J.; Moraweck, B.; Imelik, B.; Prettre, M., A study of the texture and structure of Raney nickel. *J. Catal.* **1972**, 25 (2), 212-222.
147. Chang, N.-S.; Aldrett, S.; Holtzapple, M. T.; Davison, R. R., Kinetic studies of ketone hydrogenation over Raney nickel catalyst. *Chem. Eng. Sci.* **2000**, 55 (23), 5721-5732.
148. Lohrberg, K.; Kohl, P., Preparation and use of Raney-Ni activated cathodes for large scale hydrogen production. *Electrochim. Acta* **1984**, 29 (11), 1557-1561.
149. Hu, W., Electrocatalytic properties of new electrocatalysts for hydrogen evolution in alkaline water electrolysis. *Int. J. Hydrogen Energy* **2000**, 25 (2), 111-118.
150. Belot, G.; Desjardins, S.; Lessard, J., Electrocatalytic hydrogenation of organic compounds on Devarda copper and Raney nickel electrodes in basic media. *Tetrahedron Lett.* **1984**, 25 (47), 5347-5350.
151. Cyr, A.; Chiltz, F.; Jeanson, P.; Martel, A.; Brossard, L.; Lessard, J.; Ménard, H., Electrocatalytic hydrogenation of lignin models at Raney nickel and palladium-based electrodes. *Can. J. Chem.* **2000**, 78, 307-315.

152. Mahdavi, B.; Chambrion, P.; Binette, J.; Martel, E.; Lessard, J., Electrocatalytic hydrogenation of conjugated enones on nickel boride, nickel, and Raney nickel electrodes. *Can. J. Chem.* **1995**, *73* (6), 846-852.
153. Mahdavi, B.; Lafrance, A.; Martel, A.; Lessard, J.; Ménard, H.; Brossard, L., Electrocatalytic hydrogenolysis of lignin model dimers at Raney nickel electrodes. *J. Appl. Electrochem.* **1997**, *27* (5), 605-611.
154. Martel, A.; Mahdavi, B.; Lessard, J.; Ménard, H.; Brossard, L., Electrocatalytic hydrogenation of phenol on various electrode materials. *Can. J. Chem.* **1997**, *75* (12), 1862-1867.
155. Dang, A.; Capuano, G. A.; Chapuzet, J. M.; Lessard, J., The coelectrodeposition of raney nickel alloy powder on a stainless steel grid. *Int. J. Hydrogen Energy* **1993** *18* (11), 941-944. .
156. Kanan, M. W.; Nocera, D. G., In Situ Formation of an Oxygen-Evolving Catalyst in Neutral Water Containing Phosphate and Co^{2+} . *Science* **2008**, *321*, 1072-1075.
157. Lutterman, D. A.; Surendranath, Y.; Nocera, D. G., A Self-Healing Oxygen-Evolving Catalyst. *J. Am. Chem. Soc.* **2009**, *131* (11), 3838-3839.
158. Kanan, M. W.; Surendranath, Y.; Nocera, D. G., Cobalt-phosphate oxygen-evolving compound. *Chem. Soc. Rev.* **2009**, *38* (1), 109-114.
159. Esswein, A. J.; Surendranath, Y.; Reece, S. Y.; Nocera, D. G., Highly active cobalt phosphate and borate based oxygen evolving catalysts operating in neutral and natural waters. *Energy Environ. Sci.* **2011**, *4* (2), 499-504.
160. Reece, S. Y.; Hamel, J. A.; Sung, K.; Jarvi, T. D.; Esswein, A. J.; Pijpers, J. J. H.; Nocera, D. G., Wireless Solar Water Splitting Using Silicon-Based Semiconductors and Earth-Abundant Catalysts. *Science* **2011**, *334* (6056), 645-648.
161. Yagi, M.; Kaneko, M., Molecular Catalysts for Water Oxidation. *Chemical Reviews* **2000**, *101* (1), 21-36.
162. Rüttinger, W.; Dismukes, G. C., Synthetic Water-Oxidation Catalysts for Artificial Photosynthetic Water Oxidation†. *Chemical Reviews* **1997**, *97* (1), 1-24.
163. Braun, R. D., *Introduction to chemical analysis*. McGraw-Hill Ryerson, Limited: 1982.
164. Navarro, D. M. A. F. N.; Navarro, M., *J. Chem. Educ.* **2004**, *81*, 1350-1352.
165. Santana, D. S.; Lima, M. V. F.; Daniel, J. R. R.; Navarro, M., *Tetrahedron Lett.* **2003**, *44*, 4725-4727.

166. Menini, R.; Martel, A.; Ménard, H.; Lessard, J.; Vittori, O., *Electrochim. Acta.* **1998**, *43*, 1697-1703.
167. Mahdavi, B.; Los, P.; Lessard, M. J.; Lessard, J., *Can. J. Chem.* **1994**, *72*, 2268-2277.
168. Cheong, A. K.; Lasia, A.; Lessard, J., *Electrochem. Soc.* **1994**, *141*, 975-982.
169. Dang, A.; Capuano, G. A.; Chapuzet, J. M.; Lessard, J., *Int. J. Hydrogen Energy* **1993** *18*, 941-944. .
170. Robin, D.; Comtois, M.; Martel, A.; Lemieux, R.; Cheong, A. K.; Belot, G.; Lessard, J., *Can. J. Chem.* **1990**, *68*, 1218-1227.
171. Gang, W.; Liyin, B.; Rongchun, X., *Electrochimica Acta.* **2010**, *55*, 4030-4038. .
172. Cry, A.; Chiltz, F.; Jeanson, P.; Martel, A.; Brossard, L.; Lessard, J.; Ménard, H., *Can. J. Chem.* **2000**, *78*, 307-315.
173. Pivovar, B. S., *Polymer* **2006**, *47*, 4194-4202.
174. Sergeev, A. G.; Hartwig, J. F., Selective, Nickel-Catalyzed Hydrogenolysis of Aryl Ethers. *Science* **2011**, *332* (6028), 439-443.
175. Kelley, P.; Lin, S.; Edouard, G.; Day, M. W.; Agapie, T., Nickel-Mediated Hydrogenolysis of C–O Bonds of Aryl Ethers: What Is the Source of the Hydrogen? *J. Am. Chem. Soc.* **2012**, *134* (12), 5480-5483.
176. Tobisu, M.; Chatani, N., Catalytic Hydrogenolysis of C-O Bonds in Aryl Ethers. *ChemCatChem* **2011**, *3* (9), 1410-1411.
177. Fedorov, A.; Toutov, A. A.; Swisher, N. A.; Grubbs, R. H., Lewis-base silane activation: from reductive cleavage of aryl ethers to selective ortho-silylation. *Chem. Sci.* **2013**, *4* (4), 1640-1645.
178. Delle Site, L.; Alavi, A.; Abrams, C. F., Adsorption energies and geometries of phenol on the (111) surface of nickel: An ab initio study. *Physical Review B* **2003**, *67* (19), 193406.
179. Kishi, K.; Chinomi, K.; Inoue, Y.; Ikeda, S., X-ray photoelectron spectroscopic study of the adsorption of benzene, pyridine, aniline, and nitrobenzene on evaporated nickel and iron. *J. Catal.* **1979**, *60* (2), 228-240.
180. Aller, B. V., Raney cobalt hydrogenation catalysts. III. Applications and promoter effects. *Journal of Applied Chemistry* **1958**, *8* (8), 492-495.

181. Bao, L.; Xiong, R.; Wei, G., Electrochemical polymerization of phenol on 304 stainless steel anodes and subsequent coating structure analysis. *Electrochim. Acta* **2010**, *55* (12), 4030-4038.
182. Wheelhouse, R. T.; Stevens, M. F. G., DECOMPOSITION OF THE ANTITUMOR DRUG TEMOZOLOMIDE IN DEUTERIATED PHOSPHATE BUFFER - METHYL-GROUP TRANSFER IS ACCOMPANIED BY DEUTERIUM-EXCHANGE. *J. Chem. Soc.-Chem. Commun.* **1993**, (15), 1177-1178.
183. Cyr, A.; Huot, P.; Belot, G.; Lessard, J., The efficient electrochemical reduction of nitrobenzene and azoxybenzene to aniline in neutral and basic aqueous methanolic solutions at devarda copper and raney nickel electrodes: electrocatalytic hydrogenolysis of N=O and N=N bonds. *Electrochim. Acta* **1990**, *35* (1), 147-152.
184. Adkins, H.; Cramer, H. I.; Connor, R., THE RATE OF HYDROGENATION OF ACETOACETIC ESTER, DEHYDROACETIC ACID, BENZENE, PHENOL AND ANILINE OVER NICKEL AT PRESSURES FROM 27 TO 350 ATMOSPHERES. *J. Am. Chem. Soc.* **1931**, *53* (4), 1402-1405.
185. Ogumi, Z.; Nishio, K.; Yoshizawa, S., *Denki-Kagaku* **1981**, (49).
186. Ogumi, Z.; Yamashita, H.; Nishio, K.; Takehara, Z.-I.; Yoshizawa, S., Application of the SPE method to organic electrochemistry—III. Kolbe type reactions on Pt-SPE. *Electrochim. Acta* **1983**, *28* (11), 1687-1693.
187. Ogumi, Z.; Nishio, K.; Yoshizawa, S., Application of the SPE Method to Organic Electrochemistry - II. Electrochemical Hydrogenation of Olefinic Double Bonds. *Electrochim. Acta.* **1981**, *26*, 1779-1782.
188. Ogumi, Z.; Ohashi, S.; Takehara, Z., Application of the SPE method to organic electrochemistry—VI. Oxidation of cyclohexanol to cyclohexanone on Pt-SPE in the presence of iodine and iodide. *Electrochim. Acta* **1985**, *30* (1), 121-124.
189. Ogumi, Z.; Inaba, M.; Ohashi, S.-i.; Uchida, M.; Takehara, Z.-i., Application of the SPE method to organic electrochemistry—VII. The reduction of nitrobenzene on a modified Pt-nafion. *Electrochim. Acta* **1988**, *33* (3), 365-369.
190. Ogumi, Z.; Inatomi, K.; Hinatsu, J. T.; Takehara, Z.-i., Application of the SPE method to organic electrochemistry—XIII. Oxidation of geraniol on Mn,Pt-Nafion. *Electrochim. Acta* **1992**, *37* (7), 1295-1299.
191. Ogumi, Z.; Yasuzawa, M.; Kunugi, A.; Inaba, M., Electroreduction of acetophenone on Pt-Nafion composite electrodes. *Denki Kagaku* **1994**, *62* (12), 5.
192. Takenaka, H.; Torikai, E., *Kokai Tokkyo Koho (Japan Patent)* **1980**, *55*, 38934.

193. Hicks, M. T.; Fedkiw, P. S., Kolbe Electrolysis of Acetic Acid in a Polymer Electrolyte Membrane Reactor. *J. Electrochem. Soc.* **1998**, *145* (11), 3728-3734.
194. Heyl, A.; Jörissen, J., Electrochemical detoxification of waste water without additives using solid polymer electrolyte (SPE) technology. *J. Appl. Electrochem.* **2006**, *36* (11), 1281-1290.
195. Machida, M.; Shono, E.; Kimura, M.; Yamauchi, S., Electrochemical lean-deNO_x catalyst using H⁺-conducting solid polymer electrolyte. *Catal. Commun.* **2003**, *4* (12), 631-635.
196. Wang, K.; Yan, H.; Liu, J.; Sun, X.; Wang, E. f., The Electrochemical Behavior and the Quantitative Determination of Nitrogen Dioxide at a Solid Polymer Electrolyte Supported Pt-Au Electrode. *Electroanalysis* **2004**, *16* (16), 1318-1323.
197. Hasnat, M. A.; Alam, M. S.; Karim, M. H. M.-u.; Rashed, M. A.; Machida, M., Divergent catalytic behaviors of Pt and Pd films in the cathode of a sandwiched type membrane reactor. *Applied Catalysis B: Environmental* **2011**, *107* (3-4), 294-301.
198. Hasnat, M. A.; Agui, R.; Hinokuma, S.; Yamaguchi, T.; Machida, M., Different reaction routes in electrocatalytic nitrate/nitrite reduction using an H⁺-conducting solid polymer electrolyte. *Catal. Commun.* **2009**, *10* (7), 1132-1135.
199. Hasnat, M. A.; Ishibashi, I.; Sato, K.; Agui, R.; Yamaguchi, T.; Ikeue, K.; Machida, M., Electrocatalytic Reduction of Nitrate Using Cu-Pd and Cu-Pt Cathodes/H⁺-Conducting Solid Polymer Electrolyte Membrane Assemblies. *Bull. Chem. Soc. Jpn.* **2008**, *81* (12), 1675-1680.
200. Takenaka, H.; Torikai, E.; Kawami, Y.; Wakabayashi, N., Solid polymer electrolyte water electrolysis. *Int. J. Hydrogen Energy* **1982**, *7* (5), 397-403.
201. Choi, P.; Bessarabov, D. G.; Datta, R., A simple model for solid polymer electrolyte (SPE) water electrolysis. *Solid State Ionics* **2004**, *175* (1-4), 535-539.
202. Nuttall, L. J., Conceptual design of large scale water electrolysis plant using solid polymer electrolyte technology. *Int. J. Hydrogen Energy* **1977**, *2* (4), 395-403.
203. Jörissen, J., Electro-organic synthesis without supporting electrolyte: Possibilities of solid polymer electrolyte technology. *J. Appl. Electrochem.* **2003**, *33* (10), 969-977.
204. Jörissen, J., Ion exchange membranes as solid polymer electrolytes (spe) in electro-organic syntheses without supporting electrolytes. *Electrochim. Acta* **1996**, *41* (4), 553-562.
205. He, P.; Watts, P.; Marken, F.; Haswell, S. J., Electrolyte free electro-organic synthesis: The cathodic dimerisation of 4-nitrobenzylbromide in a micro-gap flow cell. *Electrochem. Commun.* **2005**, *7* (9), 918-924.

206. Inaba, M.; Ogumi, Z.; Takehara, Z. i., Application of the Solid Polymer Electrolyte Method to Organic Electrochemistry: XVII . Indirect Electrochemical Debromination Using Viologens as Microscopic Phase-Transfer Mediators. *J. Electrochem. Soc.* **1994**, *141* (10), 2579-2586.
207. Horcajada, R.; Okajima, M.; Suga, S.; Yoshida, J.-i., Microflow electroorganic synthesis without supporting electrolyte. *Chemical Communications* **2005**, (10), 1303-1305.
208. Kunugi, A.; Fujioka, M.; Yasuzawa, M.; Inaba, M.; Ogumi, Z., Electroreduction of 2-cyclohexen-1-one on metal–solid polymer electrolyte composite electrodes. *Electrochim. Acta* **1998**, *44* (4), 653-657.
209. An, W.; Hong, J. K.; Pintauro, P. N., Current efficiency for soybean oil hydrogenation in a solid polymer electrolyte reactor. *J. Appl. Electrochem.* **1998**, *28* (9), 947-954.
210. An, W.; Hong, J.; Pintauro, P.; Warner, K.; Neff, W., The electrochemical hydrogenation of edible oils in a solid polymer electrolyte reactor. I. Reactor design and operation. *J. Am. Oil Chem. Soc.* **1998**, *75* (8), 917-925.
211. Warner, K.; Neff, W. E.; List, G. R.; Pintauro, P., Electrochemical hydrogenation of edible oils in a solid polymer electrolyte reactor. Sensory and compositional characteristics of low Trans soybean oils. *J. Am. Oil Chem. Soc.* **2000**, *77* (10), 1113-1118.
212. An, W.; Hong, J.; Pintauro, P. N.; Warner, K.; Neff, W., The electrochemical hydrogenation of edible oils in a solid polymer electrolyte reactor. II. Hydrogenation selectivity studies. *J. Am. Oil Chem. Soc.* **1999**, *76* (2), 215-222.
213. Green, S. K.; Tompsett, G. A.; Kim, H. J.; Kim, W. B.; Huber, G. W., Electrocatalytic Reduction of Acetone in a Proton-Exchange-Membrane Reactor: A Model Reaction for the Electrocatalytic Reduction of Biomass. *ChemSusChem* **2012**, *5* (12), 2410-2420.
214. Green, S. K.; Lee, J.; Kim, H. J.; Tompsett, G. A.; Kim, W. B.; Huber, G. W., The electrocatalytic hydrogenation of furanic compounds in a continuous electrocatalytic membrane reactor. *Green Chem.* **2013**, *15* (7), 1869-1879.
215. Qiu, Y.; Xin, L.; Chadderton, D. J.; Qi, J.; Liang, C.; Li, W., Integrated electrocatalytic processing of levulinic acid and formic acid to produce biofuel intermediate valeric acid. *Green Chem.* **2014**, *16* (3), 1305-1315.
216. Yi-Lin, C.; Tse-Chuan, C., Metals and alloys bonded on solid polymer electrolyte for electrochemical reduction of pure benzaldehyde without liquid supporting electrolyte. *J. Electroanal. Chem.* **1993**, *360* (1–2), 247-259.
217. Li, Z.; Garedew, M.; Lam, C. H.; Jackson, J. E.; Miller, D. J.; Saffron, C. M., Mild electrocatalytic hydrogenation and hydrodeoxygenation of bio-oil derived phenolic compounds using ruthenium supported on activated carbon cloth. *Green Chem.* **2012**, *14* (9), 2540-2549.

218. Sompalli, B.; Gasteiger, H.; Mathias, M. F.; Scozzafava, M., Methods of preparing membrane electrode assemblies. Google Patents: 2003.
219. Firtina, İ.; Güner, S.; Albostan, A., Preparation and characterization of membrane electrode assembly (MEA) for PEMFC. *International Journal of Energy Research* **2011**, *35* (2), 146-152.
220. Dudley, J. R., Furfural condensation products. Google Patents: 1950.
221. Li, Z. L.; Kelkar, S.; Lam, C. H.; Luczek, K.; Jackson, J. E.; Miller, D. J.; Saffron, C. M., Aqueous electrocatalytic hydrogenation of furfural using a sacrificial anode. *Electrochim. Acta* **2012**, *64*, 87-93.
222. Housecroft, C. E.; Sharpe, A. G., *Inorganic Chemistry*. Pearson Prentice Hall: 2005.
223. Smith, M. B.; March, J., *March's Advanced Organic Chemistry: Reactions, Mechanisms, and Structure*. Wiley: 2007.
224. *Lab Manual in Biochemistry: Immunology and Biotechnology*. Tata McGraw-Hill Pub.: 2007.
225. The United States Mint About Us.
http://www.usmint.gov/about_the_mint/index.cfm?action=coin_specifications (accessed 02/01/2011).
226. Gruen, D. M.; Mendelsohn, M. H.; Dwight, A. E., Lanthanum nickel aluminum alloy. Google Patents: 1979.
227. Gay, R. N.; Raymond, W. K., Process for electroplating nickel over stainless steel. Google Patents: 1988.
228. Mroczkowski, R. S., *Electronic Connector Handbook: Theory and Applications*. McGraw-Hill: 1998.
229. Mallory, G. O.; Hajdu, J. B.; Electroplaters, A.; Society, S. F., *Electroless Plating: Fundamentals and Applications*. The Society: 1990.
230. Menini, R.; Martel, A.; Ménard, H.; Lessard, J.; Vittori, O., The electrocatalytic hydrogenation of phenanthrene at Raney nickel electrodes: the influence of an inert gas pressure. *Electrochim. Acta*. **1998**, *43* (12-13), 1697-1703.